2013

Rheological behavior of oxide nanopowder suspensions

Simge Cinar
Iowa State University

Rheological behavior of oxide nanopowder suspensions

by

Simge Çınar

A dissertation submitted to the graduate faculty

in partial fulfillment of the requirements for the degree of

DOCTOR OF PHILOSOPHY

Major: Materials Science and Engineering

Program of Study Committee:
Mufit Akinc, Major Professor
David Grewell
Matthew J. Kramer
Surya K. Mallapragada
Sriram Sundararajan

Iowa State University
Ames, Iowa
2013

`

To my mother, Gülseren Çınar, who unconditionally supports me each step of my life…

`

TABLE OF CONTENTS

ACKNOWLEDGEMENT v

ABSTRACT……..... vi

CHAPTER I. INTRODUCTION 1
I.1 Thesis Organization 1
I.2 Introduction 3
I.3 Background 6
Rheological Behavior of Colloidal Suspensions 6
Interparticle Interactions in Colloidal System 11
Development of Surface Particle Charge in Liquid Suspensions 17
Processing Additives 19
Nanopowder Suspensions and Bound Water 21
References 23

CHAPTER II. ELUCIDATION OF VISCOSITY REDUCTION MECHANISM OF NANO ALUMINA SUSPENSIONS WITH FRUCTOSE ADDITIONS BY DSC 27
Abstract 27
Introduction 28
Experimental Procedure 31
Results and Discussion 34
Conclusions 50
Acknowledgments 51
References 51

CHAPTER III. ELECTROSTATIC STABILIZATION OF ALUMINA NANOPOWDER SUSPENSIONS 54
Abstract 54
Graphical Abstract 55
Introduction 55
Experimental 58
Results and Discussion 61
Conclusions 76
Acknowledgements 77
References 78

CHAPTER IV. COMBINED EFECT OF FRUCTOSE AND NaCl ON THE VISCOSITY OF ALUMINA NANOPOWDER SUSPENSIONS 81
Abstract 81
Introduction 82
Experimental 84

`

Results and Discussion 87
Conclusions 100
Acknowledgement 101
References 101

CHAPTER V. ASCORBIC ACID AS A DISPERSANT FOR CONCENTRATED NANOPOWDER SUSPENSIONS 106
Abstract 106
Introduction 107
Experimental 110
Results and Discussion 113
Conclusion 122
Acknowledgement 123
References 123

CHAPTER VI. BOUND WATER LAYER AND ITS INFLUENCE ON THE VISCOSITY OF CERAMIC OXIDE NANOPOWDERS SUSPENSIONS 128
Abstract 128
Introduction 129
Experimental 130
Results and Discussion 134
Conclusion 152
Acknowledgement 153
References 153

CHAPTER VII. GENERAL CONCLUSIONS 158

`

ACKNOWLEDGEMENT

I am heartily thankful to my major professor, Dr. Mufit Akinc, for his supervision, patience and support throughout my research as well as for his guidance that broaden my vision and for urging me to develop as an independent researcher. I am very grateful to him for his understanding, and help not only technical, but also personal matters.

I would also like to thank the members of my dissertation committee, Dr. Matthew J. Kramer, Dr. Michael R. Kessler, Dr. Surya K. Mallapragada, Dr. Sriram Sundararajan and Dr. David Grewell, for generously offering their time and expertise for this work.

I would like to thank Dr. Tanya Prozorov and Dr. Sanjay Kashyap for their collaboration.

All my group members, especially Dr. Pratik Ray and Dr. Imteyaz Ahmad, deserve many thanks for their helpful discussions and comments, which added significant value to my work.

I warmly thank to Irmak Sargin, Olga Nikolova, Arda Colak, Ceren Gunsoy and Tugce Karakulak, who have endured me in this significant challenge and being wonderful friends. I would thank to Sevinc Akinc for her friendship and support. I sincerely thank to Hakan Yavas for his faith on me, for the motivating conversations and for his endless support in the last years of my Ph.D.

Last but not the least, I would like to express my gratitude to my family, Gulseren, Mehmet and Cem Cinar, and my cousin, Sinem Kosar, for believing in and supporting me in every aspects of my life.

`

ABSTRACT

Ceramic nanopowders offer great potential in advanced ceramic materials and many other technologically important applications. Because a material's rheological properties are crucial for most processing routes, control of the rheological behavior has drawn significant attention in the recent past.

The control of rheological behavior relies on an understanding of how different parameters affect the suspension viscosities. Even though the suspension stabilization mechanisms are relatively well understood for sub-micron and micron size particle systems, this knowledge cannot be directly transferred to nanopowder suspensions. Nanopowder suspensions exhibit unexpectedly high viscosities that cannot be explained with conventional mechanisms and are still a topic of investigation.

This dissertation aims to establish the critical parameters governing the rheological behavior of concentrated oxide nanopowder suspensions, and to elucidate the mechanisms by which these parameters control the rheology of these suspensions. Aqueous alumina nanopowders were chosen as a model system, and the findings were extrapolated to other oxide nanopowder systems such as zirconia, yttria stabilized zirconia, and titania. Processing additives such as fructose, NaCl, HCl, NaOH, and ascorbic acid were used in this study.

The effect of solids content and addition of fructose on the viscosity of alumina nanopowder suspensions was investigated by low temperature differential scanning calorimetry (LT-DSC), rheological, and zeta potential measurements. The analysis of bound water events observed in LT-DSC revealed useful information regarding the rheological behavior of nanopowder suspensions. Because of the significance of interparticle interactions in nanopowder suspensions,

`

the electrostatic stabilization was investigated using indifferent and potential determining ions. Different mechanisms, e.g., the effect of the change in effective volume fraction caused by fructose addition and electrostatic stabilization, were combined to optimize the viscosities and the ability to control the suspension viscosity. The intrinsic viscosities of nanopowder systems were estimated using the Krieger-Dougherty relation. Both the individual and the combined effects were evaluated using slip casting of green bodies. Also, ascorbic acid was used to disperse the alumina nanopowders (described here for the first time in the open literature). The mechanism of viscosity reduction was investigated by *in situ* attenuated total reflectance Fourier infrared spectroscopy (ATR-FTIR), rheological, suspension pH, and zeta potential measurements. Lastly, the findings were extrapolated to several other oxide systems. The rheological behavior of zirconia, yttria stabilized zirconia, and titania nanopowder systems was investigated as a function of solids content, bound water, and intrinsic viscosity.

The results indicated that nanopowder suspensions differ from sub-micron powder suspensions because of the higher bound water content and the short separation distances between particles causing increased interparticle interactions. The bound water event was associated with the powder surface. This layer differed from the electrostatic double layer in that it was modified by fructose molecules as well as by specifically adsorbed ions such as H^+ and OH but not by indifferent electrolytes, such as NaCl. Because of the large surface area of nanopowders, this additional layer increased the effective solids content and led to higher viscosities. While the alumina suspensions were studied in detail, it was also shown that the bound water was not unique to the alumina nanopowder suspensions, but also present in other oxide systems. However, the bound water content was unique for each system and provided information about its origin. The presence of bound water resulted in lower the maximum

`

achievable solids fractions for nanopowder systems. In order to achieve higher solids contents, the bound water layer had to be modified.

Because of the limited separation distances and large surface areas of nanopowders, the electrostatic double layer has an amplified effect on the viscosity of the suspensions. The addition of NaCl decreased the viscosity of alumina nanopowder suspensions significantly by compressing the double layer hence limiting the repulsion length.

We also discovered that ascorbic acid can be used to disperse the alumina nanopowder suspensions. By adding only 1 wt% of ascorbic acid, the viscosity of the suspensions decreased significantly. It was shown that ascorbic acid molecules adsorbed to the alumina surfaces and when the adsorption reached equilibrium, the lowest viscosities were observed. By lowering the viscosities, the maximum achievable solids content (where $[\eta] \leq 1$ Pa·s at a shear rate of 100 s^{-1}) could be increased up to about 0.35, which is the highest solids content achieved with readily available processing additives reported in the open literature.

Even though it is almost impossible to isolate the individual effects, three dominant mechanisms were observed in nanopowder suspensions: (i) increase in effective volume fraction (bound water), (ii) interparticle interactions (electrostatic), and (iii) adsorption of organic molecules. It was shown that the understanding of the system's parameters enables the optimization of the rheological behavior of the suspensions and the prediction of the green body quality.

`

CHAPTER I. INTRODUCTION

I.1 Thesis Organization

This dissertation adopts a journal paper format composed of original manuscripts preceded by an introduction and followed by a conclusion as described in the Graduate College Thesis Manual. References cited have been placed at the end of each chapter.

Chapter II contains the first paper, titled "Elucidation of Viscosity Reduction Mechanism of Nano Alumina Suspensions with Fructose Addition by DSC" was published in the *Journal of the American Ceramic Society*. Here, the effect of solids content and fructose concentration on the viscosity of alumina suspensions was revealed through the bound water content. The viscosity reduction mechanism of fructose was elucidated.

The second paper presented in Chapter III, "Electrostatic Stabilization of Alumina Nanopowder Suspensions", was accepted for publication by the *Science of Advanced Materials*. In this paper, the stability of concentrated alumina nanopowder suspensions at specific ranges of ionic strength and pH was investigated and possible mechanisms effective in controlling the suspension viscosity were discussed.

The third manuscript presented in Chapter IV, titled "Combined Effect of Fructose and NaCl on the Viscosity of Alumina Nanopowder Suspensions", will be submitted to the *Journal of European Ceramic Society*. In this study, we exemplify the success of combining electrostatic (NaCl) and specific surface adsorption (fructose) on the viscosity of alumina nanopowder suspensions. The suspension viscosity was also modeled by the Krieger-Dougherty relation. The relation was modified by accounting for the presence of the bound water layer.

`

Chapter V, “Bound Water Layer and its Influence on Viscosity of Ceramic Oxide Nanopowder Suspensions”, extrapolates our findings to other oxide nanopowder systems, such as zirconia, yttria stabilized zirconia, and titania. It was shown that bound water is not unique for alumina suspensions, but also observed in other oxide systems which were studied. Modified Krieger-Dougherty equation was applied to better understand the viscosity mechanism of suspensions. This paper will be submitted to the *Journal of European Ceramic Society*.

Chapter VI contains the fifth manuscript, “Ascorbic Acid as a Dispersant for Concentrated Nanopowder Suspensions”, which was accepted by the *Journal of European Ceramic Society*. In this paper, we report the use of ascorbic acid for the dispersion of alumina nanopowder suspensions for the first time in the open literature. Adsorption of ascorbic acid on alumina surface was studied by use of *in situ* ATR-FTIR Spectroscopy, zeta potential measurements and suspension pH changes. Concentration of ascorbic acid was optimized to obtain the lowest viscosity and highest achievable solids content.

Although all five manuscripts are mainly the work of this author, Mufit Akinc, major professor, has made significant contributions to these manuscripts and appears as a co-author. Laura van Steenhuyse (in the first paper, Elucidation of Viscosity Reduction Mechanism of Nano Alumina Suspensions with Fructose Addition by DSC), and Daniel D. Anderson (in the third, Combined Effect of Fructose and NaCl on the Viscosity of Alumina Nanopowder Suspensions, and the fourth manuscripts, Bound Water Layer and its Influence on Viscosity of Ceramic Oxide Nanopowder Suspensions), who are listed as co-authors were undergraduate students contributing to the work by conducting some of the experiments and analyses.

`

I.2 Introduction

Ceramic nanomaterials are applied in electronics (in capacitors, insulators, substrates, integrated circuit packages, piezoelectrics, magnets, superconductors, etc.), coatings (for engine components, cutting tools, industrial wear parts, etc.), chemical processing and environmental components (as filters, membranes, catalysts, catalyst supports, etc.), nanofluids (in hybrid powered engines, refrigerators, heat exchangers, nuclear reactor coolants, etc.) as well as in solid oxide fuel cells, paints, pigments, printing inks, adhesives, abrasives, ferrofluids, sunscreens and others.

Many of the processes using nanopowders involve dispersing the powder in a liquid, either as an intermediate step or to as the end product. In either case, the rheological properties of the suspensions are critical for almost all processes. The viscosity of a suspension generally determines its stability and its homogeneity, both of which are crucial for product quality. For application where strength is essential, the solids content determines the packing density and therefore also becomes an important parameter dependent on the viscosity. Rheological properties of suspensions not only play role in selecting and designing of production techniques, but also reduce production cost when the suspension viscosities are lowered.

Manipulation of the interparticle interactions (solid-solid and solid-liquid interactions) allows to control the rheological behavior, providing an approach to optimize the suspension properties. This manipulation process is called colloidal processing. Processing additives and conditions are chosen specific to the properties of the powders and liquids under consideration; the goal is to control the interactions between the powder particles, to stabilize the suspension, and retain reasonable rheological properties while obtaining optimum solids content.

`

When nanometer range powders are used in production, homogeneous dispersion and high particle loading become quite challenging because of the agglomeration tendency and high surface area of nanoparticles. The smaller the particle size, the higher the number of particles introduced to the system for given amount of powder, creating shorter interparticle distances between the individual particles (Figure 1 a). For small particles in close proximity, even small disturbances in the system, such as Brownian motion, may result in agglomeration. Higher viscosities of nanopowder suspensions can't be explained by conventional models [1-4].

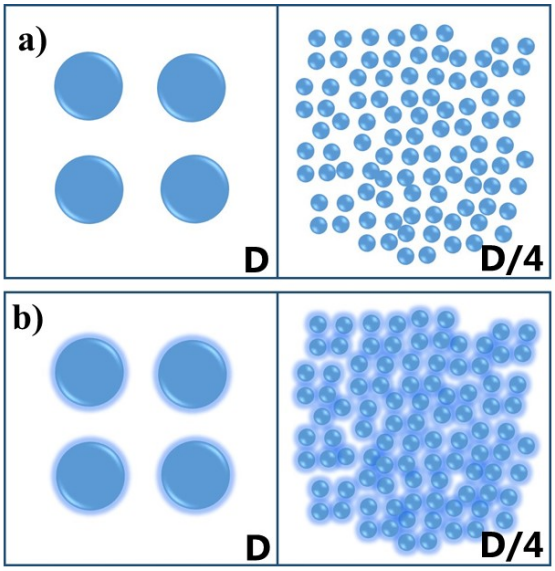

Figure 1: Crowding of particles as particle size decreases (a). The effect becomes more significant when interfacial layers are considered (b). In the above illustration when the particle size is reduced to ¼, the number of particles will increase by 64-fold for a constant solids content.

In aqueous media, the surface of a ceramic particle interacts with the medium and develops a charge on its surface. This interaction builds an interfacial layer between the particle surface and the medium. While the interfacial layer thickness (electrostatic double layer) is negligible with respect to the particle size for large particles, it becomes significant in nanopowders (Figure 1 b). Because the oxide particles are surrounded by their interfacial layer in the suspension, the effective particle size and hence the effective solids content increase and consequently limit the

`

maximum packing density of the particles. That brings us to question, “What kind of adjustments can be made to obtain and control the properties of highly loaded ceramic nanopowder suspensions?” Answer of this question requires a clear understanding of the system, especially the dominant interaction forces where the conventional models fail to explain. Only after then, the dominating parameters may be adjusted for optimum suspension viscosity.

The attractive van der Waals (vdW) forces, the repulsive electrostatic forces, and the steric (polymer-induced) forces are the operative system forces commonly examined to predict and explain the behavior of particle suspensions, especially when the particles size is in the micrometer scale. The Derjaguin-Landau-Verwey-Overbeek (DLVO) theory is used to calculate the net interaction potential between particles as a function of separation distance using the summation of individual forces. The net potential helps to predict the stability and rheological properties of the suspensions. Processing additives are used to stabilize the colloidal systems because they restrict the attractive forces or enhance the repulsive interactions between particles to increase stability [5, 6]. Even though the critical parameters for stabilization of micron- and submicron-size powder suspensions are well established, the knowledge cannot be transferred directly to nano-size powder systems.

It was reported that conventional additives used to decrease the viscosities of sub-micron size powder suspensions either increase the viscosity of the suspensions rather than decrease it, or limit the maximum achievable solids content because they may induce bridging or depletion flocculation in concentrated suspensions of nanopowders [7].

Alumina is one of the most commonly used and as such most extensively studied ceramic oxides. In particular, synthesis and characterization of alumina powders, as well as its various processing routes have been widely documented [8-15]. Alumina provides a broad operational

`

pH range because of low solubility and its slightly alkaline isoelectric point. The isoelectric point, IEP, is defined as the pH value of a suspension at which the net electric charge of the particles is zero. Because the repulsive forces are created by the surface charge, stable suspensions can be obtained at pH values away from the IEP and makes the range of study with alumina particles more flexible.

It was observed that low molecular weight saccharides serve as good dispersing agents for highly loaded alumina suspensions [16-20]. Although there are some predictions regarding the viscosity reduction mechanism of low molecular weight saccharides and other processing additives for a variety of ceramic nanopowder systems, they are generally only applicable to specific chemicals and under a given set of experimental conditions, hence far from being general models for nanopowder suspensions [16-21]. The aim of this research is to establish critical parameters governing the rheological behavior of highly loaded nanopowder suspensions and elucidate the mechanisms by which these parameters control the rheology of ceramic nanopowder suspensions. Alumina nanopowder suspension was used as a model and the findings were extrapolated to other ceramic systems, such as zirconia, yttria stabilized zirconia, and titania.

I.3 Background

Rheological Behavior of Colloidal Suspensions

Rheology is the study of the flow and deformation behavior of materials in response to applied stresses. Viscosity is a constant value, expressing the resistivity of the fluid to flow at a given shear rate; it can be expressed as the ratio of the stress applied, τ, to the rate of displacement of the fluid, $\dot{\gamma}$ (Equation 1). If the fluid exhibits a constant, characteristic response

`

at all shear rates, it is called a Newtonian fluid. Simple fluids, such as water, show Newtonian behavior.

$$\eta = \frac{shear\ rate}{strain\ rate} = \frac{\tau}{\dot{\gamma}} \tag{1}$$

Perturbations in the structure of fluids will create perturbations in the rheological responses. For the colloidal suspension of hard spheres, the equation of the state for viscosity can be written as [22]

$$\eta_s = f(\dot{\gamma}, t, \eta_l, \rho_l, R, n, \rho_P, kT) \tag{2}$$

where η_s is the suspension viscosity, $\dot{\gamma}$ is the shear rate; t is the time; η_l and ρ_l are the viscosity and the density of the liquid; R, n, and ρ_p are the radius, concentration (number density) and density of the particles, and kT is the thermal energy reflecting Brownian motion.

Hard spheres are rigid, inert, spherical particles which do not experience interparticle forces, but infinite repulsion at contact. In the presence of charged particles rather than hard spheres, additional parameters are introduced to the equation of state, such as the charge of particle, q, the ionic strength of the suspension, I, and the dielectric constant of the medium, ε. For colloidal systems containing the same type of particles and medium at constant temperature, pressure and shear rate, all variables can be grouped into two groups; solids content, Φ, and interactions between particles, ψ. Some of the rheological models reported in the literature are summarized in Table 1.

`

Table 1: Rheological models for colloidal suspensions.

Reference	Equation	Parameters	Properties
Einstein [5, 23]	$\eta_r = 1 + 2.5\Phi$	$\boldsymbol{\eta_r}$:reduced viscosity; $\boldsymbol{\Phi}$: solids content	Hard sphere model suspensions (1st order hydrodynamic interactions are introduced.) applicable for $\Phi \lesssim 0.03$
Batchelor [5, 23]	$\eta_r = 1 + 2.5\Phi + 6.2\Phi^2$		Hard sphere model suspensions (1st and 2nd order hydrodynamic interactions are introduced.) applicable for $\Phi \lesssim 0.10$
Krieger-Dougherty [5, 23]	$\eta_r = \left(1 - \frac{\Phi}{\Phi_{\max}}\right)^{-[\eta]\Phi_{\max}}$	$[\boldsymbol{\eta}]$: intrinsic viscosity ($[\eta]$= 2.5 for spherical hard spheres); $\boldsymbol{\Phi_{max}}$: maximum packing ($\Phi_{\max}$ = 0.64 for random close packing; 0.74 for the closest packing of monodispersed spheres[24])	Hard sphere model suspensions shape effects are introduced.
Starov *et al*. [25]	$\eta_r = \left(1 - \frac{\Phi}{\bar{\Phi}_{\max}}\right)^{-2.5\bar{A}}$	$\boldsymbol{\bar{\Phi}_{max}}$: average packing density of all clusters; $\boldsymbol{\bar{A}}$: average resistance coefficient of all clusters	Hard sphere model suspensions clustering effect is taken into account.
Liu [26]	$\eta_r = [a\,(\Phi_{\max} - \Phi)]^{-n}$; $\Phi_{\max} = 1 - \frac{b}{a}$	**a, b:** experimental parameter describing the viscosity behavior of suspension; **n:** flow dependent suspension specific parameter (n=2 for high shear applications)	Empirical model aims to calculate the value of $\Phi_{\max}$ for highly concentrated ceramic suspensions. For viscosity calculations, extrapolation of the experimental data is used.
Horri *et al*.[27]	$\eta_r = 1 + 2.5\Phi + K\Phi\left(\frac{\Phi}{\Phi_{\max} - \Phi}\right)^2$	$\boldsymbol{K}$: model coefficient	Empirical model addition of residual relative viscosity term for the concentrated suspensions.
Ruiz-Reina[28]	$\eta_r = 1 + 2.5\Phi S(\Phi)(1 + p)$	$\mathbf{S(\Phi)}$: the Simha function (concentration effect) **p**: electroviscous coefficient	Theoretical model, solids content and electro-viscous effects are introduced.
Ogawa *et al*.[29]	$\eta_r = \left(1 - \frac{\Phi}{\Phi_{\max}}\right)^{-2.5\Phi_{\max}} + k_2\Phi \exp\left(\frac{U_v(\Phi)}{k_B T} - \frac{k_1 a^3 \sigma_p}{\Phi k_B T}\right)$; $U_v(\Phi) = k_3 V(a)$	$\mathbf{k_1}$, $\boldsymbol{k_2}$, $\mathbf{k_3}$: certain constants; a: particle size; $\boldsymbol{\sigma_p}$: elastic particle stress arises from interparticle potential forces; $\mathbf{U_v(\Phi)}$: activation energy; $\mathbf{V(r)}$: interparticle potential	Effects of interparticle interactions on viscosity are introduced via activation process.

`

The presence of charged particles in the system introduces attractive and/or repulsive interparticle interactions. The double layer around the particles formed as a result of the interparticle interactions has a profound influence on the rheological behavior of the suspensions [30]. As long as the thickness of the layer, δ, is relatively small, the hard sphere model represents the system fairly well. If that is not the case, the effective radii of the particles become much larger than the core radius, as does the effective solids content, leading to yield stress and higher viscosity than expected. The effective solids content can be approximated by adding the double layer thickness to the particle core radius. The effective solids content, Φ_{eff}, is calculated as shown in Equation 3 [5].

$$\Phi_{\text{eff}} = \Phi\left(1 + \frac{\delta}{\text{R}}\right)^3 \tag{3}$$

As the particle concentration approaches the dense packing values for the charged particles, the double layers around the particles will start to overlap because of the small separation distances between them independent of the repulsive forces, and results in the agglomeration (or flocculation) of the particles. The degree of overlapping can be visualized by calculating the average separation distance,$< S_0 >$, between individual particles.

$$< S_0 > = a\left[\left(\frac{\Phi_{\text{max}}}{\Phi}\right)^{1/3} - 1\right] \tag{4}$$

The degree of flocculation depends on the strength of the interparticle attraction. Weakly flocculated systems ($1 < -\frac{V_{min}}{k_B T} < 20$) show reversible flocculation and strong shear thinning behavior because the shear during the flow breaks the weak links between the structures [15, 30, 31]. In flocculated systems where particles are held strongly ($-\frac{V_{min}}{k_B T} > 20$) on the other hand, flocculation (or aggregation) is irreversible and these systems exhibit substantial yield stress as

`

well as shear thinning behavior. In this case, the aggregates are considered as the primary flow units and with an increase in shear rate, the viscous forces reduce the size of the aggregates and release the immobilized water within the aggregates. This in turn, leads to a decrease in the effective solids content and hence in the viscosity of the suspension [15, 30-33]. Even though this explanation is widely accepted, the cause of the shear thinning behavior is still controversial [34-38]. Recently, it was reported that a decrease in interparticle forces at high shear rates caused by strong hydrodynamic forces leads to shear thinning behavior [37].

The rheological models can be improved by accounting for the effects of the agglomerate structures (Starov model), the thickness of electrical double layer (Ruiz-Reina model) as well as the overall interparticle interaction energy (Ogawa model). Also, the agglomerate structure can be introduced into the effective solids content term and the intrinsic viscosities discussed accordingly [34, 36, 39]. However, all equations available in the literature underestimate the viscosities of nanopowder suspensions, even when the dilute solutions are considered [1, 2, 40, 41].

In summary, the addition of particles into the solutions increases the viscosity of the suspensions mainly because of the hydrodynamic and interparticle interaction effects between charged particles. Higher particle concentrations and smaller sizes make these effects profound. Current rheological models available in the literature do not accurately predict the viscosities of nanopowder suspensions. A better understanding of the suspension behavior is needed to improve the available models or derive new ones.

`

Interparticle Interactions in Colloidal System

As stated in the previous section, the rheological properties of suspensions primarily depend on the interactions in the system. Although the contribution of the interactions varies significantly for different systems, they can be classified into three groups: solvent-solvent, particle-particle and solvent-particle interactions. The viscosity of the pure fluid is determined by solvent-solvent interactions. With the addition of particles, these interactions are interrupted and new ones are introduced depending on the interfacial properties between particles and solvent. Higher particle loadings result in particle-particle interactions.

It is widely accepted that there are two main forces present in all colloidal systems; they are known as attractive van der Waals and repulsive electrostatic forces. Additional interactions may also play a significant role depending on the system conditions.

Van der Waals Interactions

Van der Waals (vdW) interactions are the main attractive forces in the system and arise from the interactions between atomic or molecular oscillations or rotating electrical dipoles in the medium, so-called dipole-dipole interactions. If the molecules can rotate freely, the dipoles try to maximize the attractive dipolar attractions and minimize the repulsive forces by aligning the dipoles with respect to each other. Because there is no permanent orientation in isotropic liquids, the molecules try to correlate themselves due to its neighbor so the net attractive forces occur among the molecules. These are the forces that hold most fluid molecules together. The total attraction potential can be calculated on the molecular level, but it is useful to account these forces on a continuum for complex fluid systems. Hamaker calculated the vdW interaction free energy, V_{vdW}, by a pair-wise summation over all atoms in the bodies from the polarizabilities and number densities of the atoms in the two interacting bodies. According to this calculation, V_{vdW}

`

between two approaching spherical particles with radius a in a medium (different than the particle) is:

$$V_{vdW} = -\frac{A_H}{12}\left\{\frac{1}{(x+1)^2-1}+\frac{1}{(x+1)^2}+2ln\left[1-\frac{1}{(x+1)^2}\right]\right\} \quad (5)$$

Where $x = D/2a$; D is the gap between two spheres and A_H is the Hamaker constant.

With the Derjaguin approximation ($D \ll a$ or $x \ll 1$), the equation can be simplified to

$$V_{vdW} = -\frac{A_H a}{12D} \quad (6)$$

Rather than using a microscopic approach, which Hamaker used to calculate the constant, Lifshitz's theory (macroscopic approach) can be used to estimate the Hamaker constant, treating each body as a continuum with certain dielectric properties. Then,

$$A_H = \frac{3}{4}k_B T\left(\frac{\varepsilon_A-\varepsilon_B}{\varepsilon_A+\varepsilon_B}\right)^2+\frac{3h\upsilon_e}{16\sqrt{2}}\frac{(n_A^2-n_B^2)^2}{(n_A^2+n_B^2)^{3/2}} \quad (7)$$

where, ε_A , ε_B are the dielectric constants of *A* (particle material), and *B* (medium), respectively; n_i is the refraction of material *i*, and $\upsilon_e$is the main UV absorption frequency.

For concentrated suspensions, the retardation effects observed at interparticle separations larger than 5 nm needs to be considered[5]. Gregory equation [42] includes the retardation effect and is valid for the separations smaller than particle size (Equation 8).

$$E_{vdW} = -\frac{A}{6}\frac{a_1 a_2}{h(a_1+a_2)}\left[1-\frac{bh}{\lambda}ln\left(1+\frac{\lambda}{bh}\right)\right] \quad (8)$$

where *A* is the Hamaker constant, a_1 and a_2 are the radii of the spherical particles at the separation distance of *h, b* is a constant equal to 5.32 and λ is the characteristic wavelength for the internal molecular motion which is generally taken as 100 nm.

`

Electrostatic Interactions

Electrostatic interactions are present in any system containing ions. The natural surface charges of the particles in water or any media with high dielectric constant result in repulsive interactions between particles. Ionization or dissociation of surface groups, adsorption or binding of ions to the particle surface, or charge exchange mechanisms such as acid-base type interactions are the basis of ions present in the suspensions (discussed in details in the next section). The interfacial layer observed around the particles is called the electrical double layer (EDL) because it is shaped by the electrical properties of the particles and the solvent.

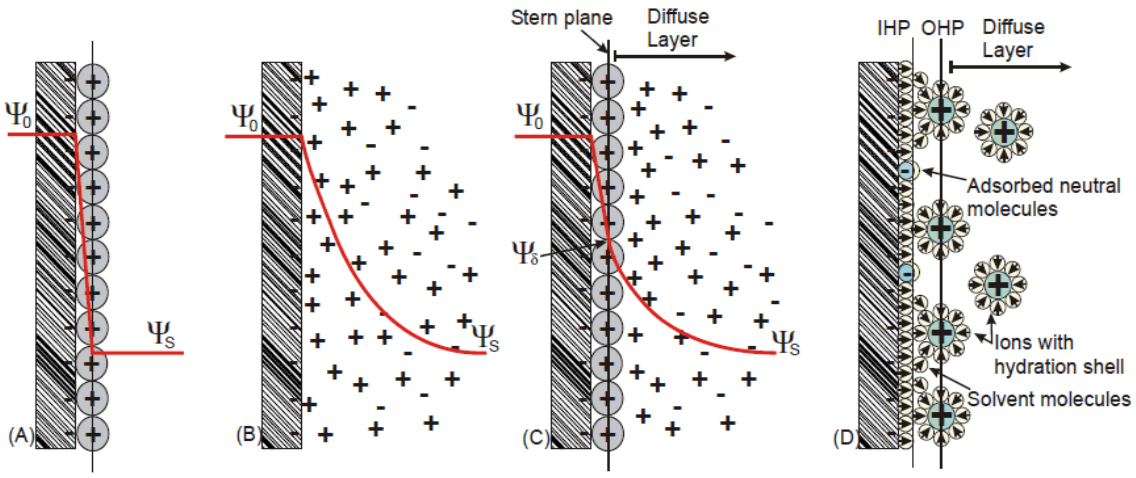

Figure 2: Electric double layer models: Helmholtz (a), Gouy-Chapman (b), Stern (c), and BDM (d) model [43].

The first model for EDLs was defined by Helmholtz (1853) as the accumulation of a monolayer of counter ions on the metal surface. Later, Gouy (1910) and Chapman (1913) described the diffuse layer by accounting on the thermal motion of the ions. Stern (1924) improved the Gouy-Chapman model by combining it with Helmholtz's model [5]. According to this model, the adjacent layer is limited with the saturation adsorption of counter ions due to their hydrated radii and after this layer, the ion diffusion occurs. Grahame (1947) added the specific adsorption of ions to the Stern model. Here, the EDL was divided into three regions: inner and

outer Helmholtz plane (IHP, OHP, respectively) and diffuse region. The Bockris, Devanathan and Muller (BDM) model (1963) [44] suggested that a layer of water was present within the IHP at the surface of the electrode. The dipole of these molecules would be fixed because of the charge in the electrode; other layers of water would follow the first layer and the polarity of the water molecules would increase. In the presence of specifically adsorbed ions, water molecules within the IHP would be displaced by ions. Figure 2 summarizes these EDL models. The Stern layer and the BDM model are widely accepted by the scientific community.

It is not easy to measure the surface potential of particles directly, but it can be approximated from zeta potential, ζ, as shown in Equation 9 in which d_s is the distance from the surface where the measurement is taken. This distance is generally taken as the shear plane and is taken as 0.5 nm for aqueous solutions [45].

$$\psi = \zeta \exp(\kappa d_s) \tag{9}$$

The interfacial layer thickness, κ^{-1}, known as the Debye length was derived from the Poisson-Boltzmann equation (PBE) by using the Gouy-Chapman model (Equation 10). In this model, the surface charge density and the dielectric constant of the medium within the double layer are assumed constant; the specific adsorption of ions and the surface charge variation on the particle surface are neglected; and the ion concentration within the interfacial layer is approximated as equal to the bulk concentration. In addition, the Debye-Hückel (DH) approximation ($|z\psi_0| \leq \frac{kT}{e} \approx 25$ mV) is used and the surface charge profile is approximated as an exponential decay. With these assumptions, the double layer thickness, κ^{-1}, is given by:

$$\kappa^{-1} = \sqrt{\frac{\varepsilon\varepsilon_0 k_B T}{2e^2 z^2 n_\infty}} = \sqrt{\frac{\varepsilon\varepsilon_0 k_B T}{2000 e^2 I}} \tag{10}$$

where the ionic strength, I, is given by:

`

$$I = \frac{1}{2}\sum c_i z_i^2 \tag{11}$$

where κ^{-1} is the double layer thickness; e is the charge of the electron; z is the valence of the ion; n_∞ is the bulk ion concentration; ε is the static dielectric constant of the medium; ε_0 is the permittivity of the free space; k_B is the Boltzmann constant; T is the temperature; and c_i is the molar concentration of ions in suspension. For 1:1 monovalent ions in water at room temperature, Equation 10 becomes

$$\kappa^{-1} = 0.034\sqrt{\frac{\varepsilon}{n_\infty}} \tag{12}$$

As two particles approach to each other, osmotic pressure increases because of the overlapping of double layers and leads to long range, electrostatic repulsive forces between particles. For concentrated suspensions, total electrostatic potential can be expressed with the Hogg, Healy, and Furstenau (HHF) equation [46]. The HHF equation involves linearization of the Poisson-Boltzmann equation and Derjaguin`s approximation which is valid for only small surface potentials (< 50 - 60 mV). It is also assumed that the thickness of the double layer and particle-particle separation is small compared to the size of the particles. HHF interaction potential is given in Equation 13, where κ^{-1} is the Debye length, and ψ is the surface potential.

$$E_{es} = \frac{\pi\varepsilon_r\varepsilon_0 a_1 a_2}{a_1 + a_2}[(\psi_1 + \psi_2)^2 ln[1 + exp(-\kappa h)] + [(\psi_1 - \psi_2)^2 ln[1 + exp(-\kappa h)] \tag{13}$$

DLVO Theory

The stability of colloidal systems is determined by the net interaction potential between particles, which the DLVO (Derjaguin and Landau, 1941; Verwey and Overbeek, 1948) theory represents as the summation of vdW and electrostatic potentials [23].

`

$$V_{net} = V_{vdW} + V_{elect} \tag{14}$$

By plotting the net interaction energy as a function of distance, the stability of the colloidal system can be estimated (Figure 3). The potential energy barrier, V_{max}, represents the maximum repulsive energy barrier between the particles. If the particles get closer than the separation distance corresponding to this energy barrier, they will be drawn toward one another to the primary minimum and aggregate unless the potential could not exceed by the energy provided by the Brownian motion. In some cases, a secondary minimum may appear, but these aggregates are very weak and easily disrupted.

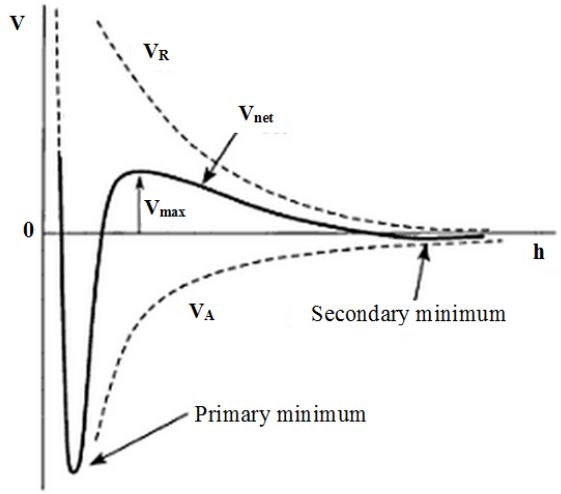

Figure 3: Net interaction energy curve [5].

The DLVO theory is vital for studying colloidal systems because it links the system forces to the total suspension properties; however, it is only the starting point for most systems because of restriction of the forces with vdW and electrostatic forces and oversimplification of the system parameters. Many papers in the literature suggest additional terms and modifications to the DLVO theory; however, none of these are able to describe the behavior of concentrated nanopowder suspensions satisfactorily, because they violate primary assumptions regarding vdW

and electrostatic forces made in the DLVO theory [47]. Currently, the DLVO theory can be used only qualitatively for nanopowder suspensions.

Development of Surface Particle Charge in Liquid Suspensions

The properties of the double layer are defined by the surface properties of the particles and the ion concentration of the suspensions. Therefore, the charging behavior of the particles is of importance in nanoparticle suspensions.

The surface chemistry of the ceramic particles typically controls the charging behavior because of the low solubility and high surface to volume ratio of the particles. Desorption of ions from the particle surface and preferential adsorption of specific additive or impurity ions are the common charging mechanisms on the surface.

Specific Adsorption/Desorption of Lattice Ions

This mechanism is usually seen in soluble, crystalline materials such as silver halides. In silver halide suspensions, some of the silver and iodide ions are dissolved and iodide ions are preferentially adsorbed to the crystal surface because of their effective chemical potential differences. As a result, the surface is negatively charged and some silver ions will be liberated into the solvent. Because the surface potential is strongly dependent on the lattice ion concentration in the solutions, these ions are called the “potential determining ions, or pdi’s”. At some concentration of ions, the surface potential can become neutral. This concentration is called the “iso electric point” (IEP).

If the ions do not involve in any interaction with surface is called “indifferent electrolyte”.Oxides with hydrated surface generally behave as constant potential surfaces with potential determining ions of hydroxyl (OH^-) and hydrogen (H^+). Although the hydrogen and

`

hydroxyl ions do not exactly fit the description of potential determining ions, they are still considered pdi's, because hydroxyl groups of oxide surfaces are able to regulate themselves by acquiring or losing protons at different pH levels (Equation 14[5, 6]).

$$M - OH_2^+ \overset{H^+}{\leftrightarrow} M - OH \overset{OH^-}{\longleftrightarrow} M - O^- \quad [14]$$

Therefore, the concentration of pdi's determines the surface potential. At lower pH values than the value corresponding to the IEP, the surface will be positively charged, while it will exhibit negative potential at higher pH values.

Specific Adsorption

When the charged species present in the system chemically adsorb on the particle surface, it is referred to as specific adsorption. Surfactants, polyelectrolytes, and polyvalent ions are common examples of specific adsorption and they are generally used to disperse colloidal particles because of the electrostatic repulsive forces they establish. Because the mechanism is related to electrostatic interactions and the charge concentration, it is highly sensitive to the ionic strength and the pH of the suspensions.

Solubility of the material liberates ions to the system. Different species formed at different pH values by hydration of these dissolved ions result in charging in the system. As an example, the aluminum ion, Al^{3+}, concentration change and aluminum bearing species formed as a function of suspension pH are given in Figure 4 and 5.

`

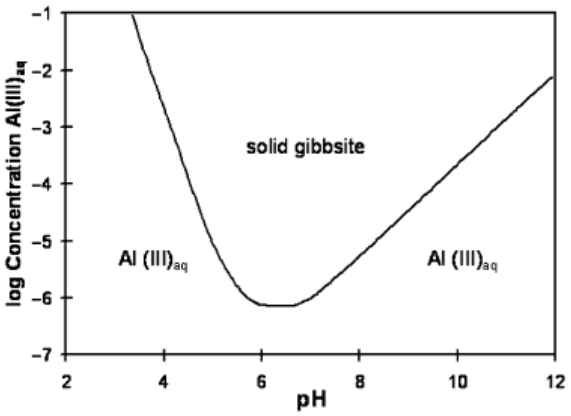

Figure 4: Solubility of $Al(OH)_3$ in water at 25 °C. The solid line indicates the maximum equilibrium solubility of Al^{3+} ions containing solution species[13].

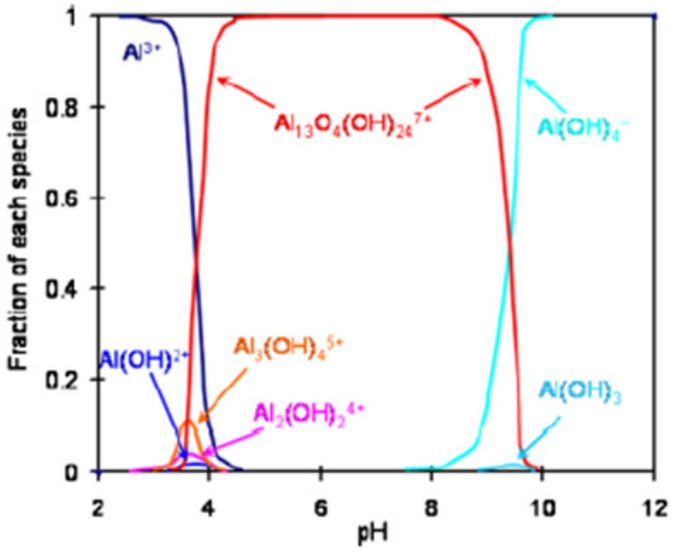

Figure 5: Fraction of solution species as a function of pH for 10^{-1} molal Al^{3+} at a total ionic strength of 1.0 molal in equilibrium with $Al(OH)_3$ at 25 °C [13].

Processing Additives

Processing additives are used in ceramic suspension systems to obtain homogeneously dispersed, stable and concentrated suspensions with reduced viscosities. They may be organic (polymers, surfactants, or other small molecules) or inorganic (such as pyrophosphates) and aim

`

to enhance and/or create the repulsive forces or restrict the attractive interactions by different mechanisms.

For oxides and/or particles with an oxide surface layer, the surface charge can be changed by adjusting the suspension pH. As going away from the IEP, the repulsive interactions are enhanced. By adding charged species that adsorb to the particles, such as surfactants, the effective surface charge can be changed, and thus the repulsive interactions can be tuned.

The use of organic molecules is also helpful in stabilizing the suspension via steric repulsion mechanisms. The soluble polymers, capable of adsorbing on the particle surface, introduce a polymeric layer between the particles and prevent the agglomeration of the particles. Because of the adsorption, the electrostatic properties of the particles may also change; in this case the combined mechanism is called electrosteric stabilization. The mechanism is based on adsorption, and therefore temperature, pH, and the concentration of the ionic species affect stabilization. For aqueous alumina suspensions, acrylic acid groups, including sodium or ammonium polyacrylates and methacrylates, are commonly used for neutral pHs [6, 13]. Oligo- or poly-saccharides (*e.g.*, dextrins, dextrans, maltodextrins) are also used as a dispersants for micron-sized ceramic particles in aqueous suspensions [19, 48-50].

When nanopowders are used, the theories mentioned previously need to be modified or replaced with entirely new theories. The organic polymers used as dispersants in conventional ceramic powder systems do not work well with nano-scale powders. The polysaccharides, for example, significantly reduce the viscosity of micron-size alumina suspensions, while resulting in an increase in viscosity for alumina nanopowder suspensions [51] whereas low molecular weight saccharides significantly reduce the viscosity of the same system [16-21, 51-53]. To understand the viscosity reduction mechanism, smaller but similar organic dispersants were

`

studied [16, 20, 50, 51]; the changes in the system parameters such as water mobility and the available water content were also studied [17, 18]; however, fundamental and complete understanding of the mechanisms is still lacking.

The electrostatic properties of nanopowder suspensions have also been studied by several groups, and attempts have been made to explain the deviations from the behavior exhibited by larger particle suspensions [13, 54-56]. Jailini *et al*. [55], for example, studied the effects of electrolyte concentration, particle size and volume fraction on zeta potential of nanopowder suspensions by using γ and α-alumina powders with average particle diameters of 11, 44, and 190 nm. They showed that the zeta potential decreased with particle size and the volume fraction of the suspensions. The increase in electrolyte concentration resulting from dissociation of ionizable surface sites on the alumina and soluble species resulting from the dissolution of alumina were offered as a possible reason.

Nanopowder Suspensions and Bound Water

Upon heating of frozen alumina nanopowder suspensions water shows two separate melting events in contrast to a single melting event observed for pure water. This interesting behavior was first observed by our group and the melting event which differs from the bulk water is called "bound water" [17, 18]. Low temperature differential scanning calorimetry, LT-DSC, thermogravimetry (TGA) and nuclear magnetic resonance (NMR) spectroscopy were used to differentiate the nature of the water associated with alumina nanopowders.

Li and Akinc reported that three types of water are present in alumina nanopowder systems: free water, physically bound water, and chemically bound water [17]. Chemically bound water was found to account for 1.1 wt.% of the powder, while the thickness of physically bound water

`

varied with solids content from 3 nm to 6 nm. The increase in solids content (> 0.30) led to an overlapping of bound water layers and resulted in a dramatic increase in viscosity. They also showed that the bound water can be modified by adding fructose. Rheological and NMR relaxation measurements indicated that the bound water layers exhibited lower molecular mobility. The introduction of fructose to the system increased the average mobility of the water molecules. It was suggested that fructose molecules release some of the bound water from the surface, increasing the availability of liquid for flow, and thus decrease the viscosity of alumina nanopowder suspensions.

Falkowski *et al*. [16] studied the effect of fructose derivatives on viscosity of alumina nanopowder suspensions. They suggest that compatibility of the additive molecule with three dimensional hydrogen structure of water affects the suspension viscosity supporting the theory suggested by Li *et al* [17, 18].

We believe that understanding the bound water mechanism and quantifying the change in melting behavior using DSC analysis will help in explaining the rheological behavior of nanopowder suspensions. Additionally, because of the high surface area, charging mechanisms of the alumina in aqueous suspensions, pH and ionic strength, will provide significant information to understand the surface properties of powders and the interparticle interactions. Use of alternative additives and extrapolation of findings to other oxide systems will expand our understanding of bound water and suspension viscosity, and make us able to generalize the conclusions.

`

References

[1] Ghadimi A, Saidur R, Metselaar HSC. A review of nanofluid stability properties and characterization in stationary conditions. Int J Heat Mass Transfer 2011; 54: 4051-68.

[2] Mahbubul IM, Saidur R, Amalina MA. Latest developments on the viscosity of nanofluids. Int J Heat Mass Transfer 2012; 55: 874-85.

[3] Singh P, Anoop K, Patel H, Sundararajan T, Pradeep T, Das S. Anomalous Size Dependent Rheological Behavior of Alumina Based Nanofluids. Int J Micro-Nano Scale 2010; 1: 179-88.

[4] Wang T, Wang X, Luo Z, Ni M, Cen K. Mechanisms of Viscosity Increase for Nanocolloidal Dispersions. J Nanosci Nanotechno 2011; 11: 3141-50.

[5] Berg JC. An introduction to interfaces & colloids: the bridge to nanoscience. World Scientific; 2009.

[6] Reed JS. Principles of ceramics processing. Wiley & Sons; 1995.

[7] Hidehiro K, Motoyuki I. Surface modification and characterization for dispersion stability of inorganic nanometer-scaled particles in liquid media. Science and Technology of Advanced Materials 2010; 11: 044304.

[8] Dörre E, Hübner H. Alumina: processing, properties, and applications. Springer; 1984.

[9] Gitzen WH. Alumina as a ceramic material. American Ceramic Society; 1970.

[10] Pohland HH. Aluminum oxide: production, properties, applications. Verl. Moderne Industrie; 1999.

[11] Bergstroem L, Blomberg E, Guldberg-Pedersen H. Interparticle forces and rheological properties of ceramic suspensions. Key Eng Mater 1999; 159-160: 119-26.

[12] Biesheuvel PM, Lange FF. Application of the Charge Regulation Model to the Colloidal Processing of Ceramics. Langmuir 2001; 17: 3557-62.

[13] Franks GV, Gan Y. Charging Behavior at the Alumina–Water Interface and Implications for Ceramic Processing. J Am Ceram Soc 2007; 90: 3373-88.

[14] Johnson SB, Franks GV, Scales PJ, Boger DV, Healy TW. Surface chemistry–rheology relationships in concentrated mineral suspensions. Int J Miner Process 2000; 58: 267-304.

[15] Lewis JA. Colloidal processing of ceramics. J Am Ceram Soc 2000; 83: 2341-59.

`

[16] Falkowski P, Bednarek P, Danelska A, Mizerski T, Szafran M. Application of monosaccharides derivatives in colloidal processing of aluminum oxide. J Eur Ceram Soc 2010; 30: 2805-11.

[17] Li C, Akinc M. Role of Bound Water on the Viscosity of Nanometric Alumina Suspensions. J Am Ceram Soc 2005; 88: 1448-54.

[18] Li C, Akinc M, Wiench J, Pruski M, Schilling CH. Relationship Between Water Mobility and Viscosity of Nanometric Alumina Suspensions. J Am Ceram Soc 2005; 88: 2762-8.

[19] Schilling CH, Sikora M, Tomasik P, Li C, Garcia V. Rheology of alumina–nanoparticle suspensions: effects of lower saccharides and sugar alcohols. J Eur Ceram Soc 2002; 22: 917-21.

[20] Yar Y, Acar FY, Yurtsever E, Akinc M. Reduction of Viscosity of Alumina Nanopowder Aqueous Suspensions by the Addition of Polyalcohols and Saccharides. J Am Ceram Soc 2010; 93: 2630-6.

[21] Singh K, Mohan S. Kinetic studies of the sucrose adsorption onto an alumina interface. Appl Surf Sci 2004; 221: 308-18.

[22] Krieger IM. Rheology Principles, Measurements, and Applications. J Colloid Interface Sci 1996; 178: 382.

[23] Larson RG. The structure and rheology of complex fluids. Oxford University Press; 1999.

[24] Hiemenz PC, Rajagopalan R. Principles of colloid and surface chemistry. Marcel Dekker; 1997.

[25] Starov V, Zhdanov V, Meireles M, Molle C. Viscosity of concentrated suspensions: influence of cluster formation. Adv Colloid Interface Sci 2002; 96: 279-93.

[26] Liu D-M. Particle packing and rheological property of highly-concentrated ceramic suspensions: φm determination and viscosity prediction. J Mater Sci 2000; 35: 5503-7.

[27] Horri BA, Ranganathan P, Selomulya C, Wang H. A new empirical viscosity model for ceramic suspensions. Chem Eng Sci 2011; 66: 2798-806.

[28] Ruiz-Reina E, Carrique F. Electroviscous Effect of Concentrated Colloidal Suspensions in Salt-Free Solutions. J Phys Chem C 2007; 111: 141-8.

[29] Ogawa A, Yamada H, Matsuda S, Okajima K, Doi M. Viscosity equation for concentrated suspensions of charged colloidal particles. J Rheol 1997; 41: 769-85.

[30] Tadros T. Interparticle interactions in concentrated suspensions and their bulk (Rheological) properties. Adv Colloid Interface Sci 2011; 168: 263-77.

`

[31] Pugh RJ, Bergström L. Surface and colloid chemistry in advanced ceramics processing. M. Dekker; 1994.

[32] Rahaman MN. Ceramic processing and sintering. M. Dekker; 2003.

[33] Tadros T. Viscoelastic properties of solid-liquid dispersions. ACS Symp. Ser. 2004; 878: 167-83.

[34] Barnes HA. A handbook of elementary rheology. University of Wales, Institute of Non-Newtonian Fluid Mechanics; 2000.

[35] Genovese DB. Shear rheology of hard-sphere, dispersed, and aggregated suspensions, and filler-matrix composites. Adv Colloid Interface Sci 2012; 171–172: 1-16.

[36] Hiemenz PC, Rajagopalan R. Principles of Colloid and Surface Chemistry, Third Edition, Revised and Expanded. Taylor & Francis; 1997.

[37] Jamali S, Yamanoi M, Maia J. Bridging the gap between microstructure and macroscopic behavior of monodisperse and bimodal colloidal suspensions. Soft Matter 2013; 9: 1506-15.

[38] Xu X, Rice SA, Dinner AR. Relation between ordering and shear thinning in colloidal suspensions. Proc Natl Acad Sci 2013; 110: 3771-6.

[39] Rubio-Hernández FJ, Ayúcar-Rubio MF, Velázquez-Navarro JF, Galindo-Rosales FJ. Intrinsic viscosity of SiO2, Al2O3 and TiO2 aqueous suspensions. J Colloid Interface Sci 2006; 298: 967-72.

[40] Rao Y. Nanofluids: Stability, phase diagram, rheology and applications. Particuology 2010; 8: 549-55.

[41] Wang X-Q, Mujumdar AS. A review on nanofluids - part I: theoretical and numerical investigations. Braz J Chem Eng 2008; 25: 613-30.

[42] Gregory J. Approximate expressions for retarded van der waals interaction. J. Colloid Interface Sci. 1981; 83: 138-45.

[43] Akle BJ. Characterization and modeling of the ionomer-conductor interface in inoc polymer transducers. 2005.

[44] Bockris JOM, Devanathan MAV, Mueller K. The structure of charged interfaces. Proc Phys Soc London Sect A 1963; 274: 55-79.

[45] Aschauer U, Burgos-Montes O, Moreno R, Bowen P. Hamaker 2: A Toolkit for the Calculation of Particle Interactions and Suspension Stability and its Application to Mullite Synthesis by Colloidal Methods. J. Dispersion Sci. Technol. 2011; 32: 470-9.

`

[46] Hogg R, Healy TW, Fuerstenau DW. Mutual coagulation of colloidal dispersions. J. Chem. Soc. Faraday Trans. 1966; 62: 1638-51.

[47] Israelachvili JN. Intermolecular And Surface Forces. 3. Saint Louis, MO, USA: Academic Press; 2011.

[48] Schilling CH, Bellman RA, Smith RM, Goel H. Plasticizing aqueous suspensions of concentrated alumina with maltodextrin sugar. J Am Ceram Soc 1999; 82: 57-66.

[49] Sikora M, Schilling CH, Tomasik P, Li C. Dextrin plasticizers for aqueous colloidal processing of alumina. J Eur Ceram Soc 2002; 22: 625-8.

[50] Tomasik P, Schilling CH, Jankowiak R, Kim J-C. The role of organic dispersants in aqueous alumina suspensions. J Eur Ceram Soc 2003; 23: 913-9.

[51] Schilling CH, Li C, Tomasik P, Kim J-C. The rheology of alumina suspensions: influence of polysaccharides. J Eur Ceram Soc 2002; 22: 923-31.

[52] Pradhan M, Bhargava P. Influence of Sucrose Addition on Rheology of Alumina Slurries Dispersed with a Polyacrylate Dispersant. J Am Ceram Soc 2005; 88: 833-8.

[53] Singh K, Mohan S. Adsorption behavior of selected monosaccharides onto an alumina interface. J Colloid Interface Sci 2004; 270: 21-8.

[54] Boström M, Deniz V, Franks GV, Ninham BW. Extended DLVO theory: Electrostatic and non-electrostatic forces in oxide suspensions. Adv Colloid Interface Sci 2006; 123-126: 5-15.

[55] Jailani S, Franks GV, Healy TW. ζ Potential of Nanoparticle Suspensions: Effect of Electrolyte Concentration, Particle Size, and Volume Fraction. J Am Ceram Soc 2008; 91: 1141-7.

[56] Zhou Z, Solomon MJ, Scales PJ, Boger DV. The yield stress of concentrated flocculated suspensions of size distributed particles. J Rheol 1999; 43: 651-71.

`

CHAPTER II. ELUCIDATION OF VISCOSITY REDUCTION MECHANISM OF NANO ALUMINA SUSPENSIONS WITH FRUCTOSE ADDITIONS BY DSC

(A paper published in the Journal of American Ceramic Society)

Simge Çınar, Laura van Steenhuyse, Mufit Akinc

Department of Materials Science and Engineering,

Iowa State University, Ames, Iowa 50011

Abstract

Control of the rheological properties of the nanoparticle suspensions is challenging. In this study influence of the solids content and the fructose addition on the viscosity of nano alumina suspensions have been investigated by low temperature differential scanning calorimetry (LT-DSC), rheometry, and zeta potential measurements. Analysis of the water melting events in LT-DSC revealed useful information for explaining the rheological behavior of the nanoparticle suspensions. It was shown that the bound water layer has a negligible effect on the viscosity of micrometer-size particle suspension while it increases the effective solid content of alumina nanoparticle suspensions significantly leading to high viscosities. The presence of fructose modifies the bound water layer, decreases the effective solids content, hence resulting in viscosity reduction. Fructose addition lowers the pH of the suspension, but has a negligible effect on the zeta potential. The origin of the bound water, and electrostatic and steric effects of the fructose addition on the viscosity are discussed.

`

Introduction

Control of the rheological behavior of powder suspensions is vital in colloidal processing, not only for easy handling but also to achieve optimum microstructure in the final product[1]. Optimum microstructures can be obtained when highly loaded, homogeneously dispersed and stable suspensions with reasonable viscosities are employed. The flow properties of the ceramic suspensions can be controlled via the electrostatic or steric stabilization mechanisms. However, control of viscosity in nanoparticle suspensions is challenging.

Johnson et al[2] reviewed the relationship between surface chemistry and rheology of the suspensions in detail. The viscosity was seen to increase powder with decreasing particle size; however, it was noted that this phenomenon has yet to be fully understood. Jailani et al[3] reported the zeta potential of alumina nanoparticle suspensions with different electrolyte concentration, particle size, and volume fraction. They concluded that the electrostatic stabilization alone does not fully explain high viscosity observed in concentrated nanoparticle suspensions. They claim the increase in available surface leads to an increase in ionizable alumina surface sites resulting in high concentration of soluble species in the suspensions. Lu[4] showed that van der Waals attractive forces are dominant in the alumina nanoparticle suspensions and the magnitude of the electrostatic repulsion is not sufficient to overcome the attractive forces. Therefore, Lu recommended steric stabilization for nanoparticle suspensions. Franks and Gan5 also suggested the use of a more robust steric repulsion for stabilization of nano oxide suspensions, and they showed that suspensions with chemically adsorbed molecules have higher stability during processing.

When the common dispersants used for steric stabilization of micrometer-sized particle suspensions are employed in nano-sized particle suspensions, several problems arise. First, as

`

available surface is much higher in a nanoparticle suspension, a larger quantity of additive is required to cover the particle surfaces. As this adlayer polymer associates with the particle surface, the effective solids content increases in proportion to the thickness of the layer and limits the maximum achievable solids content. When polyacrylic acids are used, a decrease in viscosity of the suspensions has been reported[4,6], but the maximum achievable solids content is limited to 30–40 vol%. On the other hand, when dispersants like oligo- or polysaccharides (e.g., dextrins, dextrans, maltodextrins) are used, the viscosity increases[7–9]. Schilling et al[10] showed that low molecular weight polysaccharides reduce the viscosity of submicrometer particle (0.4 lm) suspensions while the high molecular weight saccharides (>2000 kDa) result in an increase. This was attributed to the small separation distances between particles in submicrometer particle systems.

Several attempts have been made to explain the mechanism of viscosity reduction in ceramic suspensions by various additives. Tomasik et al[11] used 23 different low molecular weight additives like tetraalkylammonium hydroxides, tetraalkylammonium chlorides, phenols, and carboxylic acids to assess their effectiveness in reducing the viscosity of submicrometer (0.4 μm) alumina suspensions. They suggested that the electrostatic interactions have the most dominant effect due to a change in pH of the suspensions with the addition of these additives. However, for the nondissociating macromolecules, adsorption of these molecules on the particle surface was suggested as the viscosity reduction mechanism. The adsorption of monosaccharides on the alumina surface was also reported by Singh and Mohan[12,13]. Falkowski et al[14] showed that neither shift in the isoelectric point nor significant change in zeta potential of alumina is observed with the addition of fructose, glucose and their derivatives with carboxylic group attachments. Therefore, although the low molecular weight saccharides adsorb on the alumina

`

surface, the viscosity reduction in alumina nano suspensions cannot be explained entirely by electrostatic or steric stabilization mechanisms.

Li and Akinc[15,16] used nuclear magnetic resonance measurements to explain the effect of monosaccharides, specifically fructose, on the viscosity reduction in nano alumina suspensions and introduced the term of "water availability" and its effect on viscosity of the concentrated alumina nanoparticle suspensions. They observed a significant increase in the average water mobility with the addition of fructose to the alumina suspensions. They also observed the appearance of a second water melting event when heating frozen alumina nanoparticle suspensions by differential scanning calorimetry (DSC). This second peak was attributed to the melting of bound water. It was suggested that the addition of fructose releases (or changes the nature of) the bound water on the surface and results in a decrease in the viscosity.

However, the definition of bound water is still ambiguous and the viscosity reduction mechanism by low molecular weight saccharides or similar chemicals is still a topic of considerable debate. These concepts invoke a need for a better understanding of the rheological behavior of concentrated nanoparticle suspensions and its control. In this article, the effects of particle size, solids content, concentration of fructose, and indifferent electrolytes on the melting behavior of water in frozen alumina suspensions were investigated by DSC, rheometry, and zeta potential measurements. Fructose and nano alumina powder were chosen as model materials for the low molecular weight saccharide and the nano oxide particle system, respectively.

`

Experimental Procedure

Materials

Two types of alumina powders were used in this study. The micrometer size powder (Premalox 0.3 DA; Ocean State Abrasives Inc., RI) consisted of high purity (≥ 99.99%), deagglomerated and calcined α-alumina ($\rho \approx 3.98$ g/cm^3) particles with an average particle size of 0.3 lm. The nano alumina powder (with a phase distribution of $\gamma/\delta \approx 70:30$, brunauer-emmet-teller (BET) specific surface area of 36 m^2/g, density of 3.67 g/cm^3, purity ≥ 99.5%) were obtained from the Nanophase Technology Corporation (Burr Ridge, IL). Figure 1 shows a transmission electron micrograph of the nanopowders used in this study. In general, particles are spherical showing a considerable size distribution ranging from about 10 to over 100 nm with an average particle size of about 45 nm. Sharp boundaries on overlapping particles indicate that the particles are not agglomerated. Ultrapure water with resistivity of 18.2 MΩ cm and total organic content (TOC) < 5 ppm (Milli-Q Gradient A-10 model of Millipore Company, Billerica, MA) was used to prepare the suspensions. D-(L)-fructose (99% purity; Sigma Aldrich, St. Louis, MO) and sodium chloride (99.99% purity; Alfa Aesar, Ward Hill, MA) were used as additives. Density of fructose was taken as 1.6 g/cm^3.

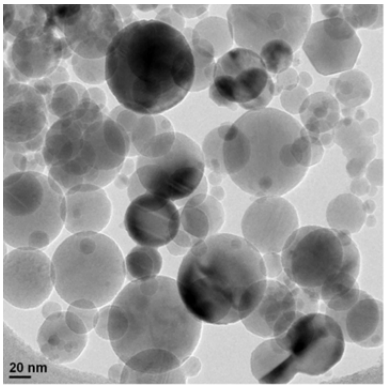

Figure 1: Transmission electron micrograph of alumina nanopowder.

`

Suspension Preparation

For the preparation of suspensions, the alumina powder content was calculated as a volume fraction of the suspension. The fraction of the fructose was calculated as a weight percentage of the alumina powder and the volume of fructose was taken into account while calculating the required volume of water. The samples were labeled as "xxAlyyF" where xx represents the volume percent of the alumina in the suspension and yy represents fructose content expressed as the weight percent of the alumina. As such, 20Al04F represents 20 vol% alumina suspension that contains 4% fructose based on dry mass of alumina. For instance, to prepare 100 mL of this particular suspension, 73.4 g (20 mL 9 3.67 g/cm^3 =73.4 g) nano alumina powder (which was dried at 110 °C for 2 h prior to weighing), and 7.34 g fructose (10 wt% of alumina) were weighed separately. Fructose was then added to the sufficient amount of ultrapure water (80 mL - (7.34 g per 1.6 g/cm^3) = 75.4 mL H_2O) to make 80 mL of fructose solution to which the alumina powder is then added slowly. Suspensions were shaken for 24 h prior to analysis to establish chemical and physical equilibrium. For ionic strength experiments, a predetermined amount of NaCl, taking account for the total solution volume, was added to the suspension 2 h before the testing.

In determining the electrolyte concentration, all the added water was assumed to be "free water". As the NaCl additions were too small, their effect on the total volume was neglected. For each experiment, a 20 mL suspension was prepared.

Rheology

A rheometer (Model AR 2000ex, TA Instruments, New Castle, DE) with 40 mm steel cone and plate geometry having a 4° cone angle was used for viscosity measurements. A solvent trap was used to prevent water evaporation. During the measurements, 10 points per decade of each

`

half loop of three consecutive complete loops in the shear rate ramping up (0.5-500s^{-1}) and down (500-0.5s^{-1}) were recorded at 25.0 ± 0.1 °C. The measurements were generally reproducible after the 1st loop and the data points corresponding to final half loop were used in data analysis.

In order to express the rheological behavior of the suspensions, Herschel-Bulkley model (power law) has been used (Equation 1) throughout the study.

$$\eta = K\dot{\gamma}^{n-1} \quad (1)$$

In the above equation, η is the viscosity of the suspension, $\dot{\gamma}$ is the shear rate, K is the consistency coefficient and n is the power law (or rate) index. Consistency coefficient, *K*, corresponds to viscosity of the fluid at a shear rate of 1 s^{-1} whereas the rate index, *n*, describes the flow behavior. The value of n is a measure of shear thinning. The suspension shows strong shear thinning behavior as $1 - n$ approaches one. For $1 - n = 0$, viscosity does not show any dependency on shear rate, so suspension show Newtonian behavior. The measurements recorded in the present study were found to obey the power law within the limits of experimental error.

Differential Scanning Calorimetry

To elucidate the association of water with the particles and quantify the amount of water interacting with the particle surface from that of bulk water, low temperature differential scanning calorimetry (LT-DSC) was employed. Nanoparticle suspensions were cooled below the freezing point of water before heating to study the melting behavior of the water. For these experiments, a DSC (Model Q20; TA Instruments, New Castle, DE) fitted with an RCS 40 cooling unit was employed. The DSC samples with similar water content (around 5–10 mg) were prepared and tested in hermetically sealed aluminum pans. The samples were cooled down to -25 °C, held at that temperature for 1 min and the temperature was then increased to 10 °C at a eating rate of 1 °C/min.

`

The area under the melting curve was deconvoluted using TA Universal Analysis software to calculate the energy absorbed during each melting event. Since the melting events spread over a broad temperature range, a linear baseline is used for deconvolution. The melting temperatures were also estimated using TA Universal Analysis software.

Zeta Potential Measurements

Zeta potential measurements were conducted on Zetasizer Nano ZS90 (Malvern Instruments, Worcestershire, UK). Alumina suspensions prepared as described above were diluted until the concentration of the alumina particles was 200 ppm by deionized water. NaCl was added to keep the ionic strength of the solutions constant and equal to 0.001 M. The pH of the suspensions was varied between 3 and 11 using 0.1 M HCl or NaOH solution.

Results and Discussion

Melting Behavior of Water

A single melting event around 0 °C was observed in the DSC experiment for pure water (Fig. 2, trace a). With the addition of 0.3 micrometer alumina particles, a shoulder appeared before the major melting event (Fig. 2, trace b). However, for nanosize powder suspensions, the second event became more prominent and emerged as separate from the free water peak (Fig. 2, trace c). This second event was designated as the “bound water” peak as it is believed to occur due to interaction of water with the alumina surface[15]. The lower melting temperature observed for the bound water may be attributed to the restricted motion and lower entropy due to its association with the particle surface.

It is interesting to note the similarity between the free water melting peaks in Fig. 2. Furthermore, when the bound water peak is separated from the free water, as in nano alumina

`

suspension (trace c), the onset of free water peak for nano alumina suspensions and pure water coincides.

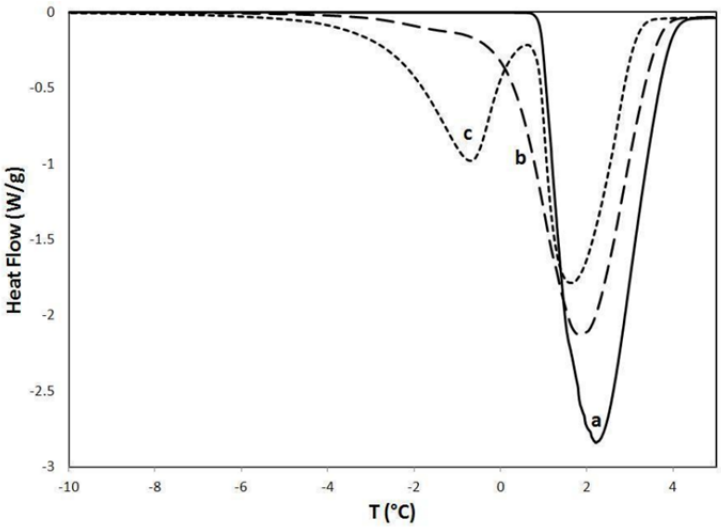

Figure 2: DSC curves for pure water (a), micrometer size (b), and nano size alumina (c) suspension with a solids content of 0.30.

Table 1: Effect of the particle size on the melting temperature and volume fraction of free and bound water as calculated from the LT-DSC data.

	$T_{m,FW}$ (°C)	$T_{m,BW}$ (°C)	$\Delta H_{f,FW}$ (J/g)	$\Delta H_{f,BW}$ (J/g)	w_{FW}	w_{BW}
Pure water	0.94	-	310	-	1.00	0.00
Φ: 0.30, D : 0.3 µm	0.15	-3.64	310	*	*	*
Φ: 0.30, D ≈ 45 nm	0.85	-3.35	310	230	0.55	0.45

T_m, ΔH_f and w represent melting temperature, heat of fusion and weight fraction, respectively. Subscripts FW and BW stand for free and bound water, respectively.

** Bound water peaks are very small and ill-defined. The content of the bound water cannot be reasonably calculated.*

To calculate the relative amounts of water associated with each event, the curves were deconvoluted [Eq. (2)]. The heat of fusion for free water is estimated by dividing the area under the peak for pure water (trace a) by the sample mass and found to be 310 J/g [Eq. (3)]. The deviation from the literature value of 333.6 J/g is about 24 J/g and corresponding to an error of 7%. Heat of fusion values estimated by DSC were consistently lower than the literature values

`

and may be attributed to the nonequilibrium (kinetic) nature of the DSC analysis. The values estimated by DSC in this report should be considered accurate to about ± 10%. The free water content (m_{FW}) of nano alumina suspensions was estimated using the value of $\Delta H_{f,\,FW}$ = 310 J/g for heat of fusion of water [Eq. (3)]. The amount of bound water was estimated from the total water content of the sample (m_{sample}) and free water amount [Eq. (4)]. The heat of fusion value for the bound water was obtained by dividing the heat associated with the second event by the amount of bound water [Eq. (5)].

$$Q_{total} = Q_{FW} + Q_{BW} \tag{2}$$

$$m_{FW} = Q_{FW} / \Delta H_{f,FW} \tag{3}$$

$$m_{BW} = m_{sample} - m_{FW} \tag{4}$$

$$\Delta H_{f,BW} = Q_{BW} / m_{BW} \tag{5}$$

where Q_{FW}, and Q_{BW} represent heat absorbed for free and bound water, and mi and $\Delta H_{f,i}$ represent the mass and heat of fusion for component i, respectively. Because of the similar melting temperatures of free water in Fig. 2, the heat of fusion values can also be assumed constant among the samples with varying solids content, if the entropy change (structural change in water due to the presence of alumina particles) is neglected for the reported melting events. By using the heat of fusion values for each event calculated from pure water and nano-sized particle suspension data, the relative amounts of free and bound water were calculated. The results have been tabulated in Table I. Bound water content for micrometer size particles could not be calculated due to ill-defined and small bound water peak. The higher bound water content for nanoparticles is expected because of nearly an order of magnitude higher specific surface area.

`

Effect of Solids Content

Figures 3 (a) and (b) show the viscosity of the alumina suspensions with different solids content and power law parameters, respectively. As seen in both figures, as the solids content increases the viscosity increases, the suspension becomes more shear thinning.

Figure 4 shows the bound water peak increases with solids content. As seen in the figure, the onset of the bound water melting shifts slightly to lower temperatures, but extrapolation

of the melting peak to the baseline results in more or less constant onset value for all samples except $\Phi = 0.50$, and was estimated to be -3.1 °C ± 0.1 °C and 0.8 °C ± 0.1 °C for bound and free water, respectively. Free water peaks show similar features except solids content, $\Phi = 0.50$. The high solids content sample has very small quantity of free water.

By using the method described in the previous section, heat of fusion of bound water and the relative amounts of bound and free water were calculated for each sample. The data for the lowest and highest alumina concentrations, Φ: 0.02, 0.05, and 0.50, were not included in the calculations because of the high error margin in deconvolution of small peaks. The average heat of fusion value for bound water was estimated to be 228 ± 8 J/g. The lower heat of fusion for the bound water relative to free water implies that entropy changes associated with bound water melting is lower than that of free water.

`

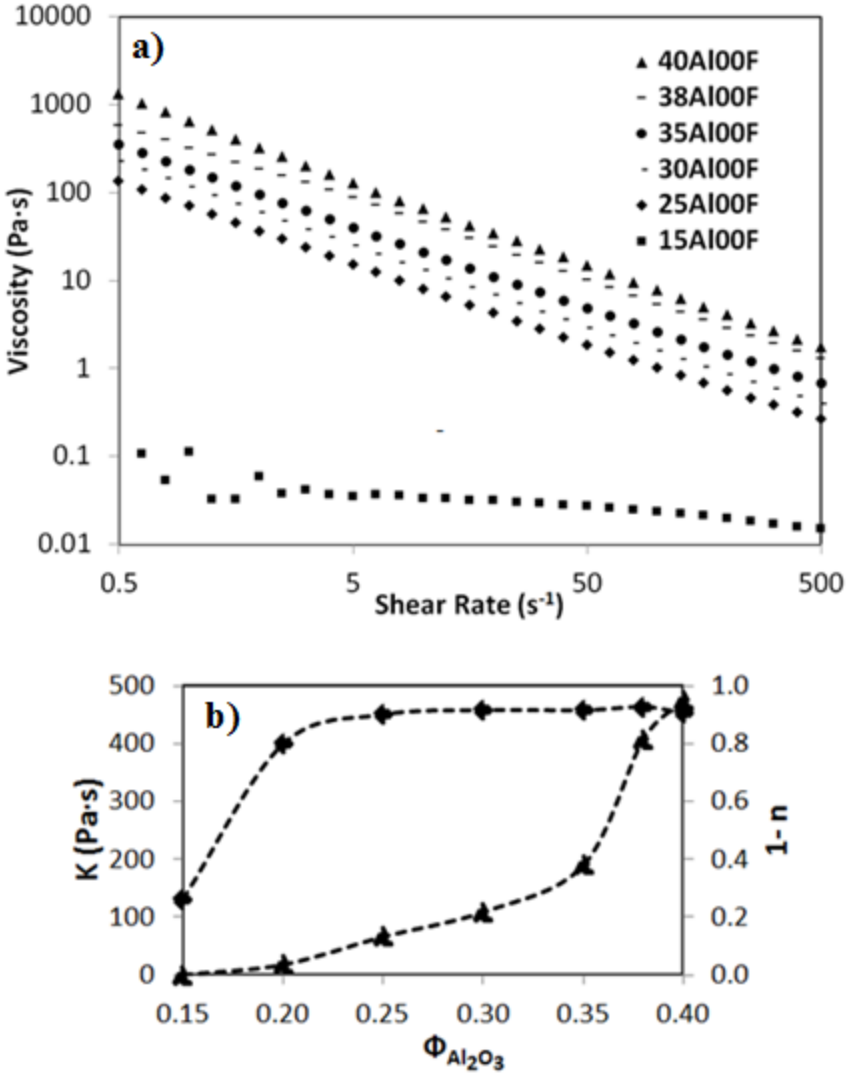

Figure 3: (a) Viscosity of the suspensions, and (b) change in power law parameters, consistency coefficient, K (▲), rate index, 1 - n (♦), with different solids content of alumina nanopowder.

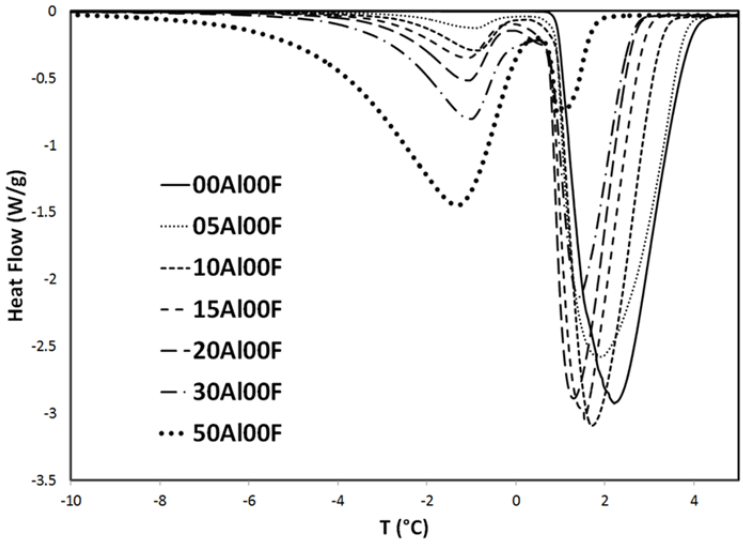

Figure 4: LT-DSC curves for melting of water in frozen alumina nanopowder suspensions as a function of alumina solids content. (The curves were normalized for total water content). 'xxAl' stands for xx volume percent of alumina content.

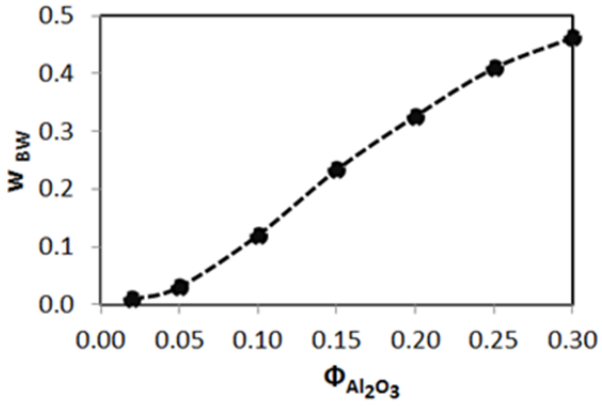

Figure 5: Change in bound water fraction with solids content of alumina nanopowder.

The bound water content as estimated by deconvolution of the DSC curves are plotted in Fig. 5. As expected, with the increase in alumina content (and therefore the surface area), the fraction of the bound water increases. However, while the increase in the fraction of bound water is monotonic, the increase in the corresponding consistency coefficient, K, (a term analogous to

`

viscosity) is much steeper as shown in Fig. 3, similar to the behavior predicted by Krieger-Dougherty relationship[17]. This behavior may be explained by the fact that beyond a certain solids loading, the particle–particle interactions play a more dominant role.

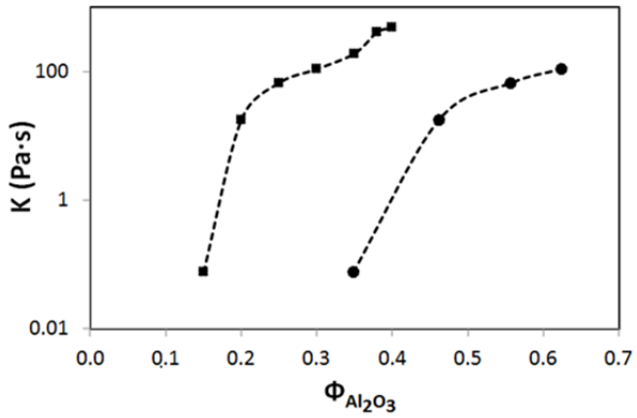

Figure 6: Effect of the bound water on the viscosity as a function of solids content (■) and effective solids content (●).

Effective solids content, $\Phi_{effective}$, may be estimated from the following equation:

$$\Delta G = \Delta H - T \cdot \Delta S \qquad (6)$$

by using the bound water fractions estimated from the DSC curves, the effective solids content of the suspensions were calculated and plotted against the consistency coefficient, K, as shown in Fig. 6. As the bound water cannot serve as a carrier for the suspension, the effective solids content in the suspension increases, and that of the liquid decreases resulting in more viscous suspensions. It should be noted that because of the unknown structure of bound water on the particle surface (or occluded within flocs), the estimated effective solids content should be considered approximate.

`

Bound Water

Chemically bound water, electrical double layer, hydration layer, and the water trapped in pores are all likely to contribute to the bound water layer discussed above.

The chemically bound water layer is the water molecules which are directly bound to the alumina surface. This layer is composed of a few water molecules in thickness which has been measured to be around 1 nm[18–26] corresponding to around 1.1 wt% of powder for 45 nm diameter particles. The chemically bound water layer is commonly referred to as "unfreezable water" as it melts at temperatures lower than - 20°C[27]. When the estimated weight fractions and melting temperatures of bound water were considered, chemically bound water does not explain the bound water curves observed in this study.

If the bound water is primarily due to the electrical double layer around the particles, we would expect the second peak in the DSC melting event to decrease and eventually diminish with an increase in indifferent electrolyte additions (i.e., NaCl) as the double layer thickness is ompressed. However, the increase in ionic strength does not diminish the bound water content (Fig. 7). On the contrary, the free water curves are shifted to lower temperatures with increasing NaCl concentration, as expected from freezing point depression. Therefore, the bound water melting peaks observed in the DSC plots cannot be explained by the electrical double layer.

`

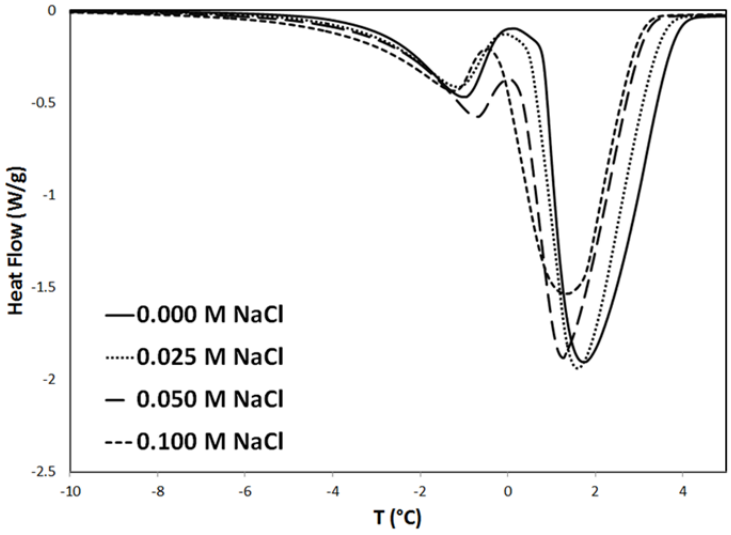

Figure 7: DSC curves for 20 vol% aqueous alumina suspensions with respect to the sodium chloride, NaCl, concentration.

Water in small pores melts at lower temperatures than bulk water as expressed by Gibbs Thompson relation [28]. Rennie and Clifford[29], and Ishikiriyama et al[30] studied the melting of ice in porous solids using DSC and reported that lower melting temperatures are observed for smaller pores. Melting points observed in our LT-DSC runs correspond to much larger pore sizes than we would expect for our suspensions.

The short range repulsive forces between the approaching surfaces, called hydration layer forces, result in the formation of a hydration layer around the particles. The properties of this hydration layer differ significantly from bulk water. The thickness, in which these forces are effective, measured around 2–3 nm for various systems[20,22,23,25,26]. The decay length of the hydration forces was reported to range from the 0.2 to 1.4 nm[21]. Although the exact origin of the hydration forces is not known, Butt et al[21] stated that they are the water–water molecular interactions unlike the chemically bound water layers which originate from the interaction between the particle surface and the water molecules. Guriyanova et al[31] recently showed by atomic force microscopy (AFM) force measurements that the short range repulsive forces, i.e.,

hydration forces, are effective up to 5 nm and different from the Derjaguin Verwey Landau Overbeek (DLVO) forces which extend to longer distances. Furthermore, at high ion concentrations such as in the presence of NaCl salts, the DLVO forces are screened, but repulsive hydration forces areretained similar to our observations in this study.

Based on the depression in the melting temperature and the fractions of water calculated from LT-DSC analysis, the bound water seems likely to represent the hydration layer. Regardless of its origin, bound water increases the effective solids content and results in high viscosities in nano alumina suspensions.

Effect of Fructose Concentration

In the absence of alumina, aqueous fructose solutions exhibit a single melting event in LT-DSC plots as shown in Fig. 8. Absence of a second peak for these samples is another confirmation that the second melting event in alumina suspensions is due to alumina–water interactions. The melting peaks shift to lower temperatures and become more asymmetric as fructose concentrations increase. The estimated melting temperatures and average heat of fusion values are given in Table II. The decrease in heat of fusion as well as the onset of lower melting temperature is due to fructose–water molecular interaction and is in agreement with the experimental and computational saccharide aqueous solutions[32].

`

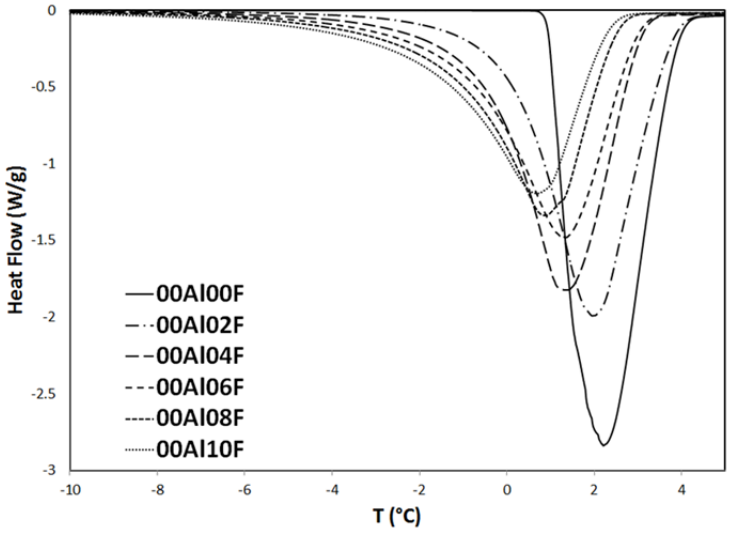

Figure 8: DSC curves for aqueous fructose solutions (corrected for total water content). 'xxF' stands for xx weight percent of fructose. The concentration of fructose examined aqueous solution is the same as in the 20 vol% aqueous alumina suspensions.

Table 2: Melting points and heat of fusion of fructose solutions as determined from LT-DSC experiments.

Fructose conc. %	T_m (°C) (±0.1)	ΔH_f (J/g) (±5%)
0	0.9	311
2	0.0	286
4	-0.5	281
6	-1.1	260
8	-1.4	240
10	-2.0	234

$T_{m,}$ and ΔH_f are melting temperature and heat of fusion.

As in the alumina water system, two distinct melting events were observed in aqueous alumina suspensions containing fructose (Fig. 9). The effect of fructose in the bound water phase is twofold: solute effect of fructose in the bound water phase and fructose adsorbed on the alumina surface. Separating the effect of adsorbed fructose from that of water is not trivial. Nevertheless, while adsorbed fructose alters the bound water content/structure, fructose in water

`

lowers the onset of the melting temperature. Heats of fusion and fractions of free and bound water contents for suspensions with varying concentration of fructose for 20 vol% alumina suspensions are listed in Table III.

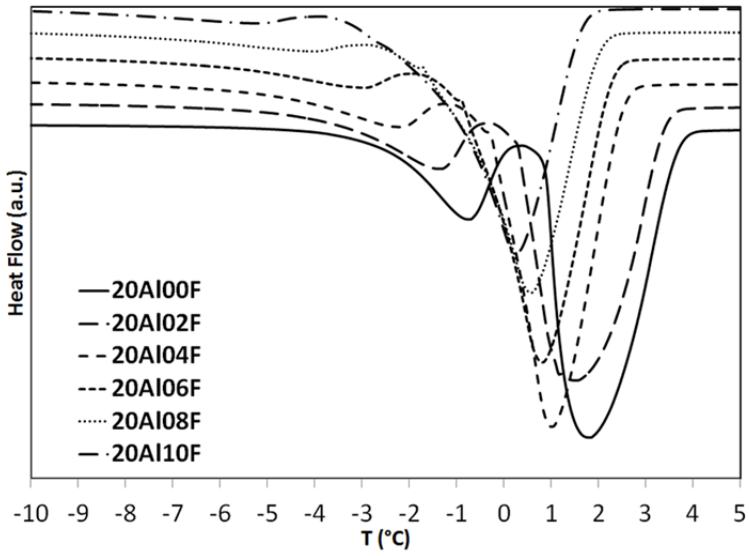

Figure 9: DSC curves for aqueous alumina suspensions with fructose addition (corrected for total water content). '20AlxxF' stands for xx weight percent of fructose with respect to the 20 vol% alumina.

Table 3: DSC results for aqueous nano alumina suspensions with fructose addition.

	FW (% Area) (±10%)	**BW (% Area) (±10%)**	**$\Delta H_{f,FW}$ (J/g) (±10%)**	**W_{FW} (±0.02)**	**$\Delta H_{f,BW}$ (J/g) (±10%)**	**W_{BW} (±0.02)**
20Al00F	22	78	311	0.72	229	0.28
20Al02F	21	79	286	0.78	273	0.22
20Al04F	19	81	281	0.81	272	0.19
20Al06F	16	84	260	0.84	263	0.16
20Al08F	13	87	240	0.89	276	0.11
20Al10F	11	89	234	0.90	262	0.10

ΔH_f and W represent heat of fusion and weight fraction, respectively. FW and BW stand for free and bound water.

`

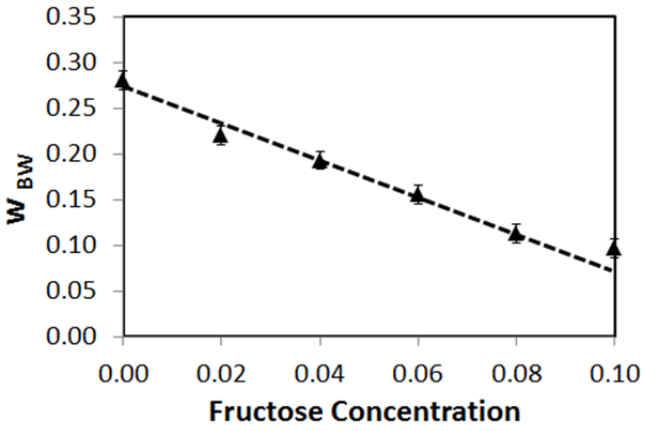

Figure 10: Change in bound water fraction with fructose concentration of 20 vol% alumina nanopowder suspensions.

Both free and bound water melting peaks exhibit asymmetry similar to the ones observed in the fructose–water system. As the concentration of fructose increases, onset of the free and bound water melting shifts to lower temperatures. That is most probably due to the presence of fructose in each phase. The heat of fusion values listed in Table II were used to calculate the heat of fusion and amount of free water. Heat of fusion values for the bound water melting events remain more or less constant for the whole concentration range studied. As the alumina content (and the available interfacial area) remains constant, the decrease in fraction of the bound water with the fructose addition (Fig. 10) supports the statement made by Li and Akinc[15,16] that fructose displaces water from the alumina surface.

The change in viscosity of the alumina suspensions for different fructose concentrations and the associated power law parameters are given in Figs. 11(a) and (b), respectively. As the concentration of fructose increases, viscosity of the suspensions decreases and flow becomes less shear thinning.

`

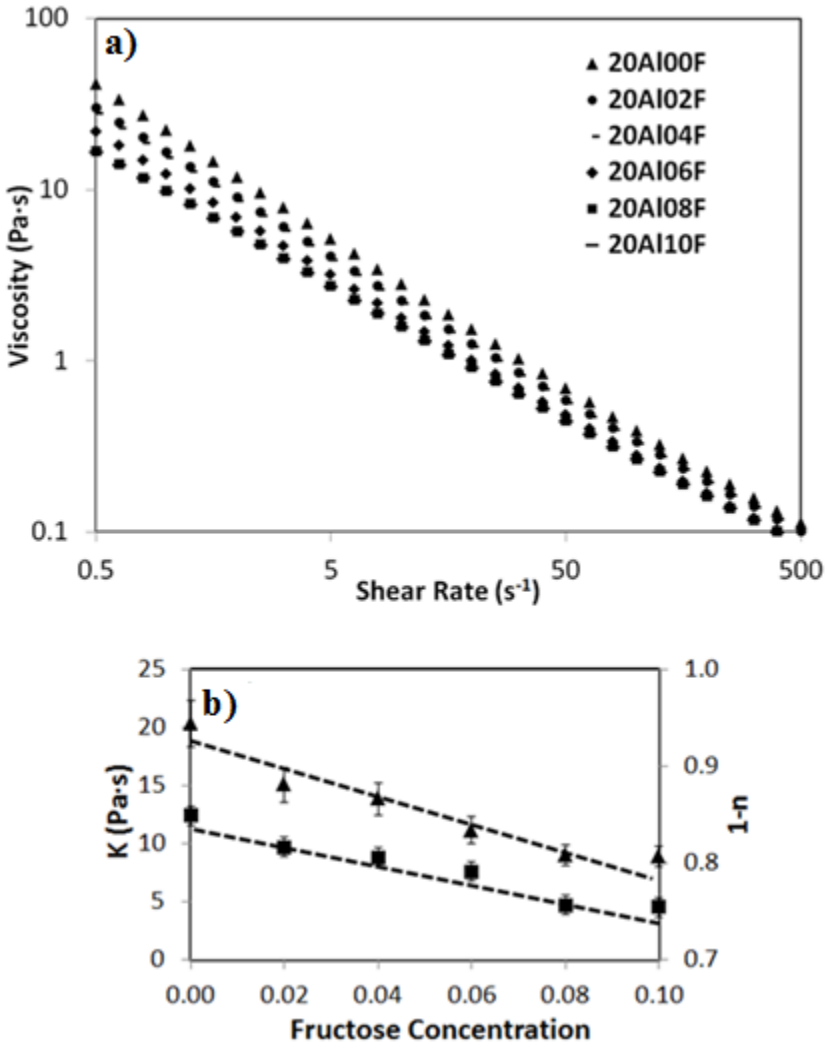

Figure 11: (a) Viscosity of the suspensions, and (b) change in power law parameters, consistency coefficient, K (▲), rate index, 1 – n (■), with fructose concentration for 20 vol% alumina nanopowder suspensions.

A comparison of the viscosity and LT-DSC results indicates that the decrease in bound water fraction with the addition of fructose leads to lower suspension viscosity. These results also imply that Low Temperature Differential Scanning Calorimetry (LT-DSC) may predict, at least semiquantitatively, variation in viscosity with processing additives. The possible role fructose plays in reducing the viscosity of nano alumina suspension is discussed below.

`

Electrostatic Effect of Fructose on Interparticle Interactions

The profound effect of potential determining ions (i.e., pH) and indifferent ions on the stability of colloids and the rheological behavior of suspensions is well-established. Fructose has a very low acid dissociation constant ($pK_a \approx 12.2$)[33]. For 20 vol% alumina suspension with an initial pH of 5.7, even with the highest fructose content (10 wt%), the reduction in pH from fructose dissociation would be negligible (pH = 5.69). However, as illustrated in Fig. 12, the pH of alumina suspensions decreased substantially to pH ≈ 5.1 at higher fructose concentrations. Obviously, alumina plays an active role in dissociation of fructose. However, neither the change in pH nor in ion concentration of the suspension results in significant change in zeta potential of the nano alumina particles (Fig. 13). In the pH regime studied ($5.0 \leq pH \leq 5.7$), the ξ potential remains relatively constant at 50 mV for various fructose concentrations. In addition, as shown in Fig. 13, fructose does not lead to any shift in the isoelectric point of the nano alumina particles. A similar observation was reported by Falkowski et al[14] It is also worth noting that the change in pH is another proof of the interaction of the fructose with the alumina surface.

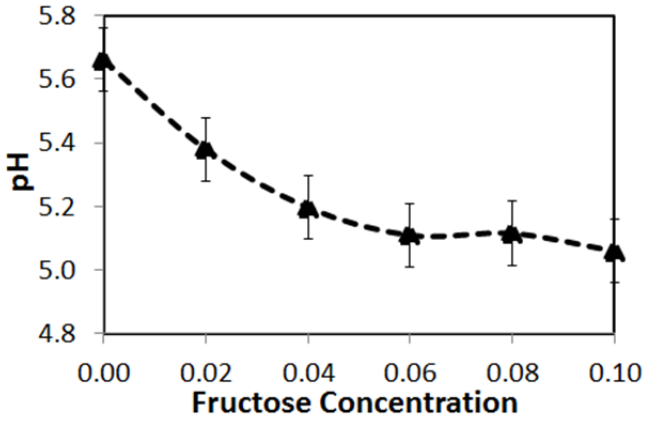

Figure 12: Change in pH of the 20 vol% alumina nanopowder suspensions with fructose concentration.

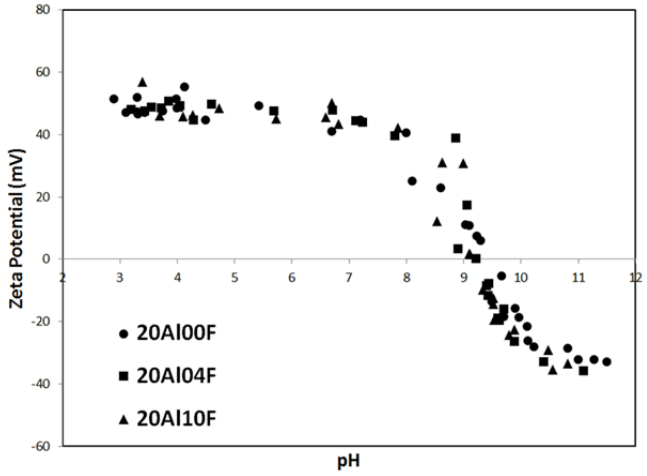

Figure 13: Zeta potential measurements of alumina suspensions with different fructose concentrations as a function of pH.

Steric Effect of Fructose on Interparticle Interactions

The adsorption of fructose on alumina surface has been studied by several groups[13,15]. It is shown that maximum adsorption of the fructose on alumina surface is limited submonolayer coverage. Therefore, even if the monolayer coverage is assumed, the thickness of the adsorbed layer will be restricted with the size of the fructose molecule which is about 0.5 nm. When the long range effects of van der Waals forces are considered[4], it is unlikely that the steric stabilization mechanism can explain the viscosity reduction brought about by fructose addition.

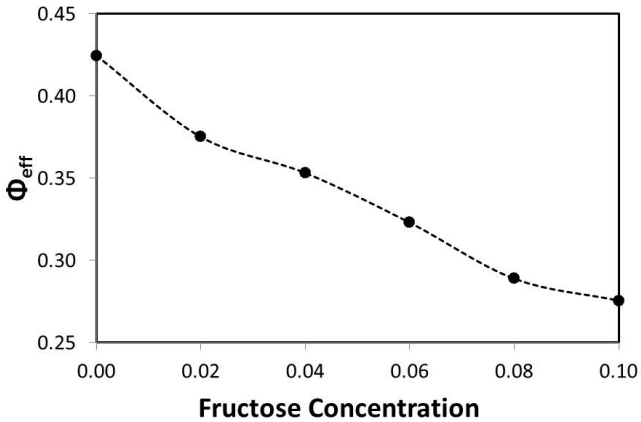

Figure 14: Effect of fructose concentration on calculated effective solids content.

`

Fructose and Effective Solids Content

As discussed in previous sections, a large surface area of the nanoparticles leads to an increase in effective solids content, therefore increasing the viscosity of the suspensions. By assuming that bound water is not available as a vehicle, the effective solids content was calculated from the values in Table III and plotted in Fig. 14. As the bound water is calculated indirectly, the trend in Fig. 14 should be considered semiqualitative. However, it is clear that any change in effective solids content is significant for the viscosity of the nanoparticle suspensions. The addition of fructose to alumina suspensions modifies the bound water content which leads to reduction in effective solids content, and therefore the viscosity of suspensions. These results show that, it is not only the interparticle forces (electrostatic and steric effects) but also surface/solvent interactions that are important in controlling the rheological behavior of the nanoparticle suspensions.

Conclusions

Low temperature differential scanning calorimetry is a useful technique for understanding the rheological behavior of nanoparticle suspensions. Variation in bound water content as a function of solids content and fructose addition was studied using LT-DSC and rheometry. Appearance of a “bound water” peak with introduction of both, micro- and nano-sized alumina particles was observed. It is plausible that bound water represents the hydration layer around the alumina particles. Effective solids contents were estimated by use of the bound water fractions obtained from the DSC plots. Significant increase in effective solids content due to bound water is believed to be responsible for the high viscosity of nanoparticle suspensions. Zeta potential measurements at several fructose concentrations indicate that the electrostatic stabilization does not play a critical role in the reduction in viscosity by fructose addition. Rather, reduction in the

`

effective solids content by modification of the bound water is the primary reason for the reduction in the viscosity by fructose addition.

Acknowledgments

This work has been supported by National Science Foundation through grant no. CBET-0931038. The authors would like to thank Yaqiao Wu for conducting TEM characterization of alumina nanopowders.

References

[1]J. S. Chong, E. B. Christiansen, and A. D. Baer, "Rheology of Concentrated Suspensions," J. Appl. Polym. Sci., 15 [8] 2007–21 (1971).

[2]S. B. Johnson, G. V. Franks, P. J. Scales, D. V. Boger, and T. W. Healy, "Surface Chemistry–Rheology Relationships in Concentrated Mineral Suspensions" Int. J. Miner. Process., 58 [1–4] 267–304 (2000).

[3]S. Jailani, G. V. Franks, and T. W. Healy, "Z Potential of Nanoparticle Suspensions: Effect of Electrolyte Concentration, Particle Size, and Volume Fraction," J. Am. Ceram. Soc., 91 [4] 141–7 (2008).

[4]K. Lu, "Theoretical Analysis of Colloidal Interaction Energy in Nanoparticle Suspensions," Ceram. Int., 34 [6] 1353–60 (2008).

[5]G. V. Franks and Y. Gan, "Charging Behavior at the Alumina–Water Interface and Implications for Ceramic Processing," J. Am. Ceram. Soc., 90 [11] 3373–88 (2007).

[6]A. R. Studart, E. Amstad, and L. J. Gauckler, "Colloidal Stabilization of Nanoparticles in Concentrated Suspensions," Langmuir, 23 [3] 1081–90 (2006).

[7]C. H. Schilling, R. A. Bellman, R. M. Smith, and H. Goel, "Plasticizing Aqueous Suspensions of Concentrated Alumina With Maltodextrin Sugar," J. Am. Ceram. Soc., 82 [1] 57–66 (1999).

[8]C. H. Schilling, M. Sikora, P. Tomasik, C. Li, and V. Garcia, "Rheology of Alumina–Nanoparticle Suspensions: Effects of Lower Saccharides and Sugar Alcohols," J. Eur. Ceram. Soc., 22 [6] 917–21 (2002).

[9]M. Sikora, C. H. Schilling, P. Tomasik, and C. Li, "Dextrin Plasticizers for Aqueous Colloidal Processing of Alumina," J. Eur. Ceram. Soc., 22 [5] 625–8 (2002).

`

[10]C. H. Schilling, C. Li, P. Tomasik, and J.-C. Kim, "The Rheology of Alumina Suspensions: Influence of Polysaccharides," J. Eur. Ceram. Soc., 22 [6] 923–31 (2002).

[11]P. Tomasik, C. H. Schilling, R. Jankowiak, and J.-C. Kim, "The Role of Organic Dispersants in Aqueous Alumina Suspensions," J. Eur. Ceram. Soc., 23 [6] 913–9 (2003).

[12]K. Singh and S. Mohan, "Kinetic Studies of the Sucrose Adsorption Onto an Alumina Interface," Appl. Surf. Sci., 221 [1–4] 308–18 (2004).

[13]K. Singh and S. Mohan, "Adsorption Behavior of Selected Monosaccharides Onto an Alumina Interface," J. Colloid Interface Sci., 270 [1] 21–8 (2004).

[14]P. Falkowski, P. Bednarek, A. Danelska, T. Mizerski, and M. Szafran, "Application of Monosaccharides Derivatives in Colloidal Processing of Aluminum Oxide," J. Eur. Ceram. Soc., 30 [14] 2805–11 (2010).

[15]C. Li and M. Akinc, "Role of Bound Water on the Viscosity of Nanometric Alumina Suspensions," J. Am. Ceram. Soc., 88 [6] 1448–54 (2005).

[16]C. Li, M. Akinc, J. Wiench, M. Pruski, and C. H. Schilling, "Relationship Between Water Mobility and Viscosity of Nanometric Alumina Suspensions," J. Am. Ceram. Soc., 88 [10] 2762–8 (2005).

[17]I. M. Krieger and T. J. Dougherty, "A Mechanism for non-Newtonian Flow in Suspensions of Rigid Spheres," Trans. Soc. Rheol., 3 [1] 137–52 (1959).

[18]D. Argyris, P. D. Ashby, and A. Striolo, "Structure and Orientation of Interfacial Water Determine Atomic Force Microscopy Results: Insights From Molecular Dynamics Simulations," ACS Nano, 5 [3] 2215–23 (2011).

[19]D. Argyris, T. Ho, D. R. Cole, and A. Striolo, "Molecular Dynamics Studies of Interfacial Water at the Alumina Surface," J. Phys. Chem. C, 115 [5] 2038–46 (2011).

[20]H. J. Butt, "Measuring Electrostatic, van der Waals, and Hydration Forces in Electrolyte Solutions With an Atomic Force Microscope," Biophys. J., 60 [6] 1438–44 (1991).

[21]H.-J. Butt, B. Cappella, and M. Kappl, "Force Measurements With the Atomic Force Microscope: Technique, Interpretation and Applications," Surf. Sci. Rep., 59 [1–6] 1–152 (2005).

[22]J. Drelich, Z. Xu, and J. Masliyah, "Structural Effects Recorded for AFM Tips Interacting With Individual Nanoparticles and Their Clusters Deposited on Substrates," Langmuir, 22 [21] 8850–9 (2006).

[23]W. A. Ducker, T. J. Senden, and R. M. Pashley, "Direct Measurement of Colloidal Forces Using an Atomic Force Microscope," Nature (London), 353, 239–41 (1991).

`

[24]J. N. Israelachvili, Intermolecular And Surface Forces, 3rd edition. p. 363. Academic Press, St. Louis, MO, 2010.

[25]S. Liu, D. Guo, and G. Xie, "Water Film Confined in a Nanoscale gap: Surface Polarity and Hydration Effects," J. Appl. Phys., 108 [8] 084315, 7 pp (2010).

[26]A. Verdaguer, G. M. Sacha, H. Bluhm, and M. Salmeron, "Molecular Structure of Water at Interfaces: Wetting at the Nanometer Scale," Chem. Rev. (Washington, DC, U. S.), 106 [4] 1478–510 (2006).

[27]N. Garti, Thermal Behavior of Dispersed Systems. pp. 161–163. Marcel Dekker, New York, NY, 2001.

[28]M. Alcoutlabi and G. B. McKenna, "Effects of Confinement on Material Behavior at the Nanometer Size Scale," J. Phys.: Condens. Matter, 17 R461– 524 (2005).

[29]G. K. Rennie and J. Clifford, "Melting of ice in Porous Solids," J. Chem. Soc., Faraday Trans., 73, 680–9 (1977).

[30]K. Ishikiriyama, M. Todoki, and K. Motomura, "Pore Size Distribution (PSD) Measurements of Silica Gels by Means of Differential Scanning Calorimetry: I. Optimization for Determination of PSD," J. Colloid Interface Sci., 171 [1] 92–102 (1995).

[31]S. Guriyanova, V. G. Mairanovsky, and E. Bonaccurso, "Superviscosity and Electroviscous Effects at an Electrode/Aqueous Electrolyte Interface: An Atomic Force Microscope Study," J. Colloid Interface Sci., 360 [2] 800–4 (2011).

[32]N. Spiliotis and D. Tassios, "A UNIFAC Model for Phase Equilibrium Calculations in Aqueous and Nonaqueous Sugar Solutions," Fluid Phase Equilib., 173 [1] 39–55 (2000).

[33]X. M. Fang, F. Y. Gong, J. N. Ye, and Y. Z. Fang, "Determination of Ionization Constants of Saccharides by Capillary Zone Electrophoresis With Amperometric Detection," Chromatographia, 46 [3] 137–40 (1997).

`

CHAPTER III. ELECTROSTATIC STABILIZATION OF ALUMINA NANOPOWDER SUSPENSIONS

(A paper accepted by the Science of Advanced Materials)

Simge Çınar and Mufit Akinc

Department of Materials Science and Engineering,

Iowa State University, Ames, Iowa 50011

Abstract

Electrostatic stabilization has an impact on a broad range of applications. Previous research has shown that concentrated alumina nanopowder suspensions can be stabilized at specific ranges of ionic strength and pH. This study investigated the stability of alumina nanopowder suspensions in terms of viscosity measurements as a function of indifferent electrolyte concentration and suspension pH. Using alumina nanopowders with an average particle size of about 50 nm, stable suspensions were obtained with $0.020 \leq [NaCl] \leq 0.040$ M or in the range $4 \leq pH \leq 7$. The observed suspension stability was investigated by zeta potential measurements and explained with the DLVO theory. The effective volume fraction of solids brought about by bound water (or swelling), surface charge, and the compression of the electrical double layer were three plausible control mechanisms for the rheological behavior and electrostatic stabilization of alumina nanopowder suspensions with high solids content.

`

Graphical Abstract

The difference in electrostatic stability of concentrated nanopowder suspensions than dilute or micron sized suspensions was related to the presence of bound water around the powder surface and changes in zeta potential values of powder.

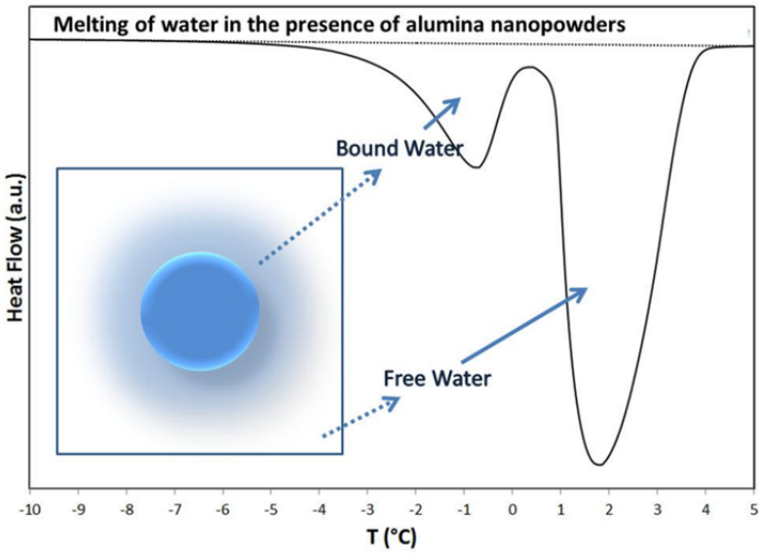

Introduction

The colloidal stability of oxide nanopowder suspensions is crucial for a variety of applications, including nanofluids[1-5], waste water treatment[6], advanced ceramics[7;8], and others. It is also relevant with regard to environmental and toxicological[9-13] concerns emerging with the wide use of nanopowders in industry.

The stability of a suspension and its rheological behavior are closely related. In general, lower suspension viscosities indicate more stable suspensions. By understanding the interaction forces among the particles in a liquid medium, the stability of a suspension, and thus its rheological behavior, can be manipulated. Interparticle interactions can be predicted by the well-

`

known DLVO (Derjaguin-Landau-Verwey-Overbeek) theory, which combines the net interaction of the main attractive (van der Waals) and repulsive (electrostatic) forces.

The major stabilization mechanisms can be categorized in three different groups: (i) steric, (ii) electrostatic, and (iii) electrosteric stabilization. The electrostatic behavior of the powders is of particular importance for several reasons: (i) powders exhibit charged surfaces in aqueous environments that need to be controlled in order to stabilize the particles; (ii) it is very difficult to obtain completely pure oxide powders, especially nanopowders because of large surface area.

Compared to micron-size suspensions with similar solids content, nanopowder suspensions have a higher surface area and smaller separation distance between particles. Therefore inter-particle interactions gain increased significance, bringing more complexities to the calculations and predictions, and the influence of electrolyte concentration becomes particularly important.

The effects of charged particles on the stability of oxide nanopowder systems have been studied by several groups. However, in these studies, the charged particles either show a steric effect in addition to their electrostatic contribution[14], or the behavior of the stabilizers (adsorbed species on oxide surface) is affected by the suspension pH or the concentration of indifferent electrolytes[9;13;15]. Only few groups reported on the effect of ions alone on the viscosity of aqueous oxide nanopowder suspensions that may reveal the fundamentals of electrostatic stabilization[16-20]. These studies either focused on dilute suspensions[18;20] or indicated that coulombic interactions alone did not improve the stability of the nanopowder suspensions[16;17;19].

Lu[19] calculated the net interaction between alumina particles with a diameter of 55 nm and a zeta potential of 43 mV (or lower) using DLVO theory and concluded that for nanopowder systems, van der Waals interactions dominated electrostatic interactions, which resulted in

`

flocculation. Jailaini *et al*.[17] reported that a decrease in particle size and an increase in solids content resulted in a reduction of the zeta potential. Because in these systems electrostatic stabilization would not be successful, they suggested imposing steric repulsion in order to stabilize nanopowder suspensions. Recently, a study by Iijima and Kamiya[16], who used DLVO calculations, showed that the resulting potential barrier in nanopowder systems would be too small to obtain kinetically stable suspensions. According to their calculations, a system with an average particle size of 30 nm requires an unreasonably high surface potential (approx. 177 mV) to create a sufficiently high potential barrier, which is difficult to obtain using additives. All of these studies indicate that nanopowder suspensions cannot be stabilized electrostatically. However, it should be noted that they base their predictions either on theories applicable to micron-sized particles or on indirect measurements.

On the other hand, anomalous stability of oxide powders at high ionic strength that cannot be directly explained by DLVO theory has also been reported, even though the origin of the behavior is still controversial[21;22]. Secondary hydration forces associated with hydrated counterions adsorbed on the particle surface[23-27] and the formation of a rigid solvent layer around the powder particles and the associated repulsive forces effective at small interparticle separations (< 5 nm) [28-30] are some of the mechanisms proposed to explain this phenomenon. For alumina suspensions, anomalous stability is observed for ionic concentrations higher than 0.1 M[23].

Our experiments with alumina nanopowder revealed an unexpected level of stability of the concentrated suspensions at very low ionic strengths, contrary to the predictions of the DLVO theory mentioned above. The present study aims to investigate the effects of both indifferent and

`

potential determining ions on the viscosity of concentrated alumina nanopowder suspensions to explain the observed unexpected stability.

Experimental

Materials

Two different batches of alumina nanopowders (AAGL 1201 and AAGL 1203) with similar characteristics were used in this study. The powders had a phase distribution of $\gamma/\delta \approx 70{:}30$, a specific surface area is approx. 36 m^2/g (38.8 and 36 m^2/g for AAGL 1201 and AAGL 1203 respectively), purity $\geq$ 99.5%, and a density of 3.67 g/cm^3 and were purchased from Nanophase Technology Corporation (Burr Ridge, IL). Transmission electron micrographs of as received powders are shown in Figure 1. The powders had an average particle size of 45 nm according to the measured BET surface area. The size distribution of the particles was determined by measuring the diameters of approximately 900 particles from TEM images. Almost 99 % of particles were between 10 and 100 nm. Average particle sizes from TEM images were calculated as 30 and 28 nm with standard deviations of 21 and 20 nm for batches of AAGL 1201 and AAGL 1203, respectively. The zeta potential values measured over a range of pH values at a constant ion concentration of 0.01M NaCl were similar and the IEP of the two batches was the same within an experimental error range of $\pm$ 0.1 (pH = 9.5 $\pm$ 0.1).

Although the powders from different batches had similar properties, the batch-to-batch variation in viscosity was significant.

`

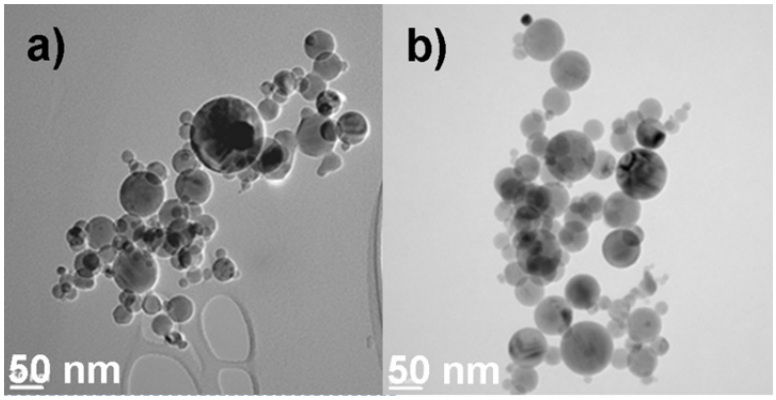

Figure 1: TEM micrographs of alumina nanopowders: Batch # AAGL 1203 (a), and AAGL 1201 (b).

Ultrapure water (Milli-Q Gradient A-10 model, Millipore Company, Billerica, MA) with a resistivity of 18.2 MOhm·cm and TOC < 3 ppm was used. ACS certified NaCl, NaOH, and KNO_3 and concentrated HCl were purchased from Fisher Scientific (Fair Lawn, NJ).

Sample Preparation

For suspension preparation, alumina nanopowders were first dried at 110 ^{o}C for 2 hours to eliminate any moisture adsorbed on the powder surface. Solids content of the suspensions were calculated as volume percent of powder in the suspension. For instance, for 10 ml suspension with a solids content of 0.20, 7.34 g of alumina powder (2 ml× 3.67 g/cm^3) were added to 8 g of water. For weighing, an electronic analytical balance with readability of 0.1 mg was used. The measurements were within an error margin of 1 – 2 %. Suspensions were shaken with a heavy duty shaker for 24 hours to achieve physical and chemical equilibrium before testing.

For the ionic strength experiments, the required amount of NaCl powder was weighed, added to the suspensions, and shaken for 2 additional hours prior to testing.

For the pH study, the total ionic strength was kept constant at 0.05 M. For pH adjustment at constant ionic strength, 1.0 M stock solutions of acid, base and salt were used. To keep the solids

`

content constant subsequent to acid/base addition, the required amount of acid or base was calculated and the amount of water needed for the suspension was reduced appropriately. For example, for a total volume of 10 ml suspension with a solids content of 0.20, 7.34 g of alumina was mixed with 7.6 ml of water rather than 8.0 ml. After 24 hours of shaking, the required volume of acid or base solution was added, then the total addition of 0.4 ml was completed by adding salt solution. Here, for a 0.025M NaOH sample, 0.2 ml NaOH solution and 0.2 ml NaCl solution (the chemical composition of each sample is listed in the legends of the related figures) were added. At the end, alumina suspensions with a solids content of 0.20 and ionic strength of 0.05 M with varying pH values were obtained. Analogous to salt additions, the suspensions were shaken for 2 more hours after adding acid or base and rheological tests as well as pH measurements were conducted.

Rheological Measurements

A rheometer (TA Instruments, model AR 2000ex, New Castle, DE) with cone and plate geometry (steel cone and plate having 4^{o} cone angle and 40 mm diameter) was used for viscosity measurements. The limit of minimum torque for the rheometer was 0.05 $\mu N \cdot m$. To prevent evaporation of water, a solvent trap was used. The temperature was kept constant at 25 ^{o}C by using a Peltier plate with a precision of ± 0.1 ^{o}C. Ten viscosity measurements were recorded per half loop of two consecutive complete loops over a shear rate range of 0.5 – 500 s^{-1}. The shear rate was ramped up in the first half, and ramped down in the second half of one complete loop. The measurements were mostly reproducible after the first loop and the data points corresponding to the final half of the second loop were used for data analysis.

`

Zeta Potential Measurements

Zeta potential was measured by Laser Doppler Electrophoresis using a Zetasizer (Nano ZS90, Malvern Instruments, Worcestershire, UK) instrument. Alumina suspensions prepared for the rheological measurements were diluted to approximately 200 ppm particles by deionized water. NaCl was added to adjust the ionic strength and the solutions were shaken for 12 h before measurements. The pH of the suspensions was varied between 3 and 11 by adding 0.01 M of HCl or 0.1 M of NaOH. The measurements were conducted after 2 – 5 min of acid/base addition and at 25 °C. The solution pH was measured before and after the electrophoretic measurements, and the average pH was assigned for the zeta potential measured. The pH values were accurate to ± 0.01. The Smoluchowski equation was used for the zeta potential calculations. Conductivity measurements were done concurrently with zeta potential measurements by the same instrument.

Differential Scanning Calorimetric Measurements

The use of low temperature differential scanning calorimetry, LT-DSC, for the determination of the bound water content and its influence on effective volume content was previously reported in detail[31]. For these tests, a DSC (Model Q20; TA Instruments, New Castle, DE) with an RCS 40 cooling unit was used. To prevent the evaporation of water during the analysis, hermetically sealed aluminum pans were employed. The samples were cooled down to -25 ^{o}C, held at that temperature for 1 min, and then heated to 10 ^{o}C at a rate of 1 ^{o}C/min.

Results and Discussion

Comparison of Powders

In the present study, powders from two different batches were used. Because of slight variations in viscosity observed for the two batches, these powders were characterized in detail.

`

Figure 2 shows the suspension viscosity differences between two batches with NaCl concentration.

The viscosity values for batch AAGL 1203 were slightly higher than those measured for batch AAGL 1201. Basic characterization of the powders showed similar properties (phase distribution, BET surface area, average particle size, size distribution, shape, and zeta potential) as presented in the experimental part. Comprehensive characterization of the powders showed only two differences between the particles: initial suspension pH and trace levels of impurity.

Powders were treated at 500 °C for 2 hours to remove organic impurities and the Fourier transform infrared (FTIR) spectra of the powders were compared with those of as received powders. No significant differences were noted that could explain the slightly different suspension viscosities of as-received powders.

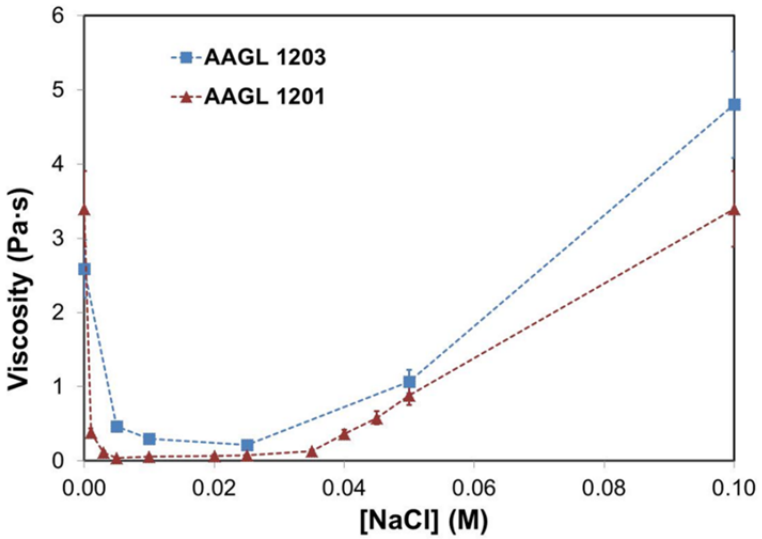

Figure 2: Comparison of viscosity variation of the two batches of powders with NaCl concentration. ($\Phi = 0.20$, and shear rate of 10 s^{-1})

The chemical analysis provided by the supplier showed that the powders had total impurity less than 0.5 %. X-Ray photoelectron spectroscopy (XPS) and inductively coupled plasma mass

`

spectroscopy (ICP-MS) showed the presence of different trace amounts of chlorine; however, the concentration of chloride was too small to quantify accurately with the aforementioned techniques.

Mikkola *et al*.[32] studied the effect of impurities on dispersion properties of submicron size α-alumina powders. They reported that while trace amounts of impurities did not result in a shift in the isoelectric point of dilute suspensions, they led to a substantial shift in concentrated suspensions. Therefore, even though the isoelectric points obtained for the powders in dilute solutions were similar to those in our experiments, impurities on the surface of particles may affect the initial pH and zeta potential of the suspensions, leading to changes in the dispersion state of the suspensions.

The initial pH values of the suspensions with $\varphi = 0.20$ were 5.3 and 5.7 for batches AAGL 1203 and AAGL 1201, respectively. For suspensions of powders from the same batch, the suspension pH increased as solids content was increased (For AAGL 1201, suspensions pH increased from 4.8 to 6.3 as the solids contents increased from 0.05 to 0.40). Similar low initial suspension pH of alumina nanopowders was also reported by Witharana and coworkers[4] (pH = 4.7 for $\varphi = 0.005$).

The pH values we measured were in the acidic range rather than being close to the expected basic IEP of alumina powders. Although some studies in literature state that impurities may cause the initial suspension pH to be much lower than the IEP, we do not have any satisfactory explanation for this phenomenon. According to their claim, the presence of chloride ions in suspensions hinders the propagation of alumina hydrolysis, bonded chlorine atoms release the acidic species to the solution which results in an acidic pH[33;34]. Several groups reported on dissolved aluminum species and their interactions with chloride ions[23;25;27].

`

Since the significant change in viscosity of the suspension was observed at low salt concentrations, as shown in Figure 2, the differences in suspension viscosities for different batches of powders may be attributed to slightly different chloride impurity levels in the powders.

Ionic Strength

The effect of ionic strength on the rheological behavior of micron-sized alumina suspensions was extensively studied and it was experimentally shown that an increase in indifferent ion concentration results in higher suspension viscosities and yield stresses as might be inferred from the DLVO theory predictions[17-19]. Of these studies, only Zhou *et al*.[35] reported that the suspension viscosity decreased first, and then increased with increasing electrolyte concentration. Results were credited, without any further analysis or discussion, to the competition of two effects of the double layer compression: (i) decrease in effective solids concentration; (ii) the reduction of the range and magnitude of the electrostatic repulsion.

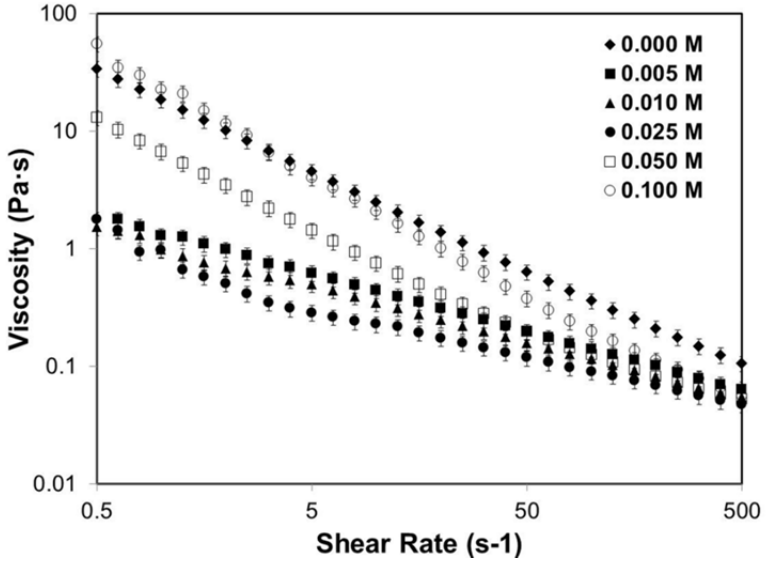

Figure 3: Viscosity of suspensions with Φ = 0.20 alumina nanopowder as a function of shear rate and NaCl concentration. (Batch #: AAGL 1203)

`

The influence of indifferent electrolyte (*i.e.*, NaCl) addition on the alumina nanopowder suspension viscosity was studied. Figure 3 shows the change in viscosity at several NaCl concentrations as a function of shear rate. The viscosity of the suspensions decreased with NaCl concentration up to 0.025 M and then increased at higher concentrations, contrary to other reports but similar to what Zhou *et al.*[35] reported on submicron alumina suspensions. A discussion of these observations and relevant DLVO predictions is presented in the next section.

Solids Content

The solids content plays a profound role in concentrated suspensions because of the strong inter-particle interactions and the overlap of double layers. Figure 4 shows the viscosity values of suspensions for several solids contents at a constant shear rate of 10 s^{-1} with varying salt concentrations. Suspensions show similar viscosity trends. However, the effect of electrolytes is almost negligible at relatively low solids content ($\varphi = 0.15$). That explains why the reduction in viscosity at low concentrations of NaCl has not been widely reported, as most of these studies focused on dilute suspensions.

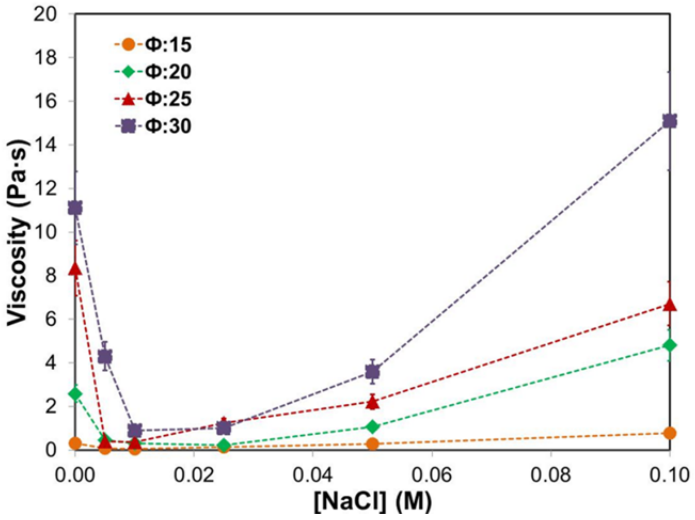

Figure 4: Viscosity of alumina nanopowder suspensions with different solids content as a function of NaCl concentration at a constant shear rate of 10 s^{-1}. (Batch #: AAGL 1203)

`

The decrease in viscosity at low NaCl concentrations can be explained with the compression of the double layer thickness, which lowers the effective volume fraction of particles. Compression of the double layer with electrolyte concentration is discussed in the subsequent section.

Because nanopowders have a higher specific surface area than micron-sized particles, the change in double layer thickness has an amplifying effect on the effective volume fraction of particles. This effect becomes even more significant as solids content increased, as seen in Figure 4.

At higher electrolyte concentrations, the powders tended to flocculate due to the screening of the surface charges. The combination of flocs and the increase in effective volume fraction caused by the occluded volume of water within the flocs resulted in higher viscosities. Critical coagulation concentrations of boehmite particles were reported as 0.05 M for NaCl at neutral pH[25].

At higher ion concentrations than the critical coagulation concentrations (> 0.1 M NaCl), anomalous stability of alumina particles was reported[23;27]. The non-DLVO behavior, stable suspensions even at the IEP, was explained by the solvation layer formed around the particles by adsorption of polymeric aluminum cations. In the present study, we focused on the stability of particles at much lower ion concentrations. The results show the importance of ionic strength on the stability of nanopowder suspensions, especially for concentrated systems. To gain better control of the viscosity of suspensions it is important to explain the origin of this behavior.

`

Zeta Potential

The zeta potential of powders is expected to decrease with increasing indifferent electrolyte concentration[36]. Figure 5a shows zeta potential measurements for alumina nanopowders as a function of pH at several ionic strengths. Unexpectedly, the zeta potential showed an increase in a narrow range of NaCl concentrations. More specifically, the zeta potential values for 0.025 M < [NaCl] < 0.05 M were higher from approx. pH = 3 all the way to the IEP, pH ≈ 9-9.5.

Another interesting observation was that the difference in zeta potential diminished as pH approached IEP, another indication that NaCl acted as an indifferent electrolyte. Concurrent measurements of conductivities showed linearity with the concentration of electrolytes (Figure 5b), proving the presence and mobility of Na^+ and Cl^- in the solution. Zeta potential measurements reported by Jailani *et al.*[17] were made at concentration higher than 0.05 M and are comparable with our measurements in this range. If it is assumed that at a particle concentration of 200 ppm the suspension is dilute enough to neglect any interactions between particles, the origin of the zeta potential changes should stem from charging mechanisms of the particles, such as dissolution kinetics or adsorption of ions on the surface. Since Na^+ and Cl^- do not specifically adsorb on the alumina surface, it is probable that the presence of these ions changed either the dissolution kinetics of the particles or the hydrolysis of the aluminum species in the solution.

It is worthwhile to note that any change in surface composition will lead to significant changes in the properties of the nanopowder suspensions. The effect of zeta potential on the colloidal stability of suspensions is discussed in the next section.

`

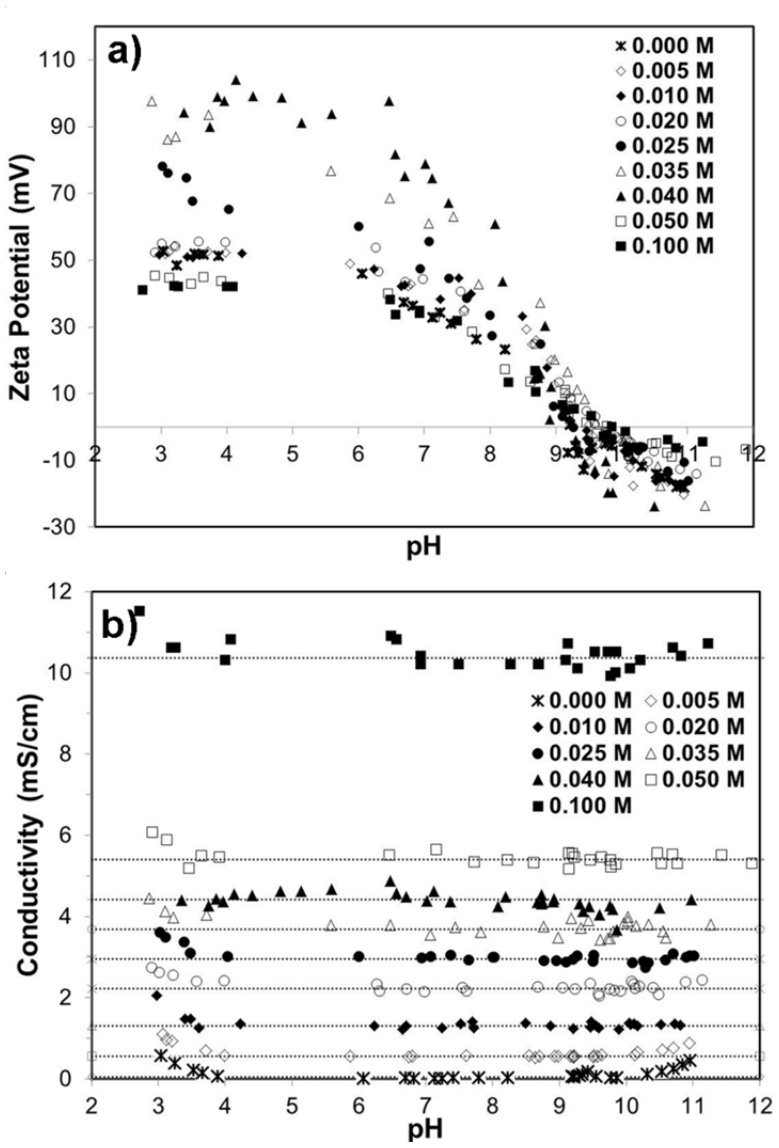

Figure 5: Zeta potential (a) and conductivity (b) measurements of alumina nanopowder suspensions for varying NaCl concentrations as a function of pH. (Batch #: AAGL 1201, and solids content: 200 ppm)

Application of the DLVO Theory

DLVO theory is widely used to predict the stability of colloidal suspensions. The theory is based on adding attractive van der Waals forces and repulsive coulombic forces to obtain net inter-particle interaction energy. If the net interaction energy barrier between the two

approaching particles is higher than the kinetic energy caused by Brownian motion, the particles do not flocculate.

For the concentrated suspensions in this study, the models proposed by Gregory[37] and by Hogg, Healy, and Fuerstenau (HHF)[38] were used to represent the van der Waals (vdW) and repulsive electrostatic interactions, respectively. Equations and their validity are discussed elsewhere[39].

In its simplest interpretation, three conclusions can be drawn from the DLVO theory: (i) the larger the Hamaker constant is, the larger the attraction between particles, (ii) higher surface potentials result in larger repulsive forces; (iii) the higher the electrolyte concentration is, the smaller the distance from the surface at which repulsive forces are effective.

Figure 6 shows the change in total interaction potential of particles with a diameter of 50 nm and a zeta potential of 50 mV at 25 °C with varying monovalent salt concentration. The Hamaker constant was taken as 3.67×10^{-20} J as reported by Bergstrom[40].

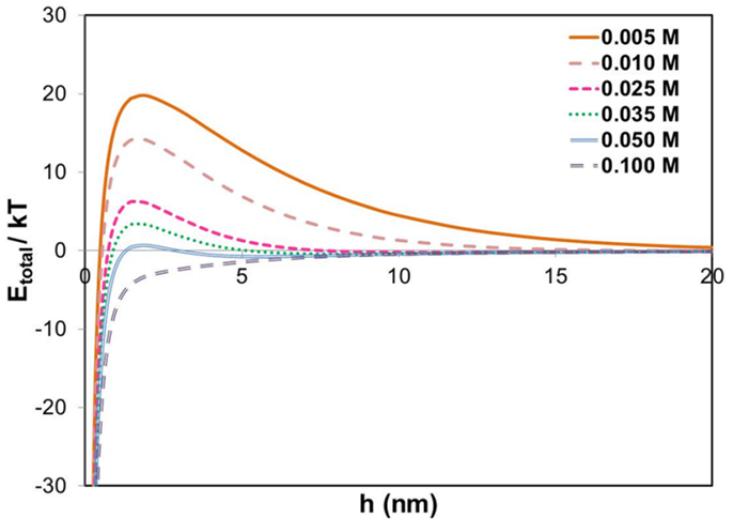

Figure 6: DLVO plots of particles with a diameter of 50 nm and zeta potential of 50 mV at various monovalent salt concentrations.

`

As expected, increasing ion concentration decreased the double layer thickness and reduced the effectiveness of electrical repulsive forces. Two significant features in Figure 6 are the height of the potential barrier, which predicts whether the particles flocculate or not, and the distance at which the net interaction energy is higher than thermal fluctuation caused by Brownian motion. This distance is considered the closest particle approach, essentially corresponding to the effective volume fraction brought about by the repulsive forces. Therefore, a large Debye length, κ^{-1}, with a correspondingly high repulsive force predicts that the system is well dispersed, and does not necessarily correspond to optimum condition for flow and compaction of highly loaded particle assemblies. The larger the distance, the higher the expected viscosity of the concentrated particle suspension. The energy barrier required to prevent flocculation can be calculated[22;39] and for 50 nm particles, this barrier was estimated to be approx. 20 – 30 kT. However, for concentrated nanoparticle suspensions, this value should be considered qualitative for reasons discussed later. Thus, suspensions with electrolyte concentrations of 0.005 M or lower were expected to be stable. Yet, from a rheological perspective (as well as in effective particle compaction), the electrolyte concentration that allows the closest approach without flocculation represents the optimum condition. This condition is not fulfilled at any salt concentration for the nanopowder suspensions in Figure 6.

Generally, the surface potential of powders is assumed to be constant for varying concentrations of indifferent electrolytes. In studies by Iijima and Kamiya[16], and Lu[19] as well as in the calculation for Figure 6, the same assumption was made. As discussed earlier, this approach does not explain the experimental viscosity observations in Figure 4. However, when the measured zeta potential values listed in Table 1 were used in the DLVO calculations (Figure 7), the observed rheological behavior of the suspensions could be explained. At very low

`

concentrations (0.005 - 0.010 M), repulsive potentials overlap at large distances (soft sphere model), leading to large effective volume fractions. As the electrolyte concentration increased (*i.e.*, 0.025 – 0.040 M), the closest particle approach, hence the effective volume fraction, decreased. In addition, the repulsive interactions between particles increased because of the increase in surface potential (as measured zeta potential indicated), leading to a higher potential barrier against flocculation. A further increase in electrolyte concentration (0.050 - 0.1 M) resulted in screening of the double layer and flocculation ensued. It can be concluded that the optimum range of ion concentration for the powder suspensions of interest ranged between 0.020 and 0.040 M, which was in agreement with the experimental observations in Figure 4.

Table 1: Suspension pH, corresponding zeta potential values, and isoelectric points of alumina nanopowders as a function of salt concentration.

[NaCl] (M)	**pH at Φ = 0.20**	**ζ (mV)**	**IEP pH**
0	5.7	47	9.2
0.005	6.2	50	9.5
0.010	6.0	48	9.5
0.020	6.4	54	9.6
0.025	6.3	60	9.3
0.035	6.5	73	9.6
0.040	6.5	98	9.1
0.050	6.7	40	9.5
0.100	6.8	37	9.7

`

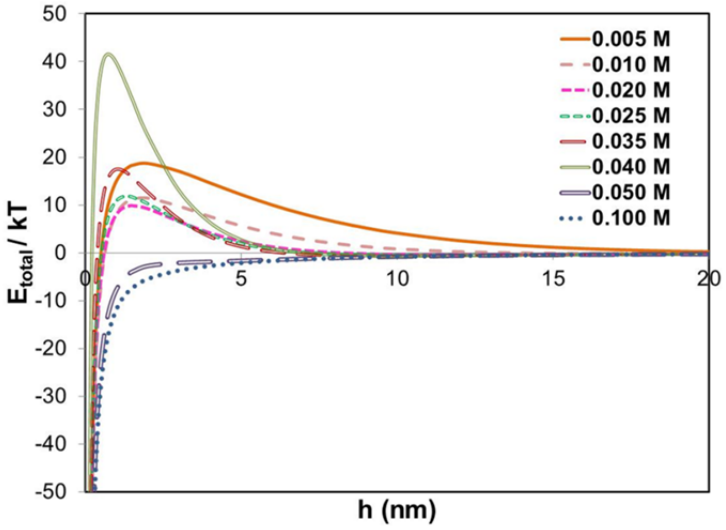

Figure 7: DLVO plots of alumina nanopowder suspensions for varying NaCl concentrations using experimental zeta potential values.

The results presented in Figures 6 and 7 should be considered qualitative. First, the HHF equation employs an approximate linear solution of the Poisson-Boltzmann equation rather than the exact nonlinear solution, which results in deviations at particle separations smaller than κ^{-1}. Secondly, the suspensions of interest are both concentrated and consist of nanopowders, which leads to a high degree of interfacial layer overlap. Van der Waals theory, for example, assumes the continuum within the system, which is only true for gaseous systems. Concentrated suspensions of nanopowders do not approximate gaseous systems, as they include a significant amount of interactions between particles. Therefore, the properties of the solvent may deviate from the bulk properties and may not be constant throughout the suspension. Moreover, a decrease of the dielectric constant of the medium caused by the presence of ions and their solvation was reported[41;42]. Carrique *et al.* [41] calculated the dielectric constant changes for concentrated suspensions and showed a decrease in dielectric constant even for particles with high zeta potentials. This decrease will result in a smaller Hamaker constant, leading to lower attraction energies and lower electrostatic repulsions between particles. Additionally, it was

shown that the zeta potential values were lower in concentrated suspensions than in dilute suspensions[17;43-45], resulting in lower repulsion between particles. Finally, two different Hamaker constant values are available in the literature and have been widely accepted for α–alumina (but none for γ– or δ–) particles in water: 3.67×10^{-20} J by Bergstrom[40] and 5.7×10^{-20} J by French[46], each resulting in different attraction energies. As for the Hamaker constant, it is also expected that the surface properties will be slightly different for particles consisting of γ– and δ–alumina phases.

Influence of Suspension pH

As we reported previously[31;48;49], there is a bound water layer around the particles that can be observed using LT-DSC and that may be used to understand the viscosity of concentrated nanopowder suspensions. Figure 9 shows the LT-DSC plots of the suspensions whose viscosities were provided in Figure 8. The similarity of the behaviors is noticeable.

Bound water melts at lower temperatures than bulk water[31;48], as seen in Figure 9a. Because the bound water layer moves with the particles, it cannot serve as a solvent. Therefore, the bound water should be considered as part of the solids and taken into account in the estimation of effective solids content. By deconvoluting the curves, the amount of bound water can be estimated[31] and Figure 9b shows the estimated bound water fractions. In calculations, we used the heat of fusion of pure water for the free water melting event, which is reasonable if only alumina nanopowder and water are present in the system[31]. The presence of additives may change the melting behavior of water. The presence of ions, for example, resulted in a depression of the freezing point as well as in a reduction in heat of fusion values. Even though the ionic strength of the suspensions was kept constant, the interaction of ions with the powder surface or with complex species formed by dissolved aluminum ions might have changed the properties of

`

the water. In fact, in Figure 9, the bound water was unaffected by the addition of NaCl, as expected for an indifferent electrolyte. However, the free water curve shifted to lower temperatures, as expected for a freezing point depression. As HCl and NaOH were added, the behavior of the bound water curves changed, indicating specific interactions of H^+ and OH^- with the alumina surface.

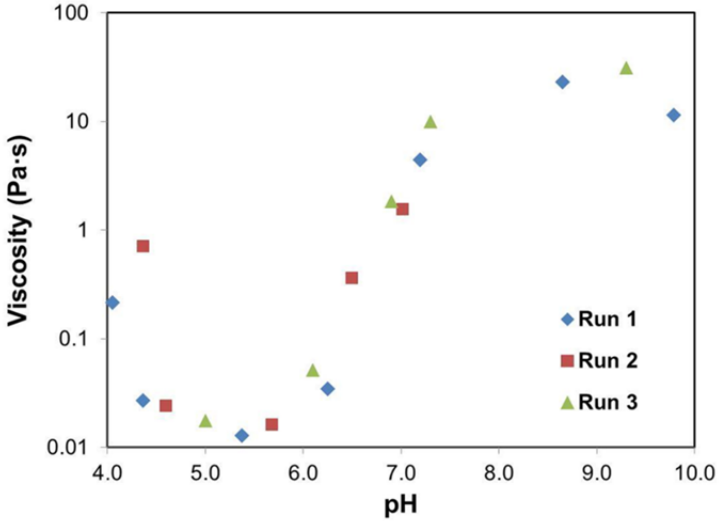

Figure 8: Effect of suspension pH on the viscosity of alumina nanopowder suspensions at constant ionic strength of 0.05 M. (Batch #: AAGL 1201, shear rate: 10 s^{-1}). Run 1, 2 and 3 represent measurements of different suspensions.

The large surface area of the nanopowders amplified the influence of the bound layer on the effective volume fraction. According to Figure 9, H^+ compressed the bound layer around the particles by releasing a fraction of the water, hence decreasing the effective solids volume fraction. On the other hand, addition of OH^- increased the bound layer thickness, increasing the effective volume fraction and viscosity of the suspensions. The bound water fractions estimated for the suspensions with pH values higher than 9.0 involved a high error margin caused by the deconvolution of highly overlapping peaks.

Our investigation suggests that the presence of a large bound water layer at high suspension pH for concentrated suspensions hindered the building of a repulsive barrier because of short interparticle separation distances. However, in dilute suspensions, the repulsive barrier may develop at high pH values because of large particle-particle separation.

The thickness of the bound layer was measured to be approx. 2 - 3 nm for various systems[50-54]. Karaman *et al*. [53] claimed that a gel layer forms around α-alumina particles. Colloidal probe atomic force microscopy showed that the thickness of the gel layer at IEP was approx. 15 nm, whereas at low pH it was approx. 3-5 nm, supporting our argument regarding bound layer and effective volume fraction. Hirata *et al*. [55] reported that by consolidating alumina compact, higher packing densities were obtained in an acidic medium compared to basic conditions.

In summary, potential determining ions, such as H^+ and OH^-, not only alter the electrostatic repulsion, but also the thickness of the bound layer, thus the effective volume fraction. The profound influence of the bound layer on concentrated suspensions led to suspension behavior that was quite different than that observed in dilute suspensions. Therefore, extreme care needs to be exercised in extrapolating experimental observations from dilute suspensions to concentrated ones. Likewise, the behavior of nanopowder suspensions is significantly different from that of large particle assemblies, hence one should be extremely cautious in extending the findings for micron-sized particle suspensions to that of nano-sized particles.

`

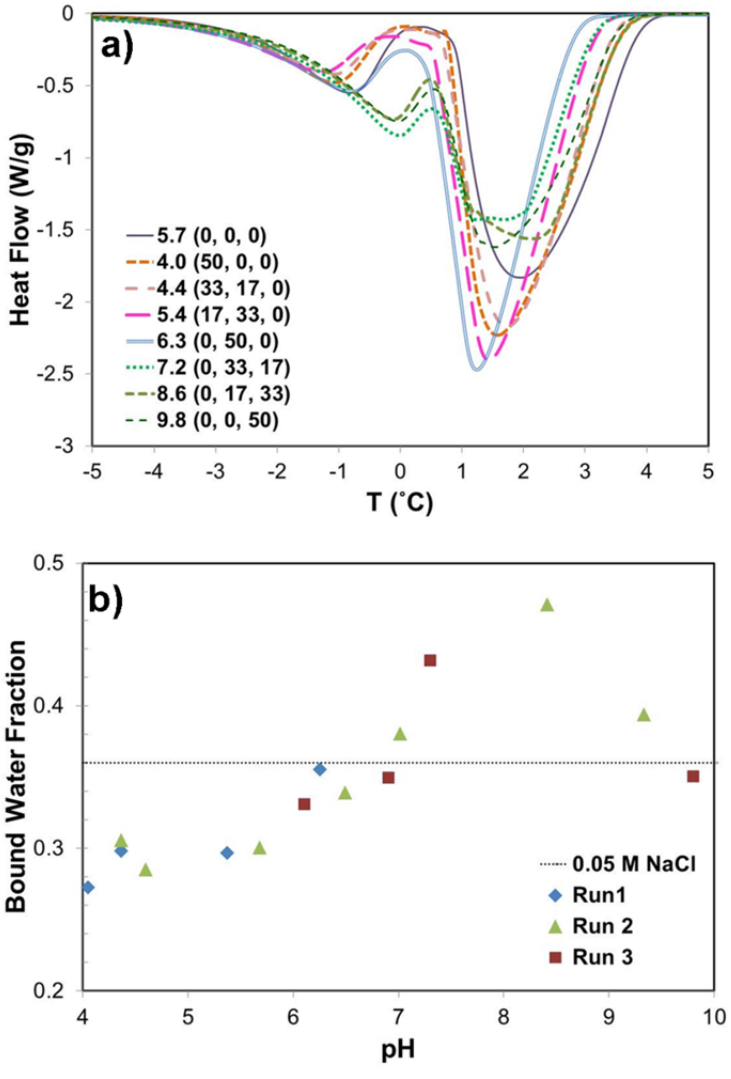

Figure 9: LT-DSC curves for alumina suspensions of Φ = 0.20 as a function of pH. (The heat flow values were expressed per gram of water for each sample. Legend: pH ([HCl], [NaCl], [NaOH] in mM))(a); Change in bound water fraction with respect to pH of the suspensions obtained by deconvolution of the LT-DSC curves. Run 1, 2 and 3 represent measurements of different suspensions (b).

Conclusions

Electrostatic stabilization of alumina nanopowder suspensions in the presence of potential determining ions (H^+ and OH^-) and indifferent electrolytes (NaCl) was studied.

Application of the DLVO theory to nanoparticle assemblies predicts that small changes in electrolyte concentrations result in significant changes in double layer thickness, hence in the

`

separation distance at which the DLVO forces are effective. That leads to a significant reduction in viscosity of concentrated alumina nanopowder suspensions ($\varphi \geq 0.20$) at low salt concentrations (*i.e.*, [NaCl] < 0.020 M). At higher salt concentrations ([NaCl] ≥ 0.040 M), higher viscosities were observed, presumably caused by screening of repulsive forces and compression of the double layer. However, at intermediate electrolyte concentrations (0.020 ≤ [NaCl] ≤ 0.040 M), higher zeta potentials resulting in low viscosities were observed. Suspension stability could be predicted by DLVO theory modified by Gregory, and Hogg, Healy, Fuerstenau (HHF) models; measured zeta potential values were also employed.

When potential determining ions were used, stable suspensions with low viscosities were obtained for $\varphi = 0.20$ in the $4 \leq pH \leq 7$ range. At pH values higher than the isoelectric point, (*i.e.*, pH ≥ 9.5), suspensions could not be stabilized by NaOH addition because of the low electrostatic repulsion and increased bound layer thickness.

LT-DSC showed that while the bound water peak remained unaffected by indifferent electrolytes, it increased with H^+ and decreased with OH^-. Thus, the potential determining ions not only tuned the electrostatic interactions, but also influenced the effective volume fraction by modifying the bound layer.

Acknowledgements

This research was supported by the National Science Foundation under grant no. CBET-0931038. The authors would like to thank Charles Glatz for making a Zetasizer available for this study and Tugce Karakulak for conducting TEM characterization of alumina nanopowders.

`

References

[1]Y. Ding, H. Chen, Z. Musina, Y. Jin, T. Zhang, S. Witharana and W. Yang, Phys. Scr., 014078 **(2010)**.

[2]A. Ghadimi, R. Saidur and H. S. C. Metselaar, Int. J. Heat Mass Transfer 54, 4051 **(2011)**.

[3]R. Prasher, P. E. Phelan and P. Bhattacharya, Nano Lett. 6, 1529 **(2006)**.

[4]S. Witharana, C. Hodges, D. Xu, X. Lai and Y. Ding, J. Nanopart. Res. 14, 1 **(2012)**.

[5]W. Yu and H. Xie, J.Nano Mat. 2012, 1 **(2012)**.

[6]S. K. Brar, M. Verma, R. D. Tyagi and R. Y. Surampalli, Waste Manage. (Oxford) 30, 504 **(2010)**.

[7]J. A. Lewis, J. Am. Ceram. Soc. 83, 2341 **(2000)**.

[8]W. M. Sigmund, N. S. Bell and L. Bergström, J. Am. Ceram. Soc. 83, 1557 **(2000)**.

[9]M. Baalousha, A. Manciulea, S. Cumberland, K. Kendall and J. R. Lead, Environ. Toxicol. Chem. 27, 1875 **(2008)**.

[10]A. M. E. Badawy, T. P. Luxton, R. G. Silva, K. G. Scheckel, M. T. Suidan and T. M. Tolaymat, Environ. Sci. Technol. 44, 1260 **(2010)**.

[11]J. M. Berg, A. Romoser, N. Banerjee, R. Zebda and C. M. Sayes, Nanotoxicology 3, 276 **(2009)**.

[12]C. Botta, J. Labille, M. Auffan, D. Borschneck, H. Miche, M. Cabié, A. Masion, J. Rose and J.-Y. Bottero, Environ. Pollut. 159, 1543 **(2011)**.

[13]S. Ghosh, H. Mashayekhi, B. Pan, P. Bhowmik and B. Xing, Langmuir 24, 12385 **(2008)**.

[14]P. Bowen, H. Hofmann, M. Staiger, R. Steiger, P. A. Brugger and K. Peternell, Key Eng. Mater. 206-213, 1977 **(2002)**.

[15]P. Bowen, C. Carry, D. Luxembourg and H. Hofmann, Powder Technol. 157, 100 **(2005)**.

[16]M. Iijima and H. Kamiya, Kona 27, **(2009)**.

[17]S. Jailani, G. V. Franks and T. W. Healy, J. Am. Ceram. Soc. 91, 1141 **(2008)**.

[18]Y. K. Leong and B. C. Ong, Powder Technol. 134, 249 **(2003)**.

[19]K. Lu, Ceram. Int. 34, 1353 **(2008)**.

`

[20]W. J. Tseng and C. H. Wu, Acta Mater. 50, 3757 **(2002)**.

[21]N. Hilal, D. Johnson, W. R. Bowen and P. M. Williams, in Atomic Force Microscopy in Process Engineering, Edited Butterworth-Heinemann Oxford **(2009)**, pp. 31.

[22]J. N. Israelachvili, Editor, *Intermolecular And Surface Forces*, 3 ed. Academic Press: Saint Louis, MO, USA **(2011)**.

[23]J. K. Beattie, J. K. Cleaver and T. D. Waite, Colloids Surf., A 111, 131 **(1996)**.

[24]M. Kobayashi, F. Juillerat, P. Galletto, P. Bowen and M. Borkovec, Langmuir 21, 5761 **(2005)**.

[25]M. P. B. van Bruggen, M. Donker, H. N. W. Lekkerkerker and T. L. Hughes, Colloids Surf., A 150, 115 **(1999)**.

[26]B. V. Velamakanni, J. C. Chang, F. F. Lange and D. S. Pearson, Langmuir 6, 1323 **(1990)**.

[27]T. D. Waite, J. K. Cleaver and J. K. Beattie, J. Colloid Interface Sci. 241, 333 **(2001)**.

[28]Y.-h. Hu, G.-z. Qiu and J. D. Miller, J Cent South Univ T 8, 18 **(2001)**.

[29]S. R. Raghavan, H. J. Walls and S. A. Khan, Langmuir 16, 7920 **(2000)**.

[30]W. E. Smith and C. F. Zukoski, J. Colloid Interface Sci. 304, 348 **(2006)**.

[31]S. Çinar, L. van Steenhuyse and M. Akinc, J. Am. Ceram. Soc. 96, 1077 **(2013)**.

[32]P. Mikkola, P. Ylhä, E. Levänen and J. B. Rosenholm, Ceram. Int. 30, 291 **(2004)**.

[33]L. F. Sharanda, A. P. Shimansky, T. V. Kulik and A. A. Chuiko, Colloids Surf., A 105, 167 **(1995)**.

[34]E. Tombácz and M. Szekeres, Langmuir 17, 1411 **(2001)**.

[35]Z. Zhou, P. J. Scales and D. V. Boger, Chem. Eng. Sci. 56, 2901 **(2001)**.

[36]R. Sprycha, J. Colloid Interface Sci. 127, 1 **(1989)**.

[37]J. Gregory, J. Colloid Interface Sci. 83, 138 **(1981)**.

[38]R. Hogg, T. W. Healy and D. W. Fuerstenau, J. Chem. Soc. Faraday Trans. 62, 1638 **(1966)**.

[39]U. Aschauer, O. Burgos-Montes, R. Moreno and P. Bowen, J. Dispersion Sci. Technol. 32, 470 **(2011)**.

[40]L. Bergstrom, Adv. Colloid Interface Sci. 70, 125 **(1997)**.

`

[41]F. Carrique, F. J. Arroyo, M. L. Jimenez and A. V. Delgado, J. Chem. Phys. 118, 1945 **(2003)**.

[42]G. Wang and P. S. Nicholson, J. Am. Ceram. Soc. 84, 1977 **(2001)**.

[43]C. R. Evanko, R. F. Delisio, D. A. Dzombak and J. W. Novak Jr, Colloids Surf., A 125, 95 **(1997)**.

[44]S. B. Johnson, A. S. Russell and P. J. Scales, Colloids Surf., A 141, 119 **(1998)**.

[45]N. J. Wagner and J. W. Bender, MRS Bulletin 29, 100 **(2004)**.

[46]R. H. French, J. Am. Ceram. Soc. 83, 2117 **(2000)**.

[47]F. Roelofs and W. Vogelsberger, J. Colloid Interface Sci. 303, 450 **(2006)**.

[48]C. Li and M. Akinc, J. Am. Ceram. Soc. 88, 1448 **(2005)**.

[49]C. Li, M. Akinc, J. Wiench, M. Pruski and C. H. Schilling, J. Am. Ceram. Soc. 88, 2762 **(2005)**.

[50]H. J. Butt, Biophys. J. 60, 1438 **(1991)**.

[51]J. Drelich, Z. Xu and J. Masliyah, Langmuir 22, 8850 **(2006)**.

[52]W. A. Ducker, T. J. Senden and R. M. Pashley, Langmuir 8, 1831 **(1992)**.

[53]M. E. Karaman, R. M. Pashley, T. D. Waite, S. J. Hatch and H. Bustamante, Colloids Surf., A 129–130, 239 **(1997)**.

[54]A. Verdaguer, G. M. Sacha, H. Bluhm and M. Salmeron, Chem. Rev. 106, 1478 **(2006)**.

[55]Y. Hirata, X. H. Wang, Y. Hatate and K. Ijichi, J. Ceram. Soc. Jpn. 111, 232 **(2003)**.

`

CHAPTER IV. COMBINED EFECT OF FRUCTOSE AND NaCl ON THE VISCOSITY OF ALUMINA NANOPOWDER SUSPENSIONS

(A paper to be submitted to the Journal of European Ceramic Society)

Simge Çınar, Daniel D. Anderson, Mufit Akinc

Department of Materials Science and Engineering,

Iowa State University, Ames, Iowa 50011

Abstract

Lower viscosities are required for many ceramic processing operations. Use of nanopowder slurries are challenging as they exhibit high viscosities. Low molecular weight saccharides were used to decrease the suspension viscosities of alumina nanopowder suspensions. It was also recently reported that suspensions with very low ionic strengths exhibit lower viscosities as they create high repulsive barrier in this range. In the present study, the effect of combination of these two additives on the viscosity is reported. Low temperature differential scanning calorimetry and *in situ* ATR-FTIR results showed that two additives act independently. Additionally, solids content term in the Krieger – Dougherty equation was modified by incorporating bound water layer and intrinsic viscosities of alumina nanopowder suspensions in the presence of additives were estimated from modified relation. Modified expression yields lower intrinsic viscosities because of the denser packing of more deformable agglomerates with the incorporation of bound water layer. The intrinsic viscosity of suspensions at the shear rate of 500 s^{-1} was decreased from 8.7 to 5.2 in the presence of combined additives. Improvement in green body microstructure in the presence of NaCl and Fructose was demonstrated with less porous bodies with higher structural integrity.

`

Introduction

Rheological properties of colloidal oxide powder suspensions greatly affect the quality of final product [1-6]. Stable suspensions of homogeneously dispersed powders yield lower viscosities than agglomerated ones. However, it is rather difficult to obtain lower viscosities when nanopowders were used. Nanopowders tend to agglomerate due to their high surface area and the small separation distances between particles in concentrated systems [1, 3, 7]. Thus, understanding the interaction between particles in concentrated suspensions is even more important.

Use of low molecular weight saccharides for viscosity reduction of alumina nanopowder suspensions was suggested by Schilling et al. [8] a decade ago. Since then, there has been several studies reported revealing their mechanism of viscosity reduction [8-13] and applications in various fields [10, 14, 15] .

Schilling et al [8] reported that additions of oligo- or polysaccharides decrease the viscosity of micron or sub-micron alumina suspensions; however, when nanopowders are used, the viscosity of suspensions increase. Bridging caused by large saccharide molecules was suggested as a reason for increase in viscosity. Instead, they used mono- or di-saccharides or sugar alcohols. Yar et al [13] studied the addition of polyalcohols which have similar chemical structure to low molecular weight saccharides. Polyalcohols have multiple hydroxyl groups on their linear or branched backbones, while saccharides have hydroxylated ring structure. They concluded that polyalcohols adsorb on the alumina surface and reduce the viscosity. Li and Akinc [11, 12] related the effect of fructose to availability of water in suspensions. They reported that a fraction of water associated with powder, called “bound water”, which has lower mobility than the bulk water. Falkowski et al [10] used a derivative of fructose molecule, 1-O-methyl-D-

`

fructose, glucose, 3-O-acrylic-D-glucose, to explain the effect of chemical structure on viscosity of alumina suspensions. They showed that substitution of $–OCH_3$ for OH group decreases the viscosity of suspensions even further. They supported the mechanism of "bound water" to explain their observation by the fact that substituted molecules are relatively less compatible with water, so they will release more bound water or associate weakly with bound water leading to lower viscosities. We recently reported that bound water is directly related with the powder surface area, so although it can be negligible in micron size powder suspensions, its influence on nanopowder suspensions is significant [9]. The effect of fructose in viscosity reduction of alumina nanopowder suspensions cannot be explained with steric or electrostatic mechanisms alone, but its presence modifies the bound water layer, decreases the effective solids content, thus the viscosity of suspensions [9].

While fructose molecules are able to modify the bound water, addition of NaCl does not lead to any changes in bound water yet it decreases the viscosity of the suspension [9]. Effect of NaCl on the viscosity of alumina nanopowder suspensions has been recently studied by our group [16]. We showed that addition of very small amounts of NaCl lead to a substantial decrease in viscosity which cannot be explained with bound water phenomena but modification of the electrostatic double layer.

In the current study, we aimed to investigate these two effects concurrently, bound layer modification and control of interparticle forces to obtain suspensions with very low viscosities while testing our ability to design better systems with our current knowledge. We first reported the rheological behavior of suspensions and compare the individual and combined effect of additives on viscosity, then carried out experiments using low temperature differential scanning calorimetry (LT-DSC) and *in situ* attenuated total reflectance Fourier transform infrared

`

spectroscopy (ATR-FTIR) to reveal the mechanism of combined effect. Viscosities of suspensions were modeled by introducing the effect of bound water content to the solids content in the Krieger – Dougherty equation [17, 18]. Physical and chemical properties of the systems were discussed in terms of the equation parameters, specifically intrinsic viscosity. Lastly, we compared the green body microstructure of slip cast alumina suspensions with and without additives.

Experimental

Materials

Alumina nanopowder (Lot number: AAGL 1201) was purchased from Nanophase Technology Corporation (Burr Ridge, IL). TEM micrograph of powders is shown in Figure 1. The powders with purity of ≥ 99.5% have phase distribution of γ/δ ≈ 70:30, density of 3.67 g/cm^3 and specific (BET) surface area of 38.8 m^2/ g. Average particle size of powders were 42 nm and 30 ± 21 nm as determined by BET surface area and TEM micrographs, respectively. More than 99 % of the powders were in the range between 10 nm and 100 nm in diameter.

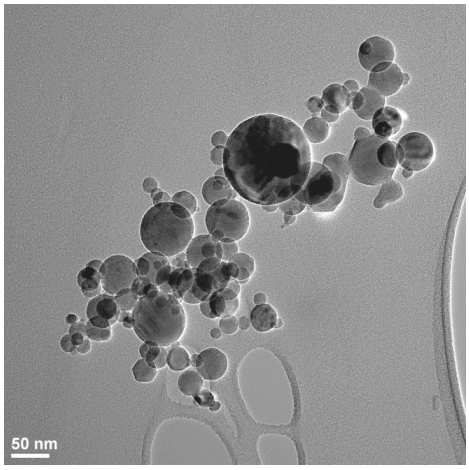

Figure 1: TEM micrograph of alumina nanopowder. In general particles are spherical with considerable size distribution. Sharp boundaries on overlapping particles indicate that particles are not agglomerated.

`

D-fructose (99%) and NaCl (ACS certified) were purchased from Alfa Aesar (Lancashire, UK) and Fisher Scientific (Fair Lawn, NJ), respectively. Figure 2 shows the chemical structure of fructose molecule.

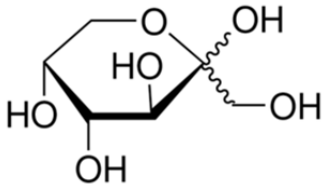

Figure 2: Chemical structure of D-fructose. Fructose has five membered ring with five hydroxyl groups.

Ultrapure water with the resistivity of 18.2 MΩ·cm and total organic content (TOC) < 3ppm (Milli-Q Gradient A-10 model, Millipore Company, Billerica, MA) was used for sample preparation.

Suspension Preparation

For the preparation of suspensions, the alumina content was calculated as the volume percentage of the suspension. The fructose addition was calculated as weight percentage of the dried alumina powder. The volume of fructose was taken into account in calculating the required volume of water to maintain volume percent of solids in suspension accurate. NaCl amount was determined as a molarity of solvent (water + fructose) content. Its effect in suspension volume was negligible.

Alumina nanopowder was dried at 110 ˚C for 2 hours prior to preparation of suspension to minimize the level of moisture content. Required amount of fructose was mixed with water, then alumina powder was added slowly. The suspension was shaken for 24 hours to establish equilibrium condition. NaCl was added 2 hours prior to analysis.

`

Viscosity Measurements

A rheometer (AR 2000ex model, TA Instruments, New Castle, DE) with a cone and plate geometry having 4˚ cone angle and 40 mm steel plate was used for viscosity measurements. To prevent evaporation of water, a solvent trap was used. The temperature was kept constant at 25 ˚C by use of Peltier plate with a precision of ± 0.1 ˚C. Ten viscosity measurements were recorded per half loop of two consecutive complete loops over the shear rate range 0.5 – 500 s^{-1}. The shear rate was ramped up in the first half, and ramped down in the second half of the one complete loop. When the measurements were reproducible after the first loop, the data points corresponding to final half of the second loop was used for analysis.

Low Temperature Differential Scanning Calorimetry (LT-DSC)

A differential scanning calorimeter (Model Q20, TA Instruments, New Castle, DE) was used for determining the bound water content of the suspensions. Suspensions with similar water content (around 5 – 10 mg) were tested in hermetically sealed aluminum pan and lids. The samples were cooled down to -25 °C, held there for one minute for equilibrium, then the temperature was increased to 10 °C with the heating rate of 1 °C/min. DSC plots were normalized for total water content for comparison of water melting events.

In situ Attenuated Total Reflection – Fourier Transform Infrared (ATR-FTIR) Spectroscopy

A Frontier model FTIR spectroscope with a single reflection ATR attachment (Perkin Elmer, Waltham, MA) was used. Samples were directly placed on the diamond crystal. For each sample, four scans with a spectral resolution of 4 cm^{-1} were recorded at room temperature. Spectrum 10 was used for data processing. Baselines were aligned at 4000 cm^{-1} for comparing spectra.

`

Slip Casting

Pellets were cast using gypsum plate as base with an acrylic cylindrical cavity (around 2.5 cm in diameter, 1 cm in height). Alumina nanopowder suspensions with 20 vol% solids were used for casting. To account for material loss into the gypsum sink and evaporation of water, additional suspension was added as needed. The pellets were dried for 48 hours at room temperature and kept in desiccator for analysis. Pellets were fractured for visual and microscopic observation.

Results and Discussion

Viscosity

Individual effects of fructose and NaCl on the viscosity of alumina nanopowder suspensions were reported before [9-12, 16]. It was shown that while fructose reduces the viscosity by replacing the bound water on the surface, NaCl additions modifies the electrostatic double layer [9, 16]. Figure 3 and Table 1 show the effect of fructose, NaCl and their combination on the suspension viscosity. 4 wt% of fructose addition was chosen as benchmark fructose concentration since it is high enough concentration to show the reduction in viscosity. Previous work showed that 0.01 M NaCl gives the lowest viscosity for similar alumina nanopowder suspensions. The data in Table 1 shows that combination of fructose and NaCl leads to much lower viscosities than only fructose or only NaCl additions.

`

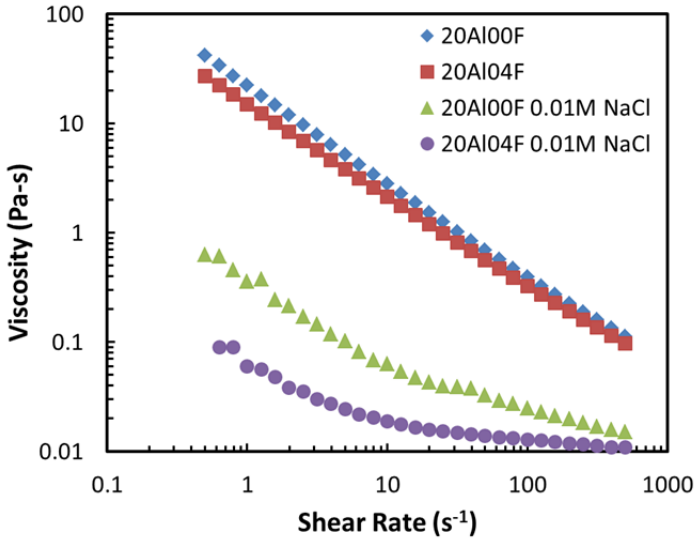

Figure 3: Viscosity of suspensions (20 vol%) with no addition (20Al00F), 4 wt% fructose (20Al04F), 0.01 M NaCl (20Al00F 0.01 NaCl) and the combination of 4 wt% and 0.01 M NaCl (20Al04F 0.01 M NaCl).

Table 1: Viscosity at shear rate of 100 s^{-1} for 20 vol% suspensions with Fructose and NaCl additions. "xxAl yyF" indicates the xx vol% of alumina suspensions with the addition of yy wt% of fructose additions.

	Viscosity (Pa·s) ($\dot{\gamma}$= 100 s^{-1})	**Viscosity Reduction* (%)**
20Al 00F	0.3922	0
20Al 04F	0.3254	17
20Al 00F 0.01 M NaCl	0.0250	94
20Al 04F 0.01 M NaCl	0.0129	97

**Relative to control suspensions of 20Al00F.*

The effect of combined addition on suspension viscosity was studied as a function of solids content and NaCl concentration by keeping the fructose to dry alumina powder ratio constant. Viscosity measurements at the shear rate of 100 s^{-1} were plotted in Figure 4.

Viscosity of suspensions increases with increase in solids content as expected. Combined additions effectively reduced the viscosity of suspensions at all solids contents. While

`

suspensions could not even be homogeneously prepared in the other cases (without addition or only fructose addition), with the combined additions, the viscosity measurements could be conducted reproducibly at solids content as high as Φ = 0.50. However, the data was limited to NaCl concentrations of 0.03 M – 0.06 M.

The viscosity showed minima at certain level of NaCl concentration. Similar behavior was observed and discussed before when only NaCl was added to the suspensions [16]. It was related to the compression of the electrostatic double layer and increase in zeta potential of powders in the specific range of NaCl concentrations leading to relatively short but strong interparticle repulsion and lower viscosities. Further increase in NaCl concentration screened the repulsive forces completely and flocculated suspensions were obtained.

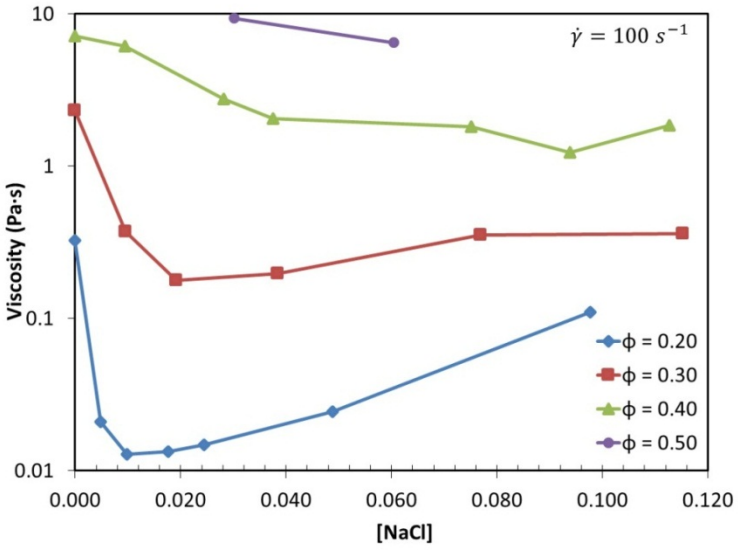

Figure 4: Viscosity of suspensions with solids loading of 0.20 as a function of solids content and NaCl concentration. Fructose concentration was kept constant at 4 wt% of dried alumina powder.

Bound water

The use of low temperature differential scanning calorimetry (LT-DSC) for determination of the bound water content was previously reported [9, 16]. Bound water content decreased with

`

fructose concentration, but was not affected by presence of NaCl. As shown in Figure 5, the presence of NaCl and fructose together do not change the behavior of bound water while shifting the melting of free water to lower temperatures as expected from melting point depression with ions. This observation indicates that NaCl does not change the bound water content whereas fructose primarily lowers it.

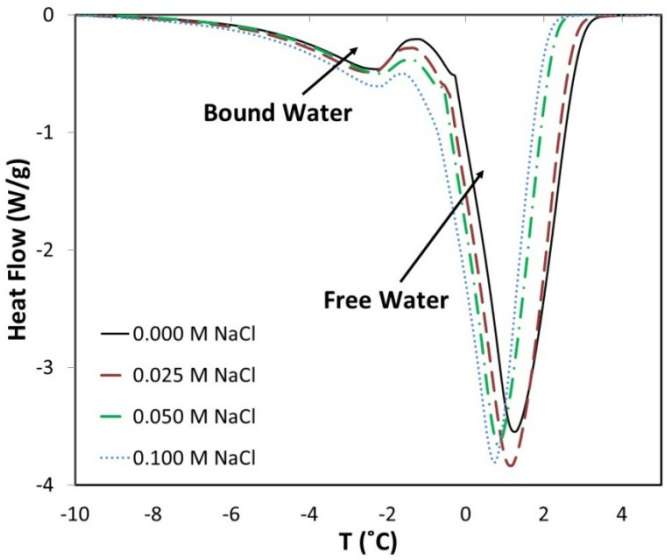

Figure 5: DSC plots of alumina suspensions with 4 wt% fructose additions and varying NaCl concentrations. Heat flow was normalized with respect to total water content. Note the shift in free water peak to lower temperatures with NaCl concentration.

Surface interactions with NaCl and Fructose

Chemical interactions between alumina, fructose and NaCl were investigated by *in situ* ATR-FTIR Spectroscopy. By subtracting the dominant water spectra from the original spectra, the changes in the spectra were amplified (Figure 6). Similar study was reported before for alumina ascorbic acid aqueous suspensions [19]. Absorbance of water hydroxyls shows a broad band between 3600 cm^{-1} and 3000 cm^{-1} (stretching), at 2150 cm^{-1} and 1627 cm^{-1} (bending). In the presence of alumina nanopowder, the intensity of asymmetric stretching (around 3515 cm^{-1}) increased while the intensity of symmetric stretching (around 3200 cm^{-1}) diminished. Gaigeot et

`

al. [20] and Sulpizi et al. [21] assigned these peaks with weak out of plane (liquid like structure) and strong in-plane (ice like structure) H-bonds arising from oxide-water interfaces. Similarly, bending vibrations at 1627 cm^{-1} diminishes when alumina was present. Since no change observed in bending vibrations at 2150 cm^{-1}, the water content of suspensions should be considered comparable.

Fructose molecule contains hydroxyls as well; however, generally those peaks are overlapped with water hydroxyl and not easily distinguished. When the water spectrum was removed, the contribution of hydroxyl stretching and bending vibrations of fructose molecule could be distinguished between 3200 cm^{-1} and 2980 cm^{-1}, and between 1780 cm^{-1} and 1400 cm^{-1} in aqueous solution spectra. These contributions lead to intensity changes in suspensions of alumina. Lower transmittance in 3200 cm^{-1} – 2980 cm^{-1} region and higher transmittance in 1780 cm^{-1} – 1400 cm^{-1} region were observed in the spectra of fructose containing alumina suspensions. Hydration of NaCl could also be distinguished between 3380cm^{-1} and 3200 cm^{-1} in alumina suspensions.

Table 2 shows chemical assignments for fructose absorptions. In the presence of alumina the bands at 1415 cm^{-1}, 1344 cm^{-1}, 1104 cm^{-1}, 1084 and 1064 cm^{-1} diminished. Changes in the spectra could be related with the interactions between alumina surface and fructose molecules. Addition of NaCl either in aqueous fructose solution or in alumina suspensions with fructose addition did not lead to any changes in fructose interactions. The fact that there is no detectable effect of NaCl in fructose – alumina interaction supports our argument that the effects of fructose and NaCl in alumina system are independent.

`

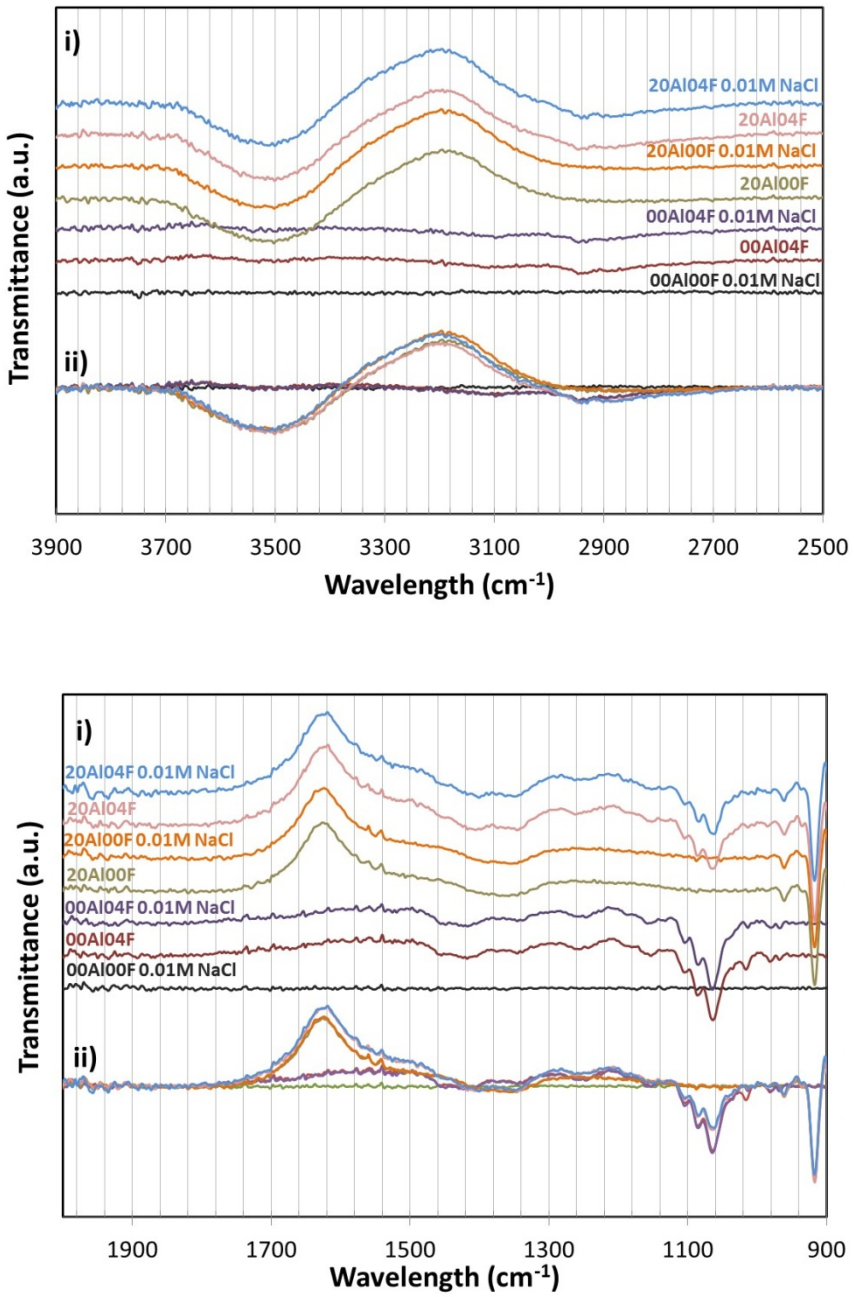

Figure 6: In situ ATR-FTIR spectra of samples in the wavelength range of 4000 cm^{-1} – 2500 cm^{-1} (a) and 2000 cm^{-1} – 900 cm^{-1} (b). "xxAlyyF" represents xx vol% alumina suspension with the addition of yy wt% fructose. Curves split at top (i) to distinguish the features of the bands and overlay at bottom (ii) to amplify the intensity differences. Horizontal lines are guide to eye.

`

Table 2: Chemical assignment of IR peaks for aqueous fructose solutions.

Band (cm^{-1})	**Assignment [22]**
2942	ν_{CH2} asymmetric
2893	ν_{CH2} symmetric
1415	$\delta_{C\text{-}O\text{-}H}$
1344 (C1)	$\delta_{C\text{-}O\text{-}H}$
1292 (C1)	$\delta_{C\text{-}O\text{-}H}$
1210	ω_{CH2}
1154	
1104 (endo)	ν_{CO}
1084 (endo)	
1064	ν_{CO}
1016	$\delta_{C\text{-}O\text{-}H}$
981 (exo)	ν_{CO}
968 (exo)	

** v: stretch, δ: deformation, ω: wagging, endo: endocyclic, exo: exocyclic, C1:Carbon 1 in fructose chain.*

Modeling Suspension Viscosity

Krieger – Dougherty (K-D) equation relates the solids content in concentrated suspensions and was selected to model the suspensions viscosities because of its effectiveness, simplicity and versatility (Equation 1). K-D equation is a semi-empirical relation whose validity was proven for micro-size powder suspensions for a broad range of solids content.

$$\frac{\eta}{\eta_0} = \left[1 - \frac{\phi}{\phi_{max}}\right]^{-[\eta]\phi_{max}} \qquad \text{(Equation 1)}$$

where η, η_0, and $[\eta]$ are the viscosity of suspension, base fluid, and intrinsic viscosity and Φ and Φ_{max} are the solids content of particles and the maximum achievable solids content for the system, respectively.

`

Even though suspension viscosity depends only on Φ, Φ_{max} and $[\eta]$, it is not straight forward to determine these parameters because of their complex nature.

First of all, suspensions in this system showed strong shear thinning behavior, especially at high solids contents; however, K-D Equation does not incorporate shear rate. Since other parameters are dependent on the shear rate, K-D equation needs to be considered at a fixed shear rate.

Recently, Jamali et al. [23] reported the origin of shear thinning behavior as lack of resistance to external/internal-particle forces on the colloidal particles. According to their study, at high shear rates hydrodynamic forces overcome interparticle forces. Since the K-D Equation is mainly dependent on hydrodynamic relations (originally derived for hard sphere systems), we preferred to use higher shear rates. The absence of plateau region [24] or shear thickening behavior [23] around 500 s^{-1}, which was the maximum shear rate applied in the present study, might indicate that the influence of interparticle interactions were not completely diminished at this shear rate. The effects of shear rate on individual parameter were also discussed below.

As mentioned before, the K-D equation was originated as hard sphere model. Therefore, solids content parameter, Φ, needs to be expressed as effective solids content, Φ_{eff}, to reflect steric [24, 25] or electrical double layer, EDL, contribution to the solids content [24, 26, 27]. Especially in nanopowder systems, existence of bound water layer amplifies the effect of the solids content on viscosity [28-30]. Therefore, estimated bound water fractions calculated from DSC data was introduced to the effective solids content term (Equation 2).

$$\phi_{eff} = \frac{V_S + V_{BW}}{V_{Total}} \qquad \text{(Equation 2)}$$

`

where, V_S, V_{BW}, and V_{Total} are the volumes of solids, bound water and total suspension, respectively. Similar treatment was employed previously to account for the swelling of the particles [31, 32]. In that case, the solids content was multiplied by the swelling ratio, α, instead.

In K-D relation, the solids content is normalized with respect to maximum achievable solids content, Φ_{max} so the physically unrealistic values packing of particles above close-packed spheres are avoided. Random packing of monodispersed hard spheres, Φ_{max} is theoretically 0.64, but experimentally may vary from 0.495 to 0.54. As shear rate is increased, the particles can pack more densely, and Φ_{max} increases to 0.74 theoretically and 0.605 experimentally [17, 33, 34]. Polydispersed particles, on the other hand, can pack even more densely, so much higher values of Φ_{max} are possible [17, 25, 35, 36]. Deformability of the particles, as in the presence of EDL or bound layer, also leads to higher Φ_{max} values [24, 25]. The K-D equation is independent of the interparticle interactions. However, because of the extreme crowding in nanopowder systems, particles tend to form agglomerates that could not be broken by shear. For these systems, the flow units are considered as primary agglomerates rather than individual particles. The formation of agglomerates lowers the value of Φ_{max} as a result of interparticle interactions [26, 35, 37-41]. However, there is no commonly accepted way to determine the value of Φ_{max} [17]. In the present study, Φ_{max} was modified with $\Phi_{eff,max}$, which is the maximum achievable solids content experimentally. The errors stemmed from this assumption are discussed later.

Using the effective solids content, Φ_{eff} and maximum effective solids content, $\Phi_{eff,max}$, we calculated the intrinsic viscosities, [η], as shown in Table 3. From the viscosity data, [η] was estimated over the solids content by regression. Table 3 compares the K-D and the modified relation at the shear rates of 0.5 s^{-1}, 50 s^{-1} and 500 s^{-1}.

`

Table 3: Application of Krieger-Dougherty equation to alumina suspensions at different shear rates.

Shear Rate (s^{-1})	**K-D relation**		**Modified K-D relation**	
	[η]	**R^2**	**[η]**	**R^2**
0.5	39.7	0.874	16.9	0.872
50	27.9	0.968	11.6	0.968
500	20.9	0.971	8.7	0.963

For the Krieger-Dougherty relation, Φ_{max} was taken as 0.495 at low shear rates (0.5 s^{-1}) and 0.54 at high shear rates (50 s^{-1} and 500 s^{-1}). Φ was assumed to be concentration of "dry" powders. In modified Krieger – Dougherty application, Φ_{max} was determined experimentally and Φ is replaced the estimated Φ_{eff} to account for the bound water layer. The equation could be fitted for the solids content between 0.0- 0.20 (five data points). At higher concentration the viscosity increased dramatically rendering these equations unreliable.

Intrinsic viscosities predicted by K-D relation were significantly higher than 2.5, which is the intrinsic viscosity value calculated for perfect hard spheres by Einstein. Rubio – Hernandez et al. [27] reported similarly high intrinsic viscosities (≈ 32.1 for similar suspension pH) for extremely dilute suspensions ($\Phi \leq 0.006$) of irregular shape γ-alumina particles with average particle size of 100 nm by including the effect of EDL. Intrinsic viscosity is known to be a function of particle size, morphology and flexibility [42]. Deviation of spherical shape leads to increase in intrinsic viscosity values because of the increase in effective particle size [24, 25] whereas deformability leads to decrease due to the capability of particles to adapt to flow or presence of other particles [17, 24]. Rubio – Hernandez related the high values of intrinsic viscosities to shape irregularities [27]. However, individual particles that are used in our study are almost perfectly spherical, but similarly high intrinsic viscosity values were obtained.

`

If the flow units were considered as agglomerates rather than individual particles, then [η] becomes a function of interparticle forces [26, 27, 37, 43, 44]. At high solids content, agglomeration is inevitable. Because of the voids in agglomerates, the intrinsic viscosities were expected to be higher [37, 45]. However, since we assume that the bound layer around powders is part of the particle, the packing of particles would be much denser than "dry" powders (Figure 7). Along with the effect of polydispersity in packing (the higher the polydispersity, the denser the packing), fully packing is plausible. Also, deformability of the agglomerates would result in more round shapes (sphere-like) flow units compared to the clusters of hard spheres leading to lower intrinsic viscosities. Therefore, lower intrinsic viscosities were expected when the modified relation was employed due to dense packing of more spherical units (Table 3).

As seen in Table 3, intrinsic viscosity of suspensions decreased with increased in shear rates as expected due to the more spherical shape of clusters [30, 45, 46]. This also leads to an increase in $\Phi_{eff,max}$ value which was not included in our calculations. Therefore, the intrinsic viscosity values reported here predict lower values.

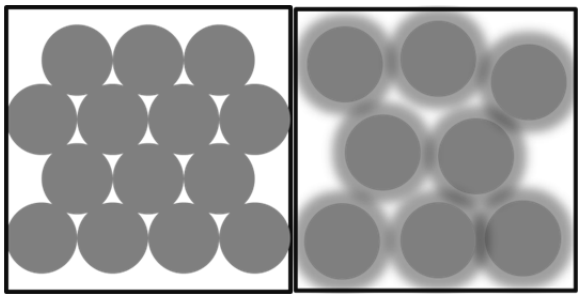

Figure 7: Crowding of particles in the presence of bound layer. Note that the system has fewer particles, but is more crowded in the presence of bound layer (right) relative to hard spheres (left).

The effects of fructose, NaCl and their combination on the intrinsic viscosity of alumina powders in aqueous suspensions were listed in Table 4. Intrinsic viscosity values estimated from

`

the K-D equation follows the same pattern with viscosity. Suspensions with lower viscosity have lower intrinsic viscosity which is generally attributed to the size of agglomerates. However, as the effective solids content due to bound water layer was is taken into consideration, intrinsic viscosity increases rather than decrease with the addition of fructose.

Table 4: Application of Krieger-Dougherty equation to alumina suspensions with NaCl and fructose at shear rate of 500 s^{-1}.

Sample	K-D relation		Modified K-D relation	
	[η]	R^2	[η]	R^2
without addition	20.9	0.971	8.7	0.963
4 wt% fructose	17.8	0.985	9.4	0.973
0.01 M NaCl	16.1	0.894	6.6	0.881
4 wt% fructose & 0.01M NaCl	11.1	0.971	5.2	0.973

For the Krieger-Dougherty relation, Φ_{max} was taken as 0.54 at 500 s^{-1}. Φ was assumed to be concentration of "dry" powders. In modified Krieger – Dougherty application, Φ_{max} was determined experimentally and Φ is replaced the estimated Φ_{eff} to account for the bound water layer.

Interparticle interaction of nanopowders can be adjusted by changing the pH or ionic strength of the solutions[16]. Since the bound layer fraction did not change in the presence of NaCl, the intrinsic viscosities of suspensions would be directly related to the interparticle forces. Therefore, the lowest intrinsic viscosity was achieved when the NaCl concentration was 0.01 M corresponding to lowest viscosity [16]. The intrinsic viscosity was calculated as 6.6 at 500 s^{-1}. The decrease in intrinsic viscosity with respect to the suspensions without addition (Table 4) shows the effectiveness of interparticle interactions in suspension.

When the two mechanisms were combined, the intrinsic viscosity of the suspensions could be decreased from 8.7 (without addition) to 5.2. Even though addition of only fructose led to

`

increase in intrinsic viscosity from 8.7 to 9.4, with the addition of NaCl the intrinsic viscosity decreased to 5.2. It can be predicted that as higher shear rates (> 500 s^{-1}) were applied to the suspensions, lower viscosities, hence lower intrinsic viscosities could be achieved if the plateau region could be obtained without forming hydroclusters. However, we would not expect to obtain intrinsic viscosities as low as 2.5 because of the agglomerated nature of nanoparticle systems.

Modeling of the alumina nanopowder suspensions showed that the K-D equation successfully predicts the behavior of suspension viscosity with respect to the solids content. However, because of having only one variable, intrinsic viscosity, [η], the equation is not equally successful as predicting the physical nature of the complex system. For better understanding of the system, effective and maximum achievable solids content terms of the K-D equation need to be modified to incorporate the bound layer and agglomeration of the primary particles so that the role of additives on viscosity reduction mechanisms can be distinguished. As a result, more realistic intrinsic viscosities were estimated.

Slip Casting

Slurries containing NaCl and fructose were slip cast and compared to the casts without additives to access the influence of these additives on the microstructure of the green body. Figure 8 shows the images and SEM micrographs of the fracture surfaces of cast pellets. Without any addition, highly porous structures were observed (Figure 8a). With the addition of fructose, more uniform structure with smaller pores was observed (Figure 8b). Montero et al. [15] reported the use of fructose as a porosity promoter for applications of porous ceramics. They obtained microstructures with submicron-sized pores after sintering the mesoporous green bodies at around 1300 - 1400 °C. The degree of porosity was seen to significantly decrease when NaCl

`

was introduced, which was attributed to the lower viscosity of the suspension (Figure 8c). Samples without fructose (Fig. 8a and 8b) had much lower green body strengths than the ones with fructose (Fig. 8c and 8d). Samples containing NaCl and fructose (Figure 8d) were free of micron-size pores and much stronger.

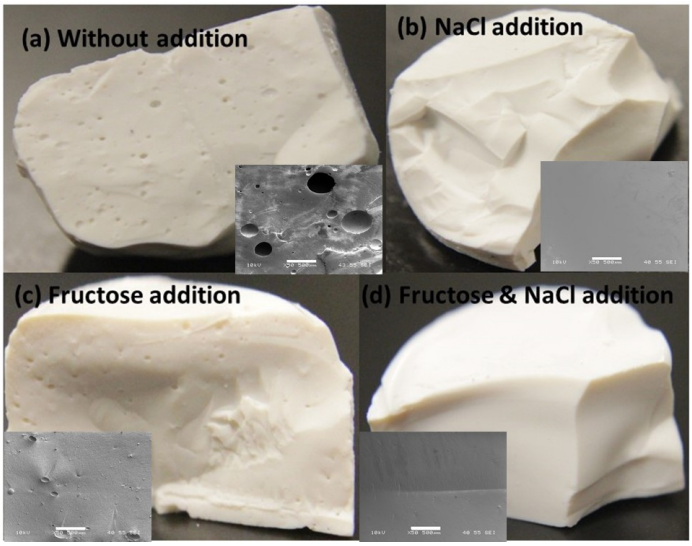

Figure 8: Images of fracture surface of slip cast pellets. All samples prepared from suspensions with 20 vol% alumina. Concentrations of additives were 4 wt% fructose and 0.01 M NaCl. SEM images (inset) are for comparison of microporosity. Scale bars for these images 0.5 are mm.

Conclusions

The effect of two additives, fructose and NaCl, operating independently were combined and the resulting suspensions were compared in terms of their effect on suspension viscosity, bound water layer content, physical behavior, and green body integrity.

Suspensions having both additives exhibited much lower viscosities than the ones with fructose and NaCl alone. Combination of fructose and NaCl was effective even at very high solids content ($\Phi \approx 0.50$). At $\Phi = 0.20$, the viscosity of suspensions could be reduced by 97% with fructose and NaCl combined addition.

`

Varying NaCl concentration did not change the melting behavior of bound water. While the chemical structure of fructose was altered in the presence of alumina, addition of NaCl did not have any effect on fructose structure. Addition of fructose and NaCl appeared to reduce the suspension viscosity independently.

The Krieger – Dougherty relation was modified by including the effect of bound water layer to the effective solids content and maximum achievable solids content parameters. Estimated intrinsic viscosities for different conditions were compared. Alumina nanopowder suspensions without any addition results in very high intrinsic viscosities (around 40) by K-D at the shear rate of 500 s^{-1}. By introduction of the bound water layer effect, the estimated value decreased to 8.7. In the presence of bound water layer, much denser agglomerates with smoother surfaces would explain the lower values. At 0.01M NaCl, which was the most effective in lowering the viscosity, the lowest intrinsic viscosity was estimated as 6.6. Combined additives lead to intrinsic viscosities as low as 5.2.

Slip cast samples without additives show low green body strength with micron size pores. Addition of fructose lowered the pore size and improved structural integrity. By combining the fructose and NaCl, stronger samples with only mesopores were obtained.

Acknowledgement

This research was supported by the National Science Foundation under grant no. CBET-0931038.

References

[1] Azar M, Palmero P, Lombardi M, Garnier V, Montanaro L, Fantozzi G, et al. Effect of initial particle packing on the sintering of nanostructured transition alumina. J Eur Ceram Soc 2008; 28: 1121-8.

`

[2] Chong JS, Christiansen EB, Baer AD. Rheology of concentrated suspensions. J Appl Polym Sci 1971; 15: 2007-21.

[3] Danelska A, Ulkowska U, Socha RP, Szafran M. Surface properties of nanozirconia and their effect on its rheological behaviour and sinterability. J Eur Ceram Soc 2013; 33: 1875-83.

[4] Lewis JA. Colloidal processing of ceramics. J Am Ceram Soc 2000; 83: 2341-59.

[5] Sigmund WM, Bell NS, Bergström L. Novel Powder-Processing Methods for Advanced Ceramics. J Am Ceram Soc 2000; 83: 1557-74.

[6] Studart AR, Pandolfelli VC, Tervoort E, Gauckler LJ. Selection of dispersants for high-alumina zero-cement refractory castables. J Eur Ceram Soc 2003; 23: 997-1004.

[7] Schneider M, Claverie J, Graillat C, McKenna TF. High solids content emulsions. I. A study of the influence of the particle size distribution and polymer concentration on viscosity. J Appl Polym Sci 2002; 84: 1878-96.

[8] Schilling CH, Sikora M, Tomasik P, Li C, Garcia V. Rheology of alumina–nanoparticle suspensions: effects of lower saccharides and sugar alcohols. J Eur Ceram Soc 2002; 22: 917-21.

[9] Çinar S, van Steenhuyse L, Akinc M. Elucidation of Viscosity Reduction Mechanism of Nano Alumina Suspensions with Fructose Addition by DSC. J Am Ceram Soc 2013; 96: 1077-84.

[10] Falkowski P, Bednarek P, Danelska A, Mizerski T, Szafran M. Application of monosaccharides derivatives in colloidal processing of aluminum oxide. J Eur Ceram Soc 2010; 30: 2805-11.

[11] Li C, Akinc M. Role of Bound Water on the Viscosity of Nanometric Alumina Suspensions. J Am Ceram Soc 2005; 88: 1448-54.

[12] Li C, Akinc M, Wiench J, Pruski M, Schilling CH. Relationship Between Water Mobility and Viscosity of Nanometric Alumina Suspensions. J Am Ceram Soc 2005; 88: 2762-8.

[13] Yar Y, Acar FY, Yurtsever E, Akinc M. Reduction of Viscosity of Alumina Nanopowder Aqueous Suspensions by the Addition of Polyalcohols and Saccharides. J Am Ceram Soc 2010; 93: 2630-6.

[14] Bednarek P, Szafran M. Thermal decomposition of monosaccharides derivatives applied in ceramic gelcasting process investigated by the coupled DTA/TG/MS analysis. J Therm Anal Calorim 2012; 109: 773-82.

[15] Montero M, Molina T, Szafran M, Moreno R, Nieto MI. Alumina porous nanomaterials obtained by colloidal processing using d-fructose as dispersant and porosity promoter. Ceram Int 2012; 38: 2779-84.

`

[16] Çınar S, Akinc M. Electrostatic Stabilization of Alumina Nanopowder Suspensions. Sci Adv Mat 2013 (accepted);

[17] Genovese DB. Shear rheology of hard-sphere, dispersed, and aggregated suspensions, and filler-matrix composites. Adv Colloid Interface Sci 2012; 171–172: 1-16.

[18] Krieger IM, Dougherty TJ. A mechanism for non-Newtonian flow in suspensions of rigid spheres. Trans. Soc. Rheol. 1959; 3: 137-52.

[19] Çınar S, Akinc M. Ascorbic Acid as a Dispersant for Concentrated Alumina Nanopowder Suspensions. 2014;

[20] Marie-Pierre G, Michiel S, Marialore S. Oxide/water interfaces: how the surface chemistry modifies interfacial water properties. J Phys: Condens Matter. 2012; 24: 124106.

[21] Sulpizi M, Gaigeot M-P, Sprik M. The Silica–Water Interface: How the Silanols Determine the Surface Acidity and Modulate the Water Properties. J Chem Theory Comput 2012; 8: 1037-47.

[22] Max J-J, Chapados C. Glucose and Fructose Hydrates in Aqueous Solution by IR Spectroscopy. J Phys Chem A 2007; 111: 2679-89.

[23] Jamali S, Yamanoi M, Maia J. Bridging the gap between microstructure and macroscopic behavior of monodisperse and bimodal colloidal suspensions. Soft Matter 2013; 9: 1506-15.

[24] Barnes HA. A handbook of elementary rheology. University of Wales, Institute of Non-Newtonian Fluid Mechanics; 2000.

[25] Hiemenz PC, Rajagopalan R. Principles of Colloid and Surface Chemistry, Third Edition, Revised and Expanded. Taylor & Francis; 1997.

[26] Mondragon R, Enrique Julia J, Barba A, Jarque JC. Determination of the packing fraction of silica nanoparticles from the rheological and viscoelastic measurements of nanofluids. Chem Eng Sci 2012; 80: 119-27.

[27] Rubio-Hernández FJ, Ayúcar-Rubio MF, Velázquez-Navarro JF, Galindo-Rosales FJ. Intrinsic viscosity of SiO2, Al2O3 and TiO2 aqueous suspensions. J Colloid Interface Sci 2006; 298: 967-72.

[28] Amorós JL, Beltrán V, Sanz V, Jarque JC. Electrokinetic and rheological properties of highly concentrated kaolin dispersions: Influence of particle volume fraction and dispersant concentration. Appl Clay Sci 2010; 49: 33-43.

[29] Ponton A, Quemada D, Lafuma F, Neel O. Studies of rheological behavior of colloidal silica suspensions with interaction potential. Colloids Surf, A 1996; 119: 255-9.

`

[30] Quemada D. Rheological modelling of complex fluids. I. The concept of effective volume fraction revisited. Eur Phys J - Appl Phys 1998; 1: 119-27.

[31] Saiki Y, Prestidge CA, Horn RG. Effects of droplet deformability on emulsion rheology. Colloids Surf, A 2007; 299: 65-72.

[32] Vickers D, Archer LA, Floyd-Smith T. Synthesis and characterization of cubic cobalt oxide nanocomposite fluids. Colloids Surf, A 2009; 348: 39-44.

[33] Chen H, Ding Y, He Y, Tan C. Rheological behaviour of ethylene glycol based titania nanofluids. Chem Phys Lett 2007; 444: 333-7.

[34] Mahbubul IM, Saidur R, Amalina MA. Latest developments on the viscosity of nanofluids. Int J Heat Mass Transfer 2012; 55: 874-85.

[35] Liu D-M. Particle packing and rheological property of highly-concentrated ceramic suspensions: φm determination and viscosity prediction. J Mater Sci 2000; 35: 5503-7.

[36] Xu X, Rice SA, Dinner AR. Relation between ordering and shear thinning in colloidal suspensions. Proc Natl Acad Sci 2013; 110: 3771-6.

[37] Anoop KB, Kabelac S, Sundararajan T, Das SK. Rheological and flow characteristics of nanofluids: Influence of electroviscous effects and particle agglomeration. J Appl Phys 2009; 106:

[38] Dong KJ, Yang RY, Zou RP, Yu AB. Role of Interparticle Forces in the Formation of Random Loose Packing. Phys Rev Lett 2006; 96: 145505.

[39] Forsyth AJ, Hutton SR, Osborne CF, Rhodes MJ. Effects of Interparticle Force on the Packing of Spherical Granular Material. Phys Rev Lett 2001; 87: 244301.

[40] Hunter RJ. Zeta Potential in Colloid Science: Principles and Applications. Academic Press; 1988.

[41] Yu AB, Feng CL, Zou RP, Yang RY. On the relationship between porosity and interparticle forces. Powder Technol 2003; 130: 70-6.

[42] García de la Torre J, Amorós D, Ortega A. Intrinsic viscosity of bead models for macromolecules and nanoparticles. Eur Biophys J 2010; 39: 381-8.

[43] Biddle D, Walldal C, Wall S. Characterisation of colloidal silica particles with respect to size and shape by means of viscosity and dynamic light scattering measurements. Colloids Surf, A 1996; 118: 89-95.

[44] Brenner H. Rheology of a dilute suspension of axisymmetric Brownian particles. Int J Multiphase Flow 1974; 1: 195-341.

`

[45] Smith TL, Bruce CA. Intrinsic viscosities and other rheological properties of flocculated suspensions of nonmagnetic and magnetic ferric oxides. J Colloid Interface Sci 1979; 72: 13-26.

[46] Argyris D, Ho T, Cole DR, Striolo A. Molecular Dynamics Studies of Interfacial Water at the Alumina Surface. J Phys Chem C 2011; 115: 2038-46.

`

CHAPTER V. ASCORBIC ACID AS A DISPERSANT FOR CONCENTRATED NANOPOWDER SUSPENSIONS

(A paper accepted by the Journal of European Ceramic Society)

Simge Çınar and Mufit Akinc

Department of Materials Science and Engineering,

Iowa State University, Ames, Iowa 50011

Abstract

The stabilization of concentrated nanopowder suspensions is crucial for many industrial applications. Yet, controlling the suspension viscosity is challenging for nanopowder suspension systems. In this study, we examined the adsorption of ascorbic acid (Vitamin C) on alumina surfaces and the related reduction in viscosity of the suspensions. Interactions between the ascorbic acid and the alumina surface were investigated by *in situ* ATR-FTIR and zeta potential measurements. It was shown that ascorbic acid forms complexes with the alumina surface through ligand exchange mechanisms. The optimum concentration of ascorbic acid for minimum suspension viscosity was determined. The maximum achievable solids content could be increased to around 0.35 by the addition of only 1.0 wt. % of dry powder ascorbic acid. Because ascorbic acid is easy to use, inexpensive, and a non-toxic organic additive, it has great potential to be used as a dispersant in a variety of industrial applications, from dilute to concentrated systems of intermediates or products.

`

Introduction

The correlation between dispersion and final product quality has been well established for the colloidal processing of oxide suspensions [1-5]. Lower viscosity of the suspensions is a good indicator of better dispersed systems. Therefore, controlling the rheological behavior of powder suspensions has been a focus of studies in recent years.

Even though the stabilization systems of micron- and submicron-size powders are well-understood, the knowhow cannot be transferred directly to nano-sized powder systems because here the number of parameters to be controlled is much higher. The main challenge with nanopowder systems is that the separation distances between particles, especially in concentrated suspensions, are much smaller than those in micron size powder systems. This fact requires much better control of interparticle interactions and limits the maximum achievable solids content. Smaller particles have larger diffusion constants. During Brownian movement, there is a high probability of particle aggregation, because the attractive van der Waals forces are more effective at small separations. Unless an electrostatic or steric barrier is built on the surface, aggregation is inevitable. Typically, steric stabilization is suggested for nanopowder suspensions because of its robustness [6-8].

Polyelectrolytes, mainly poly(acrylic acids), poly(methacrylates) and their derivatives, are studied extensively as steric stabilizers for alumina [9-21]. Oligo- and polysaccharides [22-25] and other novel additives, such as carboxymethyl lignin [26], poly(vinylpyrolidone) [27], poly(aspartic acid), and poly(epoxysuccinic acid) [28], were recently suggested as alternatives to polyelectrolytes. However, use of long chain molecules may induce bridging or depletion flocculation in concentrated suspensions of nanopowders. Kakui *et al.* [29] showed that while poly(ethyleneimine) with a molecular weight of 10,000 can disperse submicron size alumina

`

powders in ethanol solutions, the same polymer increased the viscosity of 7 nm powder suspensions. To obtain the same dispersion quality, the molecular weight of the polymer had to be decreased to 1,800, which corresponds to 1 nm adlayer thickness. They stated that larger molecules were not able to move freely around nanoparticles, decreasing the effectiveness of adsorption. Studart *et al*. [21, 30] predicted that the optimum dispersant length for 65 nm alumina powders was approx. 3.6 nm in toluene and between 3 nm and 4 nm in water, which is required to overcome the van der Waals attractive forces and optimize the excluded volume to obtain a well-dispersed system. It was also shown that low molecular weight saccharides can reduce the viscosity of alumina nanopowder suspensions more effectively than polysaccharides [31].

Small molecules as dispersants have not been as widely studied as polymeric ones. Citric acid and other aliphatic and aromatic carboxylic acids with different lengths and numbers of functional groups [5, 25, 32-36], low molecular weight saccharides and their derivatives, polyalcohols and sugar alcohols [37-43], fatty acids [44], and tailor-made molecules with pyrogallol head and short poly(ethylene glycol) tail [30] are some of the small molecules that are currently used to understand and control the rheological behavior of submicron and nanopowder alumina suspensions.

In general, adsorption of molecules occurs between the ionic functional group of the molecules and the charged oxide surface through a ligand exchange process. The lowest viscosities are obtained when the solution pH is below the isoelectric point (IEP) of the oxide powder and above the acid dissociation constant of the acidic functional group. Therefore, electrostatic interactions between the positively charged oxide surface and the negatively charged functional groups will be favorable [45]. The number, position, and type of the

`

functional groups affect the adsorption behavior [32, 46-50]. In the case of carboxylic acid, molecules with a rigid backbone with at least one carboxylic and one hydroxyl group facilitate better dispersions[35]. Low molecular weight saccharides, fructose in particular, are believed to reduce the effective solids content [37, 38, 40, 51]. Interaction of the fructose molecule with the alumina surface leads to displacement of bound water around the particles and decreases the effective volume fraction, and hence, the viscosity [37, 40, 41]. Of all of these studies, only a few examine nanopowder systems [30, 37, 38, 40, 41, 43, 44]. The maximum solids content ($\eta \leq$ 1 Pa·s at a shear rate of 100 s^{-1}) was increased to 0.35 and 0.40 by using meso-erythritol [43] or Gallol-PEG (pyrogallol head and short poly(ethylene glycol) tail) [30] for the alumina nanopowder suspensions (mean size of 44 and 65 nm), respectively. For other systems, the maximum solids loadings were limited to 0.20 – 0.25.

The aim of this study is to obtain well dispersed, concentrated nanopowder suspensions with better control of their rheological behavior. Here, we report the use of ascorbic acid (Vitamin C) for the dispersion of alumina nanopowder suspensions. To the best of our knowledge, it is the first time in the open literature that ascorbic acid is used for the stabilization of oxide suspensions.

Ascorbic acid has four hydroxyl groups, one of which dissociates in aqueous solutions. It is predicted that, while the acidic group electrostatically interacts with the positively charged alumina surface, other hydroxyl groups can help to disperse the particles in aqueous systems. In addition, ascorbic acid is a small, highly water soluble, abundant, inexpensive, and non-toxic molecule, and readily available. These properties make ascorbic acid a good candidate as an additive for oxide nanopowder suspensions.

`

Experimental

Materials

Alumina nanopowders (Lot# AAGL 1201) were purchased from the Nanophase Technology Corporation (Burr Ridge, IL). Transmission electron micrograph of these nanopowders are seen in Figure 1. Average particle size was 42 nm as calculated equivalent spherical particle diameter from a BET surface area of 38.8 m^2/ g. From the TEM images, average particle size was calculated to be 30 nm with a standard deviations of 21 nm. The powders had a density of 3.67 g/cm^3, a purity ≥ 99.5%, and a phase distribution of $\gamma/\delta \approx 70:30$.

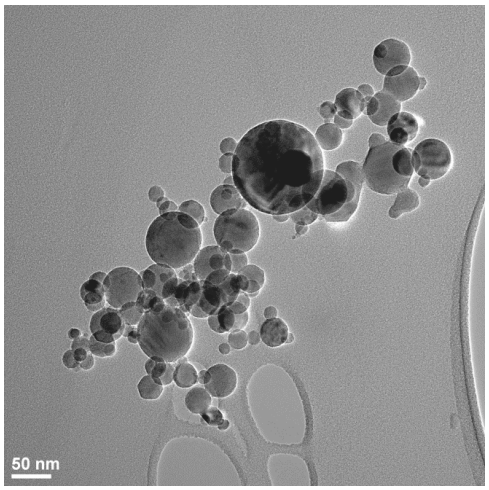

Figure 1: TEM micrograph of alumina nanopowder.

L-(+)-Ascorbic acid (ACS certified, purity > 99%) was purchased from Alfa Aesar (Ward Hill, MA). The chemical and resonance structures of ascorbic acid ($C_6H_8O_6$) are shown in Figure 2. NaCl, NaOH, and concentrated HCl were obtained from Fisher Scientific (Fair Lawn, NJ). Ultrapure water (Milli-Q Gradient A-10 model, Millipore Company, Billerica, MA) with a resistivity of 18.3 MΩ·cm and TOC < 3 ppm was used.

`

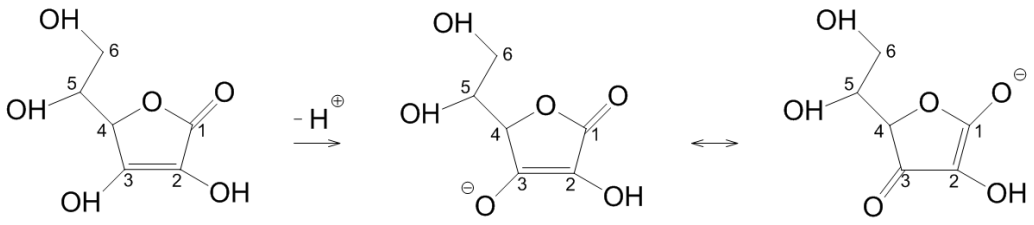

Figure 2: Chemical and resonance structures of ascorbic acid.

Suspension Preparation

The alumina powder was dried at 110 °C for 2 hours to eliminate any moisture adsorbed on the powder surface. The required amount of water and ascorbic acid was weighed and mixed. Then, alumina powder was weighed and added slowly to the solution. Suspensions were shaken in a heavy-duty shaker for 24 h at room temperature prior to rheological and ATR-FTIR measurements. While solids content of the alumina powders was calculated as a volume fraction of the suspension, the concentration of ascorbic acid was taken as a weight percentage of dried alumina nanopowder. The volume contribution of ascorbic acid to the suspension volume was negligible.

Viscosity Measurements

For the viscosity measurements, a rheometer (model AR 2000ex, TA Instruments, New Castle, DE) with a cone and plate geometry attachment (steel, 4˚ cone angle and 40 mm diameter) was used. A solvent trap was used to prevent water evaporation during the measurements. Initially, the shear rate was increased from 0.5 s^{-1} to 500 s^{-1}, then reduced back to 0.5 s^{-1} and 10 points per decade of each half loop were recorded. For reproducibility, two consecutive runs were conducted at 25.0 ± 0.1 ˚C. The data points corresponding to the final half loop of the second run were reported.

`

Zeta Potential Measurements

Zeta potentials were measured by a Laser Doppler Electrophoresis unit (Zetasizer, model Nano ZS90, Malvern Instruments, Worcestershire, UK) at 25 ˚C. The Smoluchowski equation was used for the zeta potential calculations.

A small portion of the alumina suspension (after shaking for 24 hours) was diluted to 200 ppm particles by deionized water and used for viscosity measurements. The ionic strength of the solution samples was adjusted to 0.1 M by using NaCl, a known indifferent electrolyte for alumina powders. The solution samples were shaken for an additional 24 h before zeta potential measurements were taken. The pH of the suspension was adjusted using 0.01 M or 0.1 M of HCl or NaOH. After 2 – 5 min of acid/base additions, the solution pH was measured before and after zeta potential measurements at room temperature, and the average pH was recorded for the measurement. The pH readings were accurate to ± 0.01.

ATR-FTIR Spectroscopy Measurements

An attenuated Total Reflection Fourier Transform Infrared (ATR-FTIR) spectroscope (Frontier model FTIR, Single reflection ATR attachment with diamond crystal, Perkin Elmer, Waltham, MA) was used for this study. Samples were directly put on the ATR crystal. Four scans with a spectral resolution of 4 cm^{-1} were taken at room temperature for each sample. Data was processed by Spectrum 10 software. For each spectrum, an interactive baseline correction with respect to the position of 4000 cm^{-1} was employed.

In order to resolve the individual interactions of water, ascorbic acid and alumina, four different spectra for each ascorbic acid concentration were collected and compared: spectra of (i) pure water, (ii) water mixed with required amount of ascorbic acid (the solution before adding

`

alumina powder), (iii) suspension of alumina powder with ascorbic acid (shaken for 24 hours), and (iv) alumina powder suspensions without addition of ascorbic acid.

Results and Discussion

Rheological Measurements

As a model system, a suspension with a solids content of 0.20 was chosen. Figure 3 shows the effect of ascorbic acid concentration on the viscosity of the alumina nanopowder suspensions over the shear rate range studied. Addition of ascorbic acid reduced the viscosity of the suspensions substantially, even at very high shear rates. With the addition of only 1.0 wt. % ascorbic acid, the viscosity of the suspensions decreased from 0.46 Pa·s to 0.01 Pa·s at a shear rate of 100 s^{-1}. The flow of aqueous alumina suspensions showed high shear rate dependency. However, with the addition of ascorbic acid, the dependency on the shear rate was reduced. At the optimum concentration, the flow was completely Newtonian, which indicated good dispersion of the nanopowder. Further addition of ascorbic acid resulted in higher viscosities coupled with strong shear thinning behavior, which represented the flocculated state of the nanopowders.

For easier comparison, Figure 4 shows the viscosities of suspensions at a shear rate of 100 s^{-1} as a function of ascorbic acid concentration. Increase in ascorbic acid concentration first reduced the viscosity of the suspensions. After reaching a critical concentration (1.0 wt.%), the viscosity started to increase. A similar behavior was observed when additives adsorbed on the surface. Mixing with polymeric additives shows minima when the monolayer coverage of the surface is obtained. Excess polymeric additives result in bridging and depletion flocculation [9, 11, 17, 52].

`

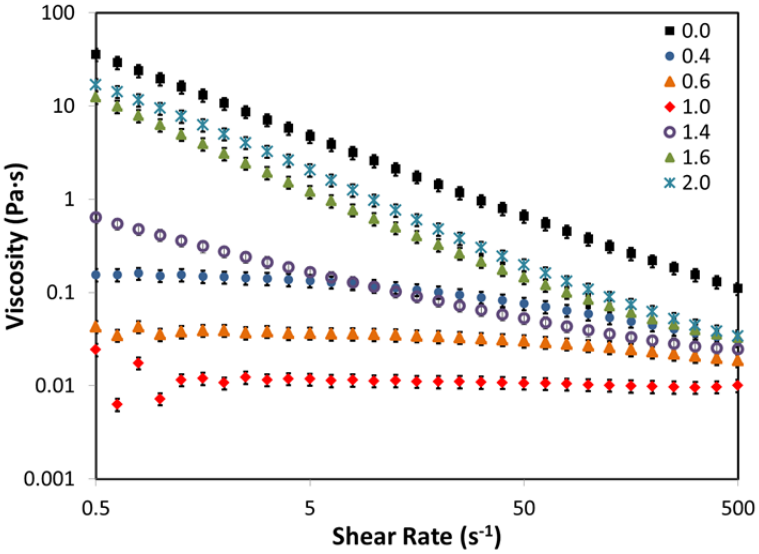

Figure 3: Viscosity of suspensions with 0.20 solids content of alumina nanopowder as a function of shear rate and ascorbic acid concentration. Note that the viscosity decreased systematically with the addition of ascorbic acid up to 1 wt.% and increased at concentrations higher than 1 wt.%.

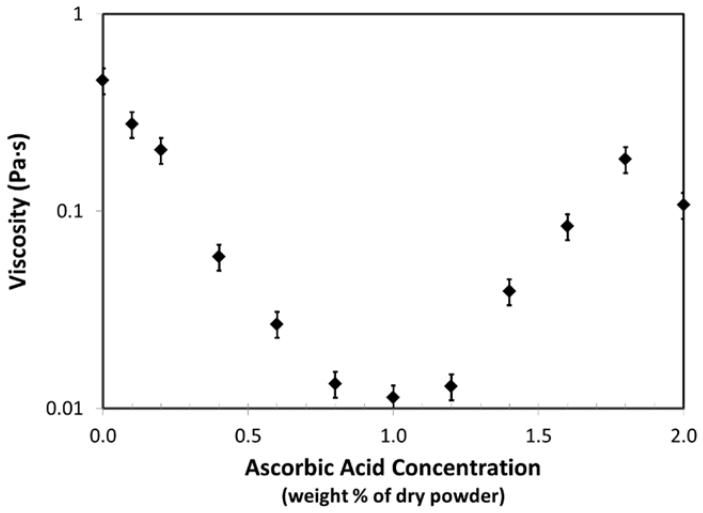

Figure 4: Viscosity of suspensions with 0.20 alumina nanopowder solids content of as a function of ascorbic acid concentration at shear rate of 100 s^{-1}.

`

Once the monolayer surface coverage is completed, excessive amounts of ascorbic acid would probably accumulate in solution. Because the separation distance is very short in concentrated nanoparticle suspensions, accumulated ascorbic acid will act a bridge between particles, resulting in higher viscosities.

By keeping the ratio of ascorbic acid to alumina powder constant at 1.0 wt.%, the solids content of the suspensions were increased to determine the maximum achievable value. Figure 5 shows the effect of ascorbic acid addition on the viscosity of suspensions with different solids contents. The effect was compared to the alumina nanopowder suspensions without ascorbic acid addition. For all solids content levels, addition of ascorbic acid led to a reduction in suspension viscosity. However, the reduction at high solids content was not as significant as that at low solids content. While the reduction was approximately 98 and 94 % for solids contents of 0.20 and 0.30, respectively, it was around 30 % for a solids content of 0.40. Changing the ratio of ascorbic acid to alumina powder (0.5 wt.% or 2.0 wt.%) did not further reduce the viscosity for suspensions with a solids content of 0.40. This relatively low effectiveness is most probably caused by the very limited separation distance between powders at high solids content. With the addition of only 1.0 wt.% of ascorbic acid, the maximum solids content was approx. 0.35.

`

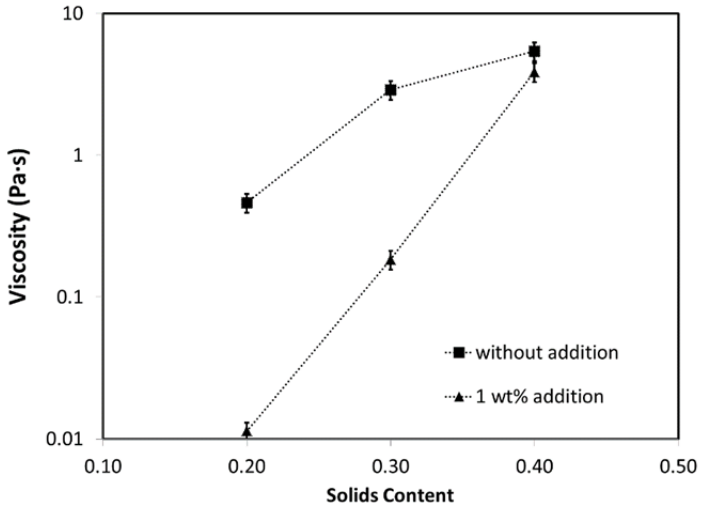

Figure 5: Viscosity of suspensions with ascorbic acid concentration of 1.0 wt.% as a function of solids content of alumina nanopowder at a shear rate of 100 s^{-1}.

In Situ ATR-FTIR Measurements

Adsorption of ascorbic acid on the surface of alumina powders has not been extensively studied. The chemical interactions between the alumina powder and the ascorbic acid were investigated by *in situ* ATR-FTIR spectroscopy. In order to distinguish the changes in the ascorbic acid structure and its interactions with alumina powder and water, each component of the suspension were studied separately. Because the strong IR absorbance of water dominates the spectrum, the pure water spectrum was subtracted from the solution/suspension spectra. Original and difference spectra are plotted in Figure 6.

The broad band between 3600 cm^{-1} and 2900 cm^{-1} in Figure 6(a) was assigned the absorbance of symmetric and asymmetric stretching of the hydroxyl groups in the water molecules. There was no change observed in this band in the spectra of the ascorbic acid/water solution. However, in the presence of alumina nanopowder, the intensity of the asymmetric stretching (around 3515 cm^{-1}) increased at the expense of the symmetric one (around 3200 cm^{-1}).

`

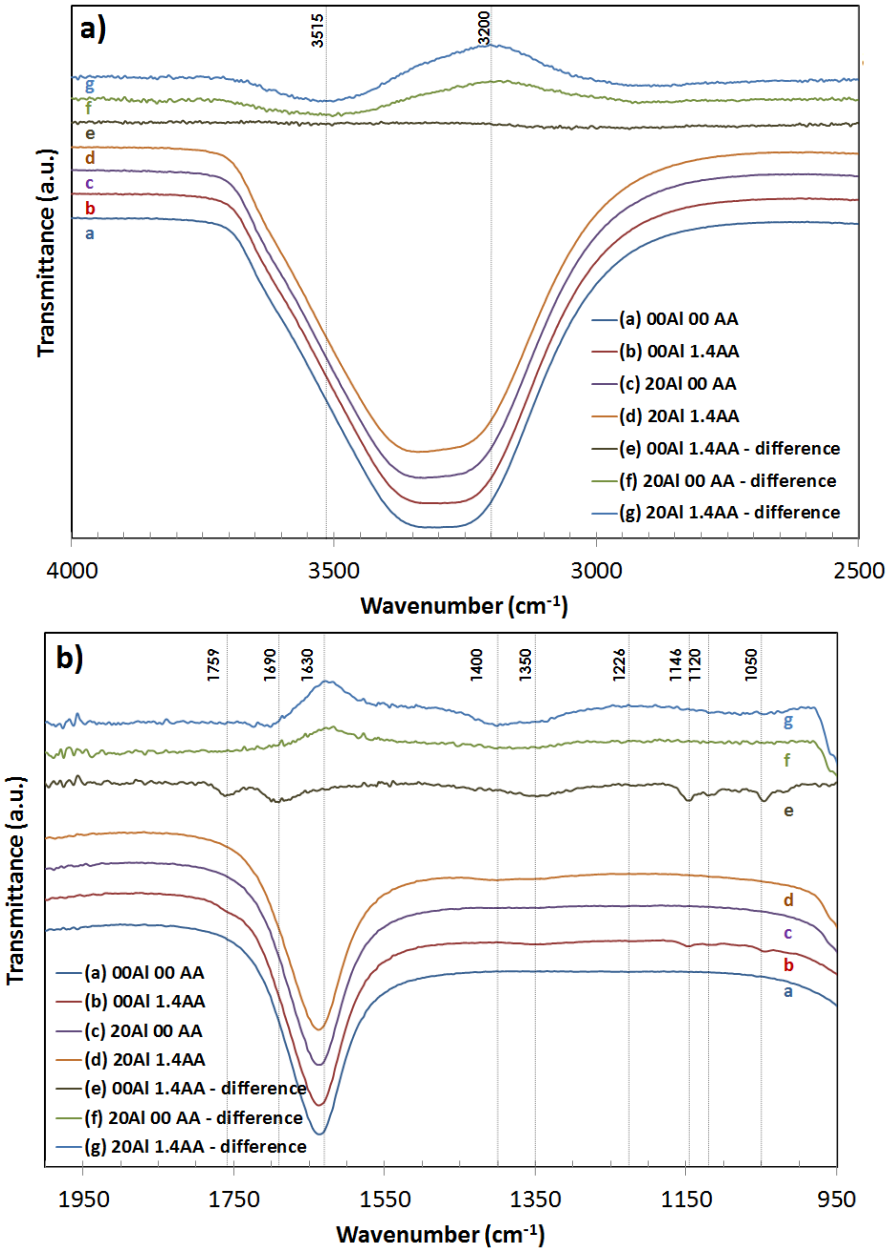

Figure 6: *In situ* ATR-FTIR spectra of samples in the wavelength range of 4000 cm^{-1} – 2500 cm^{-1} (a) and 2000 cm^{-1} – 950 cm^{-1} (b). "xxAl yyAA" represents xx volume% alumina suspensions with the addition of yy wt.% ascorbic acid.

The bands at 1630 cm^{-1} and 2150 cm^{-1} (bending) were also associated with water molecules. While there was no change in intensity and position of latter band, a decrease in intensity was observed in the former in the presence of alumina powder. Because the changes in spectra were

observed only in alumina suspensions but not in solutions, they were related to the strong interaction of water molecules with the alumina powder. The alumina surface restricts the symmetric stretching of water hydroxyls. Addition of ascorbic acid to alumina suspensions did not lead to any significant change in these peaks.

The absorbance at 1759 cm^{-1} (C_1=O asymmetric stretching) and 1690 cm^{-1} (C=C ring stretching) present in the ascorbic acid solution spectrum almost disappeared as alumina nanopowder was introduced to the solution. Very small absorbance bands around 1710 cm^{-1}, similar to C_1=O stretching, were observed. Similarly, the relatively broad band around 1350 cm^{-1}, representing C_3=O stretching vibrations in the ascorbic acid solution spectrum, shifted to 1400 cm^{-1} in the presence of alumina powder. The shifts of the band through the lower frequencies and decrease in its intensity indicated the complex formation of carbonyl groups with the alumina surface. Shifts in C_1=O band absorbance were associated with the metal-ascorbate binding earlier [53-55]. Because of the conjugated system of C_1 and C_3, the resonance structures explain the contribution of both carbons in their adsorption on the alumina surface (Figure 2).

The bands at 1226 cm^{-1}, 1146 cm^{-1}, 1120 cm^{-1}, and 1050 cm^{-1} were assigned to C-C(=O)-O stretching, C-C stretching, and C-O-H bending in the solution spectra [54, 56, 57]. These bands lost their intensities and sharpness in aqueous solution of alumina. Less intense and much broader overlapping bands were attributed to changes in ascorbic acid concentration. Even though the intensities of these peaks seemed to increase with ascorbic acid concentration, quantification of the peaks would not be reliable because of the very low absorption intensities.

Instead of carboxyl groups, ascorbic acid has hydroxyl groups. When ascorbic acid is dissolved in water, ascorbates will form and the pH of the solution decreases because of the release of H^+ (see Figure 2, first step). Negatively charged ascorbate favors adsorption to the

`

positively charged alumina surface. Because of their resonance structures (Figure 2, second step), both C_1 and C_3 favor adsorption on the alumina surface. According to the *in situ* ATR-FTIR measurements, ascorbic acids adsorbed to the alumina surface through C_1 and C_3 via ligand exchange mechanisms.

As seen in Figure 7, the pH of the suspensions decreased with ascorbic acid concentration. The acid dissociation constant, pK_a, of ascorbic acid is 4.36. At a solids content of 0.2, the initial pH of the alumina suspension was about 5.7; thus most of the ascorbic acid molecules were ionized and formed ascorbete ions. Therefore, they had a high tendency to specifically adsorb on the alumina surface. As the adsorption reaction continued, the pH of the suspension decreased because of the release of H^+ to the solution initiated by ascorbic acid dissociation. At lower pH values, the dissociation rate of ascorbic acids were expected to decrease; however, because the dissolved molecules adsorbed on the alumina surface, dissociation reaction was favorable until the alumina surface was fully covered. This supports the assumption of ligand exchange adsorption mechanisms.

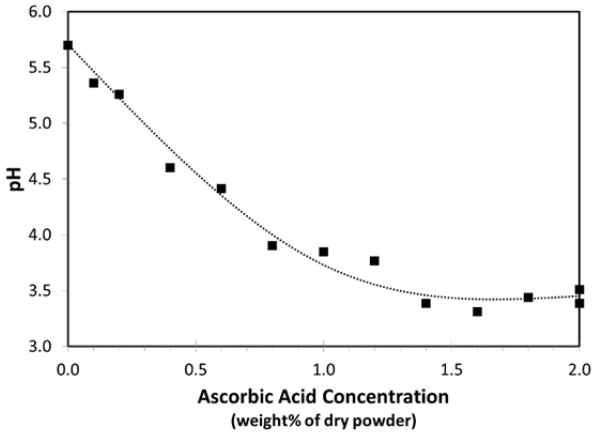

Figure 7: Change in pH of the alumina nanopowder suspensions with a solids content of 0.20 as a function of ascorbic acid concentration.

`

Zeta Potential Measurements

Adsorption of the charged molecules on the alumina surface may cause changes in surface charge. As seen in Figure 8, the zeta potential of the powders did not change much at low concentrations of ascorbic acid, but decreased when the concentration was higher than 0.4 %.

It was reported that strong adsorption resulted in shifts in IEP of the powders [33, 46, 49, 58]. Increase in ascorbic acid concentration led to shifts in IEP to lower pH values (Figure 9), which indicated the more acidic alumina surface. The values leveled off with higher concentrations of ascorbic acid (> 1.0 wt.%), which indicated that the reaction was closer to completion.

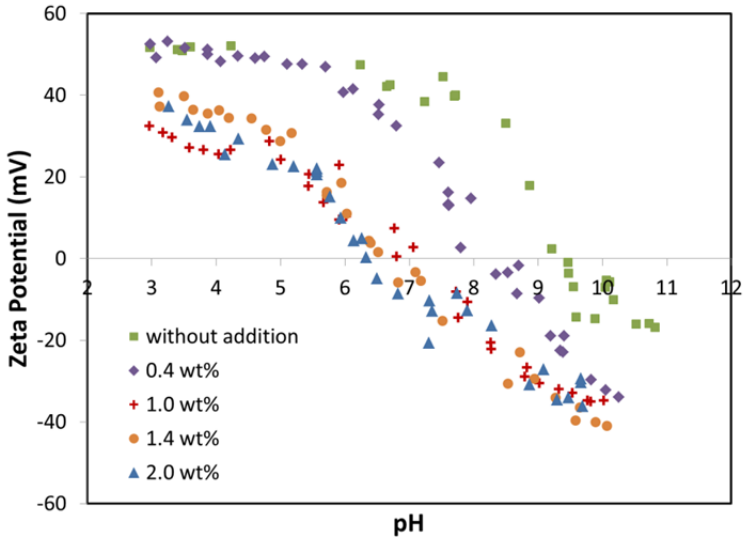

Figure 8: Zeta potential of alumina powders as a function of ascorbic acid concentration. "xx wt.%" indicates xx wt.% of ascorbic acid addition with respect to the dry alumina powder. The concentrations ascorbic acid levels before dilution.

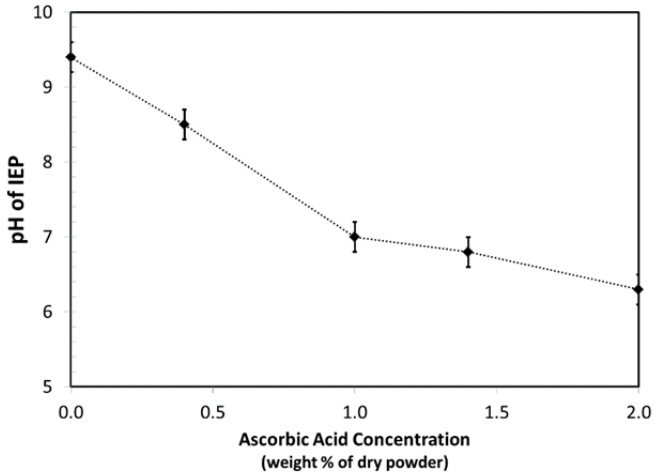

Figure 9: Shifts in pH of IEP with respect to the ascorbic acid concentration before dilution according to zeta potential measurements.

The color of the alumina suspensions changed from light to darker brown with increasing ascorbic acid concentration. It is known ascorbic acid turns to a brown color during degradation. This is another qualitative, yet independent, observation confirming a change in the molecular structure of ascorbic acid as it adsorbs on the alumina surface.

Mechanism of Viscosity Reduction

The viscosity of the nano-size alumina powder suspensions decreased dramatically with as little as 1 wt.% of ascorbic acid. The role of ascorbic acid as a dispersant is attributable to its strong specific interaction with the alumina surface. *In situ* ATR-FTIR and zeta potential measurements showed that ascorbic acid adsorbed on the alumina surface. Adsorption of ascorbate ions on the surface also led to a decrease in the IEP of alumina from 9 to approx. 6.5. Leveling of the IEP indicated that the adsorption approached a limiting value, specifically around 1.0 wt.%. In fact, the minimum viscosity was obtained at this concentration, probably representing the monolayer coverage of alumina surface. Because ascorbic acid is very soluble in water, further addition of ascorbic acid would accumulate in solution. Because of the small

`

separation distance between nanopowders in concentrated suspensions, excess ascorbic acid molecules may form bridges between the alumina powder particles. That would lead to an increase in viscosity of the suspension after the optimum value was obtained by monolayer coverage. The decreasing effectiveness of further ascorbic acid addition on lowering the viscosity at high solids contents supports our claim.

Conclusion

It was shown for the first time that ascorbic acid (Vitamin C) can be used to disperse nanopowder suspensions. With the addition of small amounts of ascorbic acid, the viscosity of the suspensions decreased significantly and Newtonian flow was obtained. The optimum concentration for minimum viscosity was determined as 1.0 wt.% of alumina powder. With optimum ascorbic acid addition, the maximum solids content (where $\eta \leq 1$ Pa·s at a shear rate of 100 s^{-1}) was increased to about 0.35.

The viscosity decrease of suspensions was directly related to the adsorption of ascorbic acid on the alumina surface. The adsorption reaction slowed down at concentrations higher than 1.0 wt.%. Further addition of ascorbic acid may form bridges between alumina particles, thus leading to an increase in viscosity. Dispersion of powders at very high concentrations was more challenging, but ascorbic acid was still effective.

In situ ATR-FTIR measurement showed that ascorbic acid bound to the surface through C_1 and C_3 via ligand exchange adsorption. As a result of ascorbate adsorption, the IEP of alumina shifted to lower pH values.

Ascorbic acid is readily available, inexpensive, and non-toxic. Because it can be removed completely during burnout process, it offers an approach to produce parts with high purity and

`

uniform microstructures. All these advantages make ascorbic acid a strong candidate for colloidal processing of concentrated oxide suspensions.

Acknowledgement

This study was supported by the National Science Foundation (Grant No. CBET 0931038). The authors would like to thank Charles Glatz for making a Zetasizer available for this study and Tugce Karakulak for conducting TEM characterization of the powders.

References

[1] Azar M, Palmero P, Lombardi M, Garnier V, Montanaro L, Fantozzi G, et al. Effect of initial particle packing on the sintering of nanostructured transition alumina. J Eur Ceram Soc 2008; 28: 1121-8.

[2] Chong JS, Christiansen EB, Baer AD. Rheology of concentrated suspensions. J Appl Polym Sci 1971; 15: 2007-21.

[3] Lewis JA. Colloidal processing of ceramics. J Am Ceram Soc 2000; 83: 2341-59.

[4] Sigmund WM, Bell NS, Bergström L. Novel Powder-Processing Methods for Advanced Ceramics. J Am Ceram Soc 2000; 83: 1557-74.

[5] Studart AR, Pandolfelli VC, Tervoort E, Gauckler LJ. Selection of dispersants for high-alumina zero-cement refractory castables. J Eur Ceram Soc 2003; 23: 997-1004.

[6] Franks GV, Gan Y. Charging Behavior at the Alumina–Water Interface and Implications for Ceramic Processing. J Am Ceram Soc 2007; 90: 3373-88.

[7] Jailani S, Franks GV, Healy TW. ζ Potential of Nanoparticle Suspensions: Effect of Electrolyte Concentration, Particle Size, and Volume Fraction. J Am Ceram Soc 2008; 91: 1141-7.

[8] Lu K. Theoretical analysis of colloidal interaction energy in nanoparticle suspensions. Ceram Int 2008; 34: 1353-60.

[9] Bhosale PS, Berg JC. Poly(acrylic acid) as a rheology modifier for dense alumina dispersions in high ionic strength environments. Colloids Surf A 2010; 362: 71-6.

[10] Bowen P, Carry C, Luxembourg D, Hofmann H. Colloidal processing and sintering of nanosized transition aluminas. Powder Technol 2005; 157: 100-7.

`

[11] Briscoe BJ, Khan AU, Luckham PF. Optimising the dispersion on an alumina suspension using commercial polyvalent electrolyte dispersants. J Eur Ceram Soc 1998; 18: 2141-7.

[12] Cesarano J, Aksay IA. Processing of Highly Concentrated Aqueous α-Alumina Suspensions Stabilized with Polyelectrolytes. J Am Ceram Soc 1988; 71: 1062-7.

[13] Cesarano J, Aksay IA, Bleier A. Stability of Aqueous α-Al2O3 Suspensions with Poly(methacrylic acid) Polyelectrolyte. J Am Ceram Soc 1988; 71: 250-5.

[14] Chera L, Palcevskis E, Berzins M, Lipe A, Jansone I. Dispersion of nanosized ceramic powders in aqueous suspensions. JPCS 2007; 93: 012010.

[15] Jiang L, Gao L. Effect of Tiron adsorption on the colloidal stability of nano-sized alumina suspension. Mater Chem Phys 2003; 80: 157-61.

[16] Kamiya H, Fukuda Y, Suzuki Y, Tsukada M, Kakui T, Naito M. Effect of Polymer Dispersant Structure on Electrosteric Interaction and Dense Alumina Suspension Behavior. J Am Ceram Soc 1999; 82: 3407-12.

[17] Lyckfeldt O, Palmqvist L, Carlström E. Stabilization of alumina with polyelectrolyte and comb copolymer in solvent mixtures of water and alcohols. J Eur Ceram Soc 2009; 29: 1069-76.

[18] Ramzi Ben, Romdhane M, Baklouti S, Bouaziz J, Chartier T, Baumard J-F. Dispersion of Al2O3 concentrated suspensions with new molecules able to act as binder. J Eur Ceram Soc 2004; 24: 2723-31.

[19] Shin Y-J, Su C-C, Shen Y-H. Dispersion of aqueous nano-sized alumina suspensions using cationic polyelectrolyte. Mater Res Bull 2006; 41: 1964-71.

[20] Singh BP, Bhattacharjee S, Besra L, Sengupta DK. Evaluation of dispersibility of aqueous alumina suspension in presence of Darvan C. Ceram Int 2004; 30: 939-46.

[21] Studart AR, Amstad E, Antoni M, Gauckler LJ. Rheology of Concentrated Suspensions Containing Weakly Attractive Alumina Nanoparticles. J Am Ceram Soc 2006; 89: 2418-25.

[22] Kim JC, Auh KH, Schilling CH. Effects of polysaccharides on the particle packing and green strength of alumina slurries. Mater Lett 1999; 40: 209-12.

[23] Schilling CH, Bellman RA, Smith RM, Goel H. Plasticizing aqueous suspensions of concentrated alumina with maltodextrin sugar. J Am Ceram Soc 1999; 82: 57-66.

[24] Sikora M, Schilling CH, Tomasik P, Li C. Dextrin plasticizers for aqueous colloidal processing of alumina. J Eur Ceram Soc 2002; 22: 625-8.

[25] Tomasik P, Schilling CH, Jankowiak R, Kim J-C. The role of organic dispersants in aqueous alumina suspensions. J Eur Ceram Soc 2003; 23: 913-9.

`

[26] Cerrutti BM, de Souza CS, Castellan A, Ruggiero R, Frollini E. Carboxymethyl lignin as stabilizing agent in aqueous ceramic suspensions. Ind Crop Prod 2012; 36: 108-15.

[27] Acosta M, Wiesner VL, Martinez CJ, Trice RW, Youngblood JP. Effect of Polyvinylpyrrolidone Additions on the Rheology of Aqueous, Highly Loaded Alumina Suspensions. J Am Ceram Soc 2013; 96: 1372-82.

[28] Xiao C, Chen H, Yu X, Gao L, Guo L. Dispersion of Aqueous Alumina Suspensions with Biodegradable Polymers. J Am Ceram Soc 2011; 94: 3276-81.

[29] Kakui T, Miyauchi T, Kamiya H. Analysis of the action mechanism of polymer dispersant on dense ethanol alumina suspension using colloidal probe AFM. J Eur Ceram Soc 2005; 25: 655-61.

[30] Studart AR, Amstad E, Gauckler LJ. Colloidal Stabilization of Nanoparticles in Concentrated Suspensions. Langmuir 2006; 23: 1081-90.

[31] Schilling CH, Li C, Tomasik P, Kim J-C. The rheology of alumina suspensions: influence of polysaccharides. J Eur Ceram Soc 2002; 22: 923-31.

[32] Desset-Brèthes S, Cabane B, Spalla O. Competition Between Ligands for Al2O3 in Aqueous Solution. J Phys Chem A 2012; 116: 6511-8.

[33] Hidber PC, Graule TJ, Gauckler LJ. Citric Acid—A Dispersant for Aqueous Alumina Suspensions. J Am Ceram Soc 1996; 79: 1857-67.

[34] Husin H, Leong Y-K, Liu J. Molecular attributes of an effective steric agent: Yield stress of dispersions in the presence of pure enantiomeric and racemate malic acids. Adv Powder Technol 2012; 23: 459-64.

[35] Leong Y-K. Role of Molecular Architecture of Citric and Related Polyacids on the Yield Stress of α-Alumina Slurries: Inter- and Intramolecular Forces. J Am Ceram Soc 2010; 93: 2598-605.

[36] Sato K, Yılmaz H, Ijuin A, Hotta Y, Watari K. Acetic acid mediated interactions between alumina surfaces. Appl Surf Sci 2012; 258: 4011-5.

[37] Çinar S, van Steenhuyse L, Akinc M. Elucidation of Viscosity Reduction Mechanism of Nano Alumina Suspensions with Fructose Addition by DSC. J Am Ceram Soc 2013; 96: 1077-84.

[38] Falkowski P, Bednarek, P, Danelska A, Mizerski T, Szafran M. Application of monosaccharides derivatives in colloidal processing of aluminum oxide. J Eur Ceram Soc 2010; 30: 2805-11.

`

[39] Kim JC, Schilling CH, Tomasik P, Auh KH. Plasticizing dense alumina slurries with mono- and di-saccharides. Mater Lett 2000; 42: 221-4.

[40] Li C, Akinc M. Role of Bound Water on the Viscosity of Nanometric Alumina Suspensions. J Am Ceram Soc 2005; 88: 1448-54.

[41] Li C, Akinc M, Wiench J, Pruski M, Schilling CH. Relationship Between Water Mobility and Viscosity of Nanometric Alumina Suspensions. J Am Ceram Soc 2005; 88: 2762-8.

[42] Schilling CH, Sikora M, Tomasik P, Li C, Garcia V. Rheology of alumina–nanoparticle suspensions: effects of lower saccharides and sugar alcohols. J Eur Ceram Soc 2002; 22: 917-21.

[43] Yar Y, Acar FY, Yurtsever E, Akinc M. Reduction of Viscosity of Alumina Nanopowder Aqueous Suspensions by the Addition of Polyalcohols and Saccharides. J Am Ceram Soc 2010; 93: 2630-6.

[44] Bell NS, Schendel ME, Piech M. Rheological properties of nanopowder alumina coated with adsorbed fatty acids. J Colloid Interface Sci 2005; 287: 94-106.

[45] Kasprzyk-Hordern B. Chemistry of alumina, reactions in aqueous solution and its application in water treatment. Adv Colloid Interface Sci 2004; 110: 19-48.

[46] Bertazzo S, Rezwan K. Control of α-Alumina Surface Charge with Carboxylic Acids. Langmuir 2009; 26: 3364-71.

[47] Hidber PC, Graule TJ, Gauckler LJ. Influence of the dispersant structure on properties of electrostatically stabilized aqueous alumina suspensions. J Eur Ceram Soc 1997; 17: 239-49.

[48] Laucournet R, Pagnoux C, Chartier T, Baumard JF. Catechol derivatives and anion adsorption onto alumina surfaces in aqueous media: influence on the electrokinetic properties. J Eur Ceram Soc 2001; 21: 869-78.

[49] Leong YK. Molecular Configuration of Adsorbed cis- and trans-1,2-Ethylene Dicarboxylic Acids and Interparticle Forces in Colloidal Dispersions. Langmuir 2002; 18: 2448-9.

[50] Teh EJ, Leong Y-K, Liu Y, Craig VSJ, Walsh RB, Howard SC. High Yield Stress Associated with Capillary Attraction between Alumina Surfaces in the Presence of Low Molecular Weight Dicarboxylic Acids. Langmuir 2009; 26: 3067-76.

[51] Singh K, Mohan S. Adsorption behavior of selected monosaccharides onto an alumina interface. J Colloid Interface Sci 2004; 270: 21-8.

[52] Leong YK, Scales PJ, Healy TW, Boger DV. Interparticle forces arising from adsorbed polyelectrolytes in colloidal suspensions. Colloids Surf A 1995; 95: 43-52.

`

[53] Rajh T, Nedeljkovic JM, Chen LX, Poluektov O, Thurnauer MC. Improving Optical and Charge Separation Properties of Nanocrystalline TiO2 by Surface Modification with Vitamin C. J Phys Chem B 1999; 103: 3515-9.

[54] Tajmir-Riahi HA. Coordination chemistry of vitamin C. Part I. Interaction of L-ascorbic acid with alkaline earth metal ions in the crystalline solid and aqueous solution. J Inorg Biochem 1990; 40: 181-8.

[55] Tajmir-Riahi HA. Coordination chemistry of vitamin C. Part III. Interaction of L-ascorbic acid with Al(III), La(III), and Pb(II) ions. Evidence for metal chelate formation in the solid and aqueous solution. J Inorg Biochem 1991; 44: 39-45.

[56] Yang H, Irudayaraj J. Rapid determination of vitamin C by NIR, MIR and FT-Raman techniques. J Pharm Pharmacol 2002; 54: 1247-55.

[57] Yohannan Panicker C, Tresa Varghese H, Philip D. FT-IR, FT-Raman and SERS spectra of Vitamin C. Spectrochim Acta Part A 2006; 65: 802-4.

[58] Leong YK. Interparticle forces arising from an adsorbed strong polyelectrolyte in colloidal dispersions: charged patch attraction. Colloid Polym Sci 1999; 277: 299-305.

`

CHAPTER VI. BOUND WATER LAYER AND ITS INFLUENCE ON THE VISCOSITY OF CERAMIC OXIDE NANOPOWDERS SUSPENSIONS

(A paper to be submitted to the Journal of European Ceramic Society)

Simge Çınar, Daniel D. Anderson, Mufit Akinc

Department of Materials Science and Engineering,

Iowa State University, Ames, Iowa 50011

Abstract

Nanopowder suspensions exhibit much higher viscosities compared to micron size powders. Recently, it was shown that a bound water layer around the particles is partially responsible for the high viscosities of alumina nanopowder suspensions. In the present study, the existence and effect of the bound water layer on suspension viscosity were validated for other oxide systems such as zirconia, yttria stabilized zirconia and titania. The water melting events were studied by low-temperature differential scanning calorimetry (LT-DSC) to investigate the nature of the bound water and how it varied by different oxide systems. Even though the free water melts around similar temperatures for different oxide systems, the melting temperatures of bound water varied from -1 °C to -7 °C. The variation in melting behavior of bound water was related to the available charged species in solution and hydroxide formation through the ΔpH values. The higher ΔpH was, the lower the melting temperature of bound water is. The bound water content was estimated and incorporated into a modified Krieger-Dougherty (K-D) equation. Intrinsic viscosities of different oxide suspensions obtained through this modified model were used to compare and understand the rheological behavior of suspensions. The modified equation

`

successfully fitted the experimental data, for all but the alumina systems. Intrinsic values were estimated as 11.6, 6.6, 5.1 and 3.1 at the shear rate of 50 s^{-1} for alumina, titania, zirconia and YSZ, respectively. Increasing shear rate predicted lower intrinsic viscosity values.

Introduction

Alumina [1-13], zirconia [14-21], yttrium stabilized zirconia (YSZ) [22-24], and titania [25-27]are some of the most widely studied ceramic nanopowder systems. Understanding of the surface properties and the rheological behavior of oxide nanopowder suspensions is essential for many applications, including nanofluids [28-32], advanced ceramics [15, 33, 34], nanocomposites [30, 35], and others. Lower suspension viscosities facilitate improved final product quality because they indicate better dispersed systems, and lower production cost.

Typically, the suspension viscosity increases with decreasing particle size [21, 36]. However, nanopowder suspensions exhibit unexpectedly high viscosities. A possible explanation is the fact that the separation distances between particles are much shorter in nanopowder systems, and therefore extreme agglomeration may be caused by enhanced interparticle forces. Existing models do not fully explain this phenomenon. The current model underestimates the viscosity of nanopowder suspensions and the issue is still a topic of debate [7, 28-31, 37-40].

The bound water layer around the nanopowder particles, which we reported earlier, leads to an increase in the effective solids content [2, 3, 12]. It was shown that while the bound water fraction is negligible for sub-micron size powders, but it becomes substantial for nanopowders, leading to much higher viscosities than predicted by existing models.

The bound water manifests itself by the appearance of lower temperature melting events in the presence of alumina powders as indicated in low temperature differential scanning

`

calorimetry (LT-DSC). It was reported that the bound water layer can be modified by low molecular weight saccharides [2, 11, 12]. This modified layer is different than an electrical double layer because its fraction is constant with varying indifferent electrolyte (NaCl) concentration. The presence of specifically adsorbed H^+ and OH^- also leads to changes in the fraction of bound water [3]. Thus, bound water is directly associated with the powder surface [3]. Because the bound water cannot serve as a solvent in the system, the effective solids content increases and is partially responsible for the high viscosities of alumina nanopowder suspensions.

The goal of the present work was to extrapolate our findings to other oxide nanopowder systems, specifically zirconia, 3 mol% yttria stabilized zirconia (YSZ), and titania. The viscosities of the suspensions by rheometry and the bound water layer by differential scanning calorimetry (LT-DSC) were studied. The effective solids content of the nanopowder suspensions was estimated using bound water fractions by LT-DSC, which were subsequently used in the modified K-D equation to predict and compare the viscosities of different oxide systems. The intrinsic viscosities predicted by this modified equation were discussed.

Experimental

Materials

While alumina (Lot number: AAGL 1201) and titania (Lot number: T90121 – 01) nanopowders were purchased from Nanophase Technology Corporation (Burr Ridge, IL), zirconia (Lot number: IAM6280NZ0) and yttria stabilized zirconia (Lot number: IAM3180NYZ3) nanopowders were purchased from Inframat Advanced Materials (Manchester, CT). All powders had a purity of at least 99.0 %. Figure 1 shows the transmission electron microscopy (TEM) images of these nanopowders. The alumina and titania nanopowders were

`

almost perfectly spherical, while the zirconia and YSZ powder particles were sphere-like. Zirconia powders were agglomerated to a degree that the boundaries between individual particles were not distinguishable. In contrast, the YSZ nanopowders were displayed on the TEM grid as almost individual particles. The alumina nanopowders had sharp boundaries, indicating that particles could be dispersed. The titania particles, on the other hand, were agglomerated. Other properties of these powders are listed in Table 1. For the estimation of the particle size based on the BET surface area, the particles were assumed to be perfectly spherical and dispersed. More than hundred particles were counted for the particle size estimation using TEM images. Measurements were done manually using ImageJ Software and particles were assumed to be spherical. The relatively high particle size results for zirconia using TEM images might have been caused by the unclear separation of individual particles and the assumption of perfect spherical shapes. In addition, fused or very small particles caused errors in size estimation using TEM images.

ACS certified NaCl, NaOH and concentrated HCl were purchased from Fisher Scientific (Fair Lawn, NJ).

`

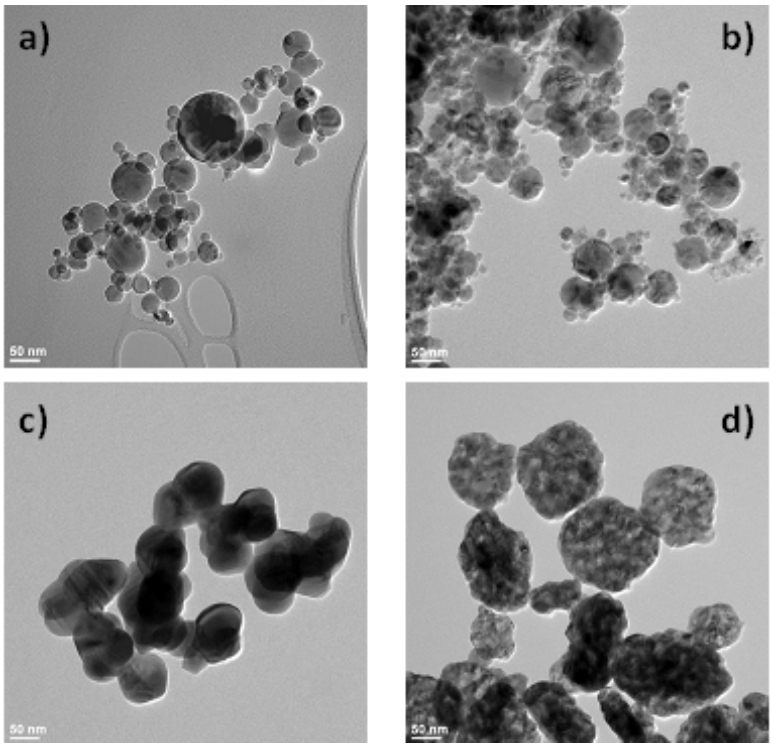

Figure 1: TEM micrographs of alumina (a), titania (b), zirconia (c), and YSZ (d) nanopowders.

Table 1: Characteristics of nanopowders studied.

	Phases present (XRD)	**Density (g/cm^3)**	**BET Surface Area (m^2/g)**	**BET Particle Size* (nm)**	**Average Particle Size** (nm)**	**Average Particle Size (TEM)*** (nm)**	**pH at IEP (± 0.2)**
Alumina	γ/δ ≈ 70:30	3.7	38.8	42	50	30 ± 21	9.5
Zirconia	Monoclinic	5.7	10.8	98	30 - 60	85 ± 25	6.2
YSZ	Tetragonal	6.1	24.4	40	30 - 60	125 ± 43	8.0
Titania	Anatase	3.9	42.8	36	38	27 ± 17	6.2

** Particles were assumed to be perfectly spherical and dispersed. **Particle size provided by manufacturer. ***Particles were assumed to be spherical and their diameters were measured manually. xx ± yy indicates the average particle size ± standard deviation. XRD: X-Ray Diffractometry, BET: surface area by Brunauer-Emmett-Teller method, IEP: Isoelectric Point, YSZ: 3 mol% yttria stabilized zirconia*

`

Suspension Preparation

In order to prepare the suspensions, all powders were first dried at 110 °C for 2 hours to eliminate moisture on the powder surface. Solids contents were calculated as percentage of the total suspension volume. The required volume was converted to mass and the powder was weighed. Ultrapure water (Milli Q Gradient A-10 model, Millipore Company, Billerica, MA) with a resistivity of 18.3 and total organic content (TOC) < 3 ppm was used. The powders were added slowly to the water and the suspensions were shaken for 24 hours in a heavy-duty shaker at room temperature.

Viscosity Measurements

A rheometer (AR 2000ex model, TA Instruments, New Castle, DE) with a cone and plate geometry attachment (steel, 4° cone angle and 40 mm diameter) was used for the viscosity measurements. Water evaporation during measurements was prevented by using a solvent trap. Two consecutive runs were conducted at 25.0 ± 0.1 °C. Each run consisted of two half loops. During the first half loop, the shear rate was ramped up from 0.5 s^{-1} to 500 s^{-1} and in the second run it ramped down to 0.5 s^{-1}. Ten points per decade of each half loop were recorded. After the second half loop of the first run, data was reproducible. Second half loop of the second run was reported.

Low Temperature Differential Scanning Calorimetry (LT-DSC)

A differential scanning calorimeter (Q20 model, TA Instruments, New Castle, DE) with an RCS 40 cooling unit was used to measure water melting events. To prevent the evaporation of water, hermetically sealed aluminum pans and lids were employed. Samples with similar water content (approx. 5 – 10 mg) were prepared. The samples were cooled down to –25 °C, held at

`

that temperature for 1 min to equilibrate the temperature. Then, the sample was heated to 10 °C at a heating rate of 1 °C/ min.

TA Universal Analysis software was used for both the deconvolution of the area under the curves and the estimation of the melting temperatures.

Zeta Potential Measurements

A Zetasizer (Nano ZS90 model, Malvern Instruments, Worcestershire, UK) was used to measure the zeta potential of the powders. The suspensions prepared for rheology and DSC measurements were diluted to 200 ppm particles by ultrapure water. The ion concentrations of the solutions were kept constant at 0.01 M with NaCl, which is known to be an indifferent electrolyte for all the powders used in this study. The details of the measurements were reported previously [3].

Results and Discussion

Rheological Measurements

The viscosity of suspensions depends on a number of variables such as particle size, shape, size distribution, surface charge, solution chemistry, solids content, deformability, flow conditions, and others [41]. Figure 2 shows the suspension viscosity of different oxide systems as a function of shear rate and solids content. Because of the large number of variables in these systems, a one-to-one comparison of the viscosity values would not be meaningful. However, some of their specific rheological characteristics are worth mentioning.

All suspensions had high viscosities and almost none of them exhibited Newtonian behavior at any solids content studied. On the other hand, shear thinning behavior was observed at almost

`

all levels of solids content, and it became more prominent at higher levels. At high shear rates and for low solids content systems, shear thickening was common.

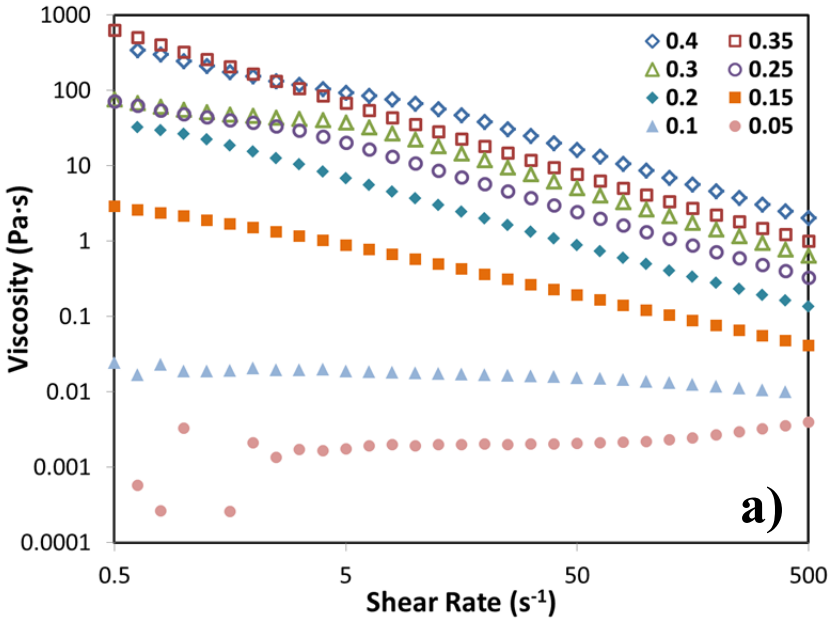

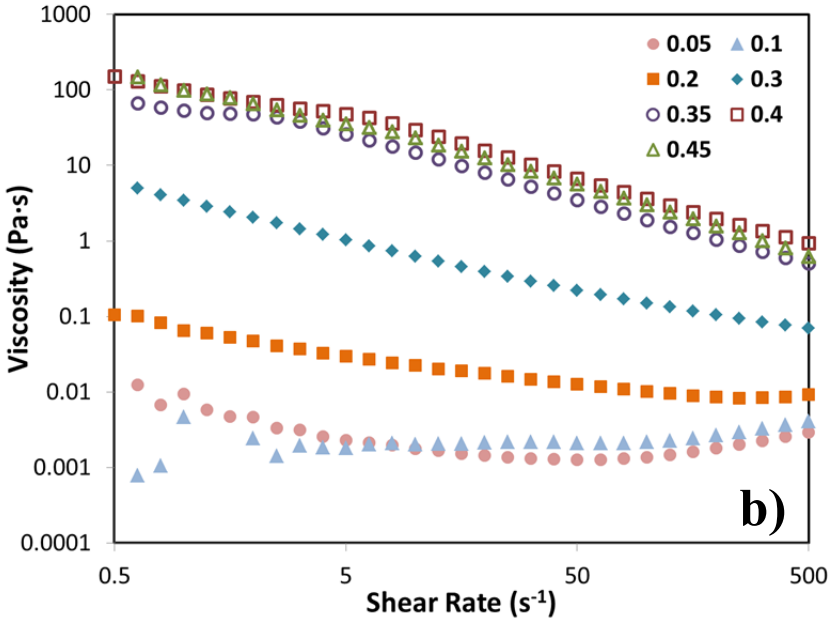

`

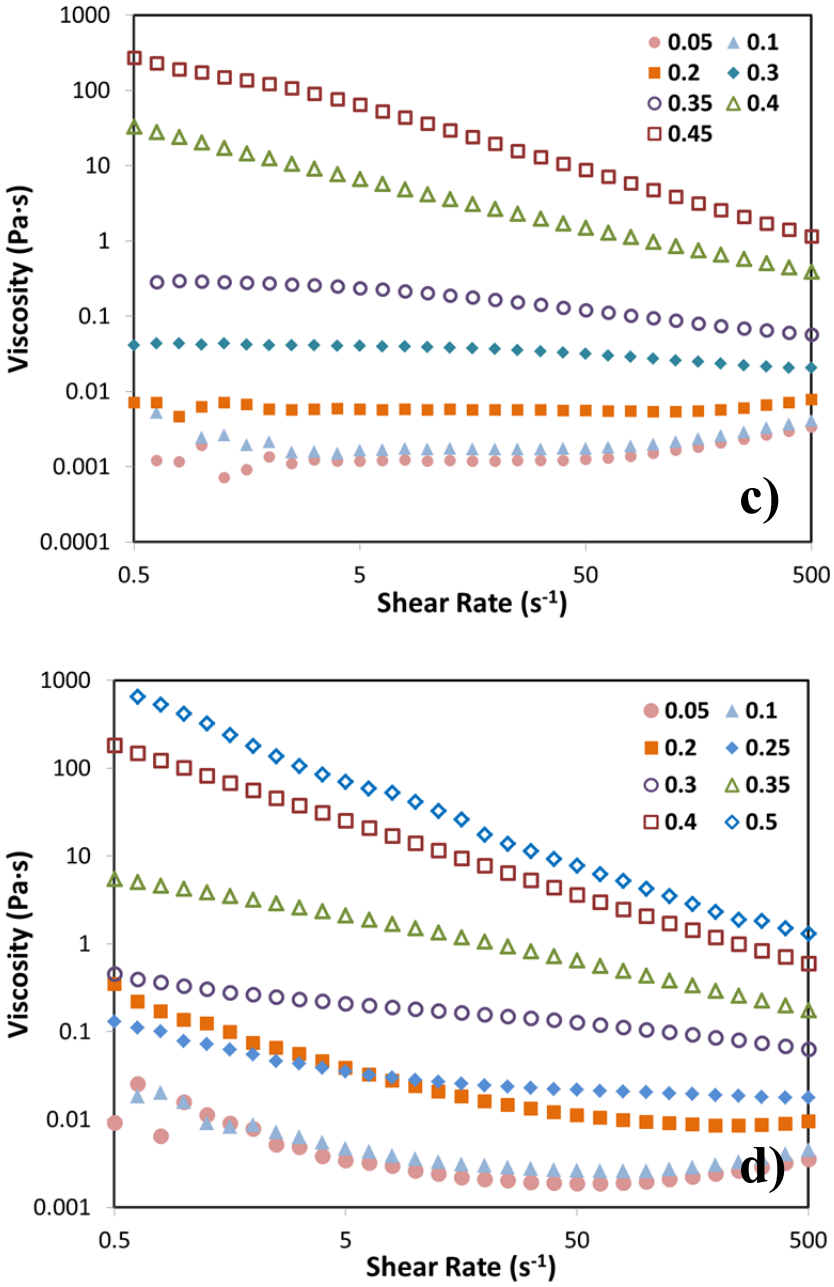

Figure 2: Viscosities of alumina (a), zirconia (b), YSZ (c), and titania (d) nanopowder suspensions with varying solids content and shear rate. Note that a log-log plot is used.

There are three main forces effective in colloidal suspensions of charged particles: Brownian, interparticle, and hydrodynamic forces. At low shear rates, Brownian and interparticle forces dominate. At high shear rates, on the other hand, hydrodynamic forces become more dominant [42-44]. Recently, Jamali *et al*. [44] used simulation to show that the shear thinning

behavior was caused by the lack of resistance to interparticle interactions or external forces. According to their study, hydrodynamic interactions overcame the interparticle interactions with increasing shear rates, and a decrease in viscosity was observed. At high shear rates, the hydrodynamic forces became so strong that hydroclusters were formed and thickening occurred [44]. According their bimodal model, shear thickening was not observed at high solids contents or when the small particle fraction was increased. Our observations for four different oxide suspensions support their findings.

A shear rate of 50 s^{-1} was chosen to compare the viscosities of different oxide systems. This is in the plateau region of low solids content suspensions where hydrodynamic interactions were assumed to be the most effective while interparticle interactions were relatively less effective. Figure 3 shows a comparison of viscosities as a function of solids content for different oxide suspensions at a constant shear rate.

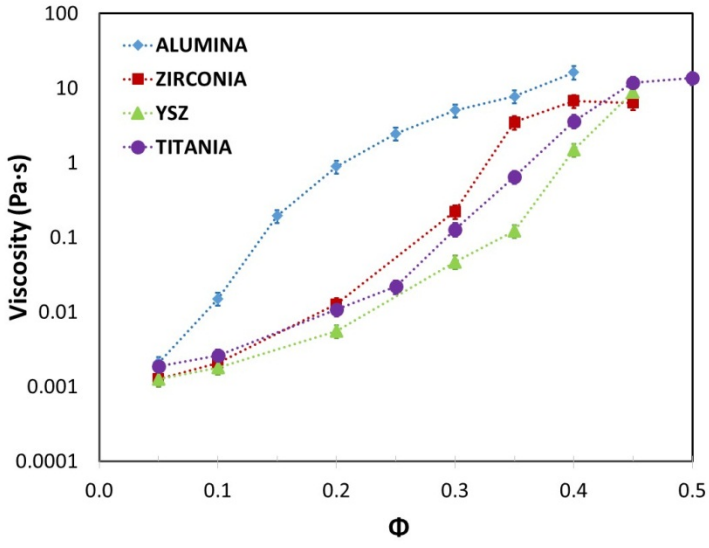

Figure 3: Comparison of suspension viscosities of different oxide systems at a shear rate of 50 s^{-1}. Note that a semi-log is used.

Figure 3 shows that the viscosity of the suspensions increased exponentially with solids content as predicted by the K-D relation. While the increase in viscosities was comparable for zirconia, YSZ and titania, the alumina nanopowders exhibited the highest viscosities at a different rate of increase than the other systems.

Neither size, shape, size distribution, nor agglomeration state of the particles (Figure 1, Table 1) can solely explain the different behavior of the alumina nanopowder suspensions or the relative viscosities of the suspensions. A more detailed study is needed to explain the subtle differences observed for these powders which is beyond the scope of this work.

Bound Water Layer

As reported previously, the secondary melting event, the "bound water", was observed in the presence of alumina nanopowders [2, 3, 12]. Figure 4 shows that melting events at lower temperatures than free water were also seen in titania, zirconia and yttria stabilized zirconia suspensions, indicating that the existence of bound water is not unique for the alumina nanopowder suspensions.

In all cases, as solids content was increased, the bound water peak was increased at the expense of the free water peak. Since the available surface area increases with solids content, increase in bound water was expected [2].

In the individual oxide systems the melting events for both free and bound water was seen at approx. the same temperatures, independent of their solids content (Figure 4, Table 2). However, the type of the oxide affected the melting temperature of the bound water, the shape of the peak as well as its amount.

`

The melting events for different oxide systems are compared in Figure 4d. The decrease in melting point temperatures in the presence of oxide nanopowders can be ranked from lowest to highest as follows: zirconia, YSZ, alumina, and titania.

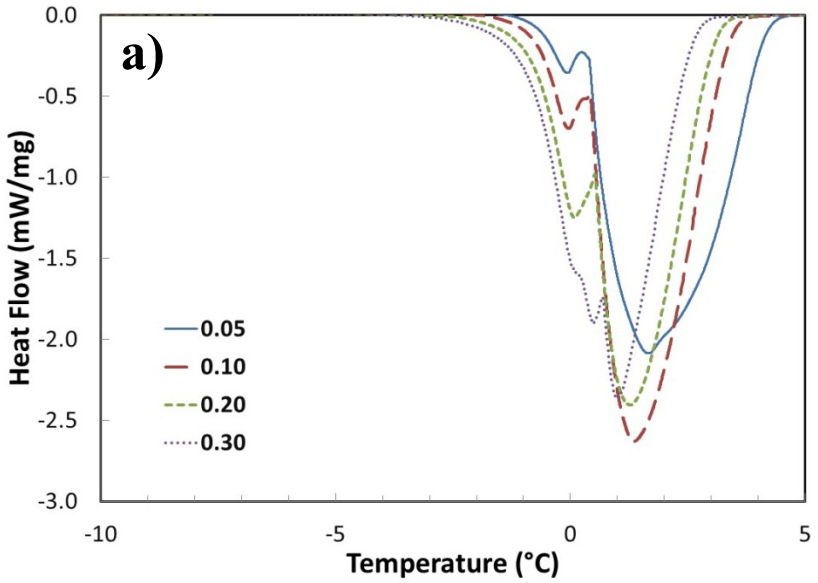

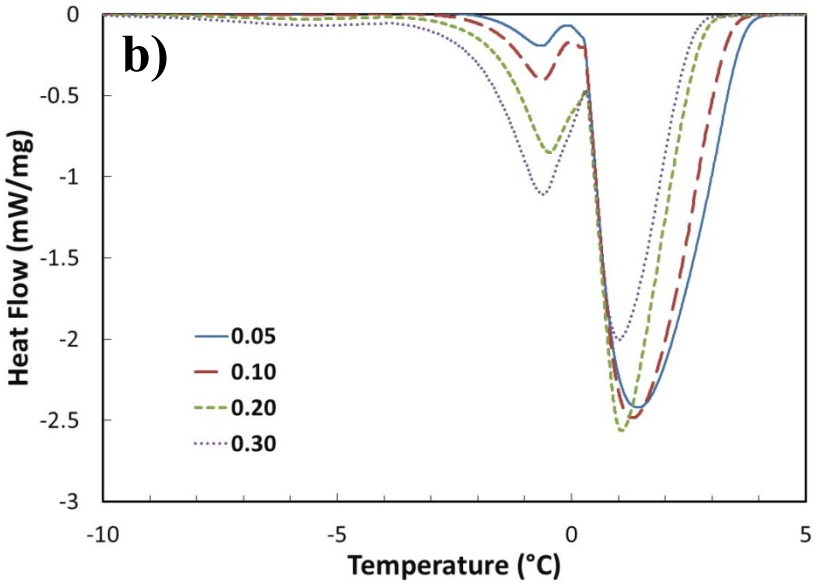

`

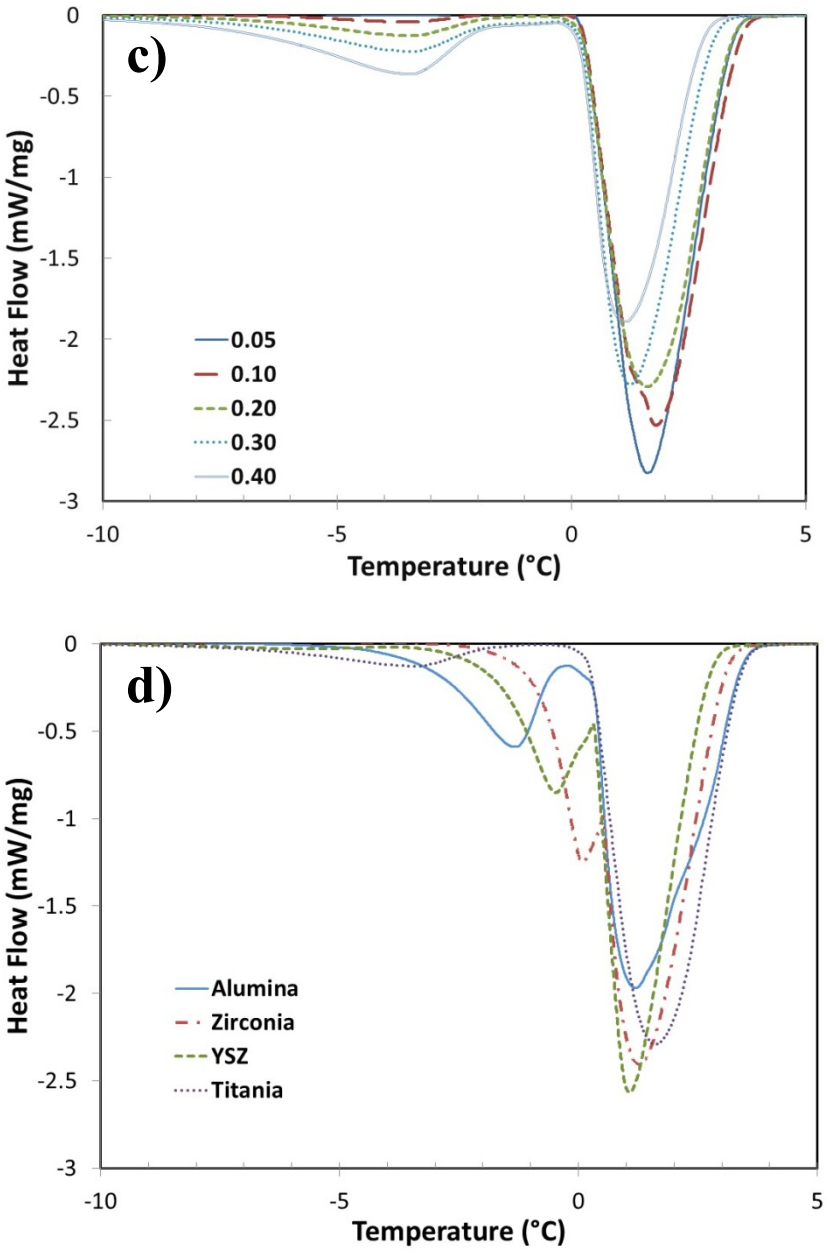

Figure 4: LT-DSC plots of zirconia (a), YSZ (b), and titania (c) nanopowder suspensions with varying solids content. A similar plot for alumina systems was reported previously [2]. LT-DSC plots were compared at Φ= 0.20 for different oxide systems (d). The melting event at lower temperatures was attributed to a bound water melting, while the other was attributed to free water. The curves were normalized with respect to the total water content.

`

In order to allow for a quantitative comparison of the bound water contents and the melting characteristics, the LT-DSC curves were deconvoluted. The details of the deconvolution process and the calculations were reported previously [2]. The heat absorbed during each event was estimated by deconvolution of the area under the melting event curve. By assuming that the heat of fusion for the free water was equal to the one of pure water, the amount of free water was estimated. Subtracting the amount of free water from the total water content provides the amount of bound water. The amount of heat absorbed for bound water melting event (estimated by deconvolution) was divided by the amount of bound water to estimate the heat of fusion values for bound water events. The heat of fusion values were averaged over solids content range and standard deviations were calculated. The entropy of fusion was estimated using Gibbs free energy equation; the results are listed in Table 2. Lower heat of fusion values were associated with lower melting temperatures and entropy changes.

Table 2: Comparison of melting events for different oxide nanopowder suspensions.

	$T_{m, FW}$ (°C)	$T_{m, BW}$ (°C)	$\Delta H_{f, BW}$ (J/g)	$\Delta S_{f, BW}$ (J/gK)	w_{BW} (Φ= 0.20)
Zirconia	0.2	-1.0	270 ± 15	0.91	0.36
YSZ	0.2	-1.8	250 ± 10	0.84	0.32
Alumina	0.3	-3.3	245 ± 15	0.83	0.30
Titania	0.2	-7.1	205 ± 10	0.71	0.19

T_m, ΔH_f, and w represent melting temperature, heat of fusion and weight fraction, respectively. FW and BW represent free and bound water, respectively.

The relative melting temperatures and heat of fusion values of bound water for different oxide systems exhibited an interesting correlation with the ΔpH values (the difference between the pH of the IEP and suspensions) and the total ion concentrations estimated from solubility products of oxides at the suspension pH (Table 3).

`

Hydrolysis reactions of the oxides in aqueous environments determine the pH of the suspensions as long as there is no other species present in the system other than pure oxide and water. These reactions yield a certain amount of charged and neutral hydroxide species, depending on solubility constants. Table 4 shows the available species at suspension pH, the solubility constants of neutral hydroxide species, the total concentrations of all species, and the overall hydrolysis reactions. For YSZ, the surfaces of the zirconia powder particles were mostly covered by yttria. Therefore, the values for YSZ should be considered in between those of yttria and zirconia.

The difference between total ion and hydroxide concentrations represents the concentration of the available charged species in the system. The charged species concentration follows the inverse relationship with the melting temperature of bound water. For increased concentration of charged species, the melting temperatures decrease and the bound water fraction becomes smaller which is expected if one considers melting/freezing point depression by electrolyte in solutions.

While the charged species consume hydrogen ions during formation, hydroxide formation reactions involving these species release hydrogen to the system. Because the hydrogen concentrations in suspensions ($[H^+] \approx 10^{-\Delta pH}$) were much higher than the solubility products of hydroxides, excess amounts of hydroxides precipitated. Therefore, the ΔpH values may be indications of precipitated hydroxides, with larger ΔpH values indicating higher concentrations of precipitated hydroxide. If the precipitation took place on the particle surface, it may be linked to the bound water event. Similar hydration reactions were also suggested for cement systems [45]. It was also reported that saccharides affect hydration of cements [46, 47]. Similarly, we

`

observed a decrease in bound water content in the presence of low molecular weight saccharides [2, 11, 12].

Table 3: Comparison of the suspension pH and zeta potentials of different oxide systems.

	pH at IEP (± 0.2)	**Suspension pH**	**ΔpH (pH_{IEP} - pH_{susp})**
Zirconia	6.2	3.7 ± 0.4	2.5
YSZ	8.0	5.1 ± 0.2	2.9
Alumina	9.5	5.5 – 6.5	≈ 3.5
Titania	6.2	2.3 ± 0.3	3.9

Table 4: Comparison of hydrolysis reactions for different oxide systems [48].

	Available Species at pH_{susp}	**K_{sp} (aq)**	**$[species]_T$ at pH_{susp}**	**Overall Hydrolysis Reactions**
Zirconia	$Zr(OH)_4$, $Zr(OH)^{3+}$ $Zr(OH)_3^+$, H_3O^+	$10^{-9.7}$	$\approx 10^{-10}$	$ZrO_2 + 2H_2O \leftrightarrow Zr(OH)_4$
YSZ		10^{-26} $[Y(OH)_3]$	-	$Y_2O_3 + 3H_2O \leftrightarrow 2Y(OH)_3$
Alumina	$Al(OH)_3$, $Al(OH)^{2+}$ $Al(OH)_2^+$, H_3O^+	10^{-15}	$\approx 10^{-5.6}$	$Al_2O_3 + 3H_2O \leftrightarrow 2Al(OH)_3$
Titania	$Ti(OH)_4$, $Ti(OH)_3^+$ $Ti(OH)_2^{2+}$, H_3O^+	$10^{-4.8}$	$\approx 10^{-4.7}$	$TiO_2 + 2H_2O \leftrightarrow Ti(OH)_4$

pH_{susp} is the pH of the suspension, K_{sp} is the solubility product of the hydroxide in aqueous environment, $[species]_T$ is the total concentration of the available species and ΔH_{hyd} is the enthalpy of hydration.

`

As mentioned earlier, the addition of NaCl did not affect the bound water, while the H^+ and OH^- led to a decrease and increase of the bound water peaks, respectively [3]. The introduction of more H^+ to the system shifted the bound water curves to lower temperatures while shrinking it. Similarly, for oxide systems, higher the ΔpH (higher the available H^+) is, lower the bound water melting temperature and smaller the bound water fraction is. With the addition of OH^-, totally opposite behavior was observed.

The changes in bound water fractions with solids content for different oxide suspensions are plotted in Figure 5. As the solids content was increased, the bound water fractions also increased, supporting our claim that the bound water was associated with the available surface area. The bound water fractions for YSZ, zirconia and alumina were relatively similar, but differed from those for titania. This trend does not correlate with their BET surface area indicating that the bound water fractions were not only function of the surface area. Different melting temperatures and heat of fusion values support this conclusion. The formation of the bound water layer may also be affected by the chemical nature and kinetics of the layer formation.

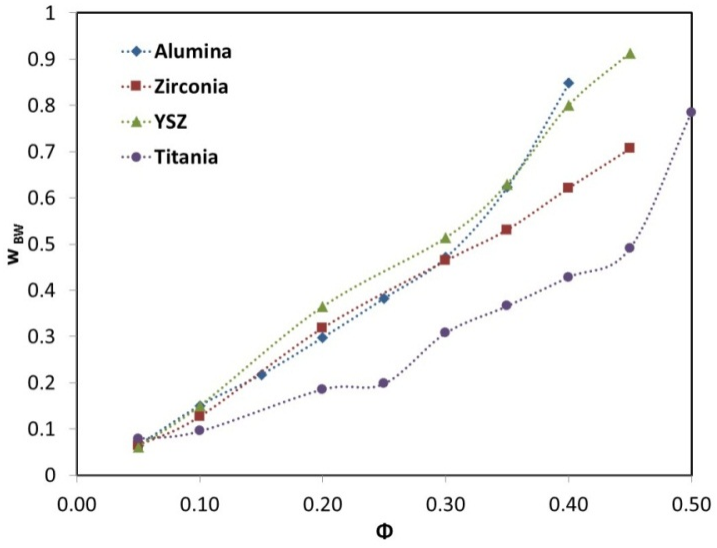

Figure 5: Variation of bound water fractions with solids content for different oxide systems.

Modeling Suspension Viscosity

The Krieger-Dougherty equation (Equation 2) is a semi-empirical relation derived for hard sphere suspensions at medium to high solids contents [43, 49, 50].

$$\frac{\eta}{\eta_0} = \left[1 - \frac{\phi}{\phi_{max}}\right]^{-[\eta]\phi_{max}} \quad \text{(Equation 1)}$$

We recently showed that the Krieger-Dougherty equation can be modified by introducing the effective solids content and maximum achievable effective solids content parameters caused by the presence of bound water layers around the particles (Equation 2) [51]. Here, we aimed to determine the intrinsic viscosities of different oxide systems to better understand the parameters affecting viscosity of nanopowder suspensions.

$$\frac{\eta}{\eta_0} = \left[1 - \frac{\phi_{eff}}{\phi_{eff,max}}\right]^{-[\eta]\phi_{eff,max}} \quad \text{(Equation 2)}$$

where η, η_0, and $[\eta]$ are the viscosity of the suspension, the base fluid and the intrinsic viscosity and Φ_{eff} and $\Phi_{eff,\ max}$ are the effective solids content of particles and the maximum effective solids content for the system, respectively.

Because the bound layer cannot serve as solvent in the system, its volume fraction, which was estimated from DSC plots, was added to the solids content parameter to obtain the effective solids content (Equation 2). For the maximum effective solids content, experimentally achieved maximum value was used.

$$\phi_{eff} = \frac{V_S + V_{BW}}{V_{total}} \quad \text{(Equation 2)}$$

where V_S, V_{BW}, and V_{total} are the volumes of solids, bound water and total suspension, respectively. Similar approaches were employed previously for steric layers [42, 49],

`

electrostatic double layers (EDL) [52, 53], and swelling of particles [35, 54]. Therefore, it was assumed that at the boundary of this layer, the powders can be assumed to be hard spheres, allowing for the application of models derived for hard spheres such as Einstein, K-D relations, and others.

The suspension viscosity of charged particles depends on many variables related to flow conditions, concentration, physical and chemical properties of the particles and suspending medium, and others [41]. Even though the K-D equation seems to be only a function of solids content, maximum achievable solids content and intrinsic viscosity, the other parameters are embedded in these three variables.

Concentrated nanopowder suspensions showed strong shear thinning behavior (Figure 1). Therefore, Φ_{eff}, $\Phi_{eff,max}$ and $[\eta]$ need to be determined for specific shear rate. We already detailed the dominant system forces caused by the applied shear rate when discussing the rheological behavior. The change in the force balance affects the prediction of the parameters. Maximum solids fraction, for example, increased with the increase in shear rate because of the denser packing of particles. For hard spheres, the highest possible packing fraction is theoretically 0.74, while experimentally it is predicted to be 0.54. At low shear rates, particles are at rest and pack loosely. While the theoretical value for random packing of monodisperse spherical particles is 0.64, experimentally it varies from 0.495 to 0.54 [29, 43, 55]. Polydispersed systems can pack more densely because the smaller particles fill the voids between larger ones [43, 49, 56, 57]. Deformability of particles also increases the packing fraction, because particles can squeeze past each other and enhance the effect of shear [42, 49]. However, there is no universally accepted way to predict the value of Φ_{max} [43].

`

Because of the lack of better approximation, we assumed that the $\Phi_{eff,max}$ is the maximum solids content achieved experimentally in our calculations independent of the shear rate. Experimental $\Phi_{eff,max}$ values are given in Table 4. Because the experimental values were already high, we did not expect large deviations with shear rate. Even when $\Phi_{eff,max}$ was assumed to be 1.0 at 500 s^{-1}, which represents the condition with the highest possible error, [η] for alumina, zirconia, YSZ and titania increased from 8.7, 4.1, 2.8, and 5.3 to 9.0, 4.9, 3.1 and 6.0, respectively.

Table 5 shows the comparison of intrinsic viscosities of different oxide systems at three different shear rates by fitting the K-D and the modified K-D expressions. Equations were fitted through regression over different solids content.

A comparison of experimental values and predictions through the modified K-D equation is shown in Figure 7. The viscosities of the alumina suspensions showed a different dependency on solids content than the other oxide systems, as was shown in Figure 3. This observation was also reflected in departure of predicted viscosity (by modified K-D expression) from the experimentally measured viscosity (Figure 7). For alumina, a good fit could only be obtained for low to medium solids contents ($0 \leq \Phi \leq 0.20$, with 5 data points). For the other oxide systems, the viscosities at higher solids contents could be estimated without significant deviations. During fitting of modified K-D relation, relatively large errors were observed at high solids contents for zirconia and YSZ suspensions ($\Phi \geq 0.40$). These deviations were probably caused by an error during deconvolution of overlapping peaks for determining the bound water content. For titania suspensions, there was no overlapping peaks even at very high concentrations, so the best fit was obtained through the full solids content range.

`

Table 5: Fitting parameters of Krieger-Dougherty equation for different oxide systems at shear rates of 0.5 s^{-1}, 50 s^{-1}, and 500 s^{-1}.

	Shear rate (s^{-1})	**K-D Relation**		**Modified K-D Relation**		**η_{exp} (Φ= 0.20) (Pa·s)**
		[η]	**R^2**	**[η]**	**R^2**	
Alumina (Φ_{max} = 0.91)	0.5	39.7	0.874	16.9	0.872	
	50	27.9	0.968	11.6	0.968	0.891
	500	20.9	0.971	8.7	0.963	
Zirconia (Φ_{max} = 0.84)	0.5	18.6	0.957	7.6	0.961	
	50	13.3	0.962	5.1	0.969	0.011
	500	10.7	0.957	4.1	0.945	
YSZ (Φ_{max} = 0.92)	0.5	9.2	0.982	3.5	0.982	
	50	8.6	0.985	3.1	0.982	0.013
	500	7.9	0.773	2.8	0.706	
Titania (Φ_{max} = 0.89)	0.5	13.3	0.849	9.5	0.936	
	50	10.6	0.979	6.6	0.990	0.006
	500	8.6	0.929	5.3	0.975	

For the Krieger-Dougherty (K-D) relation, maximum achievable solids content (Φ_{max}) was taken as 0.495 at low shear rates (0.5 s^{-1}) and 0.54 at high shear rates (50 s^{-1} and 500 s^{-1}). Φ (solids content) was assumed to be concentration of "dry" powders. For the application of the modified K-D equation, the maximum achievable effective solids content ($\Phi_{eff,max}$) was determined experimentally, and assumed constant over the shear rate range. Φ was replaced by the estimated effective solids content (Φ_{eff}) to account for the bound water layer. η_{exp} represents the experimental viscosity measurements. [η] represents the intrinsic viscosity, and the R^2 is a coefficient representing the quality of the fit. R^2=1.0 is the best possible fit.

`

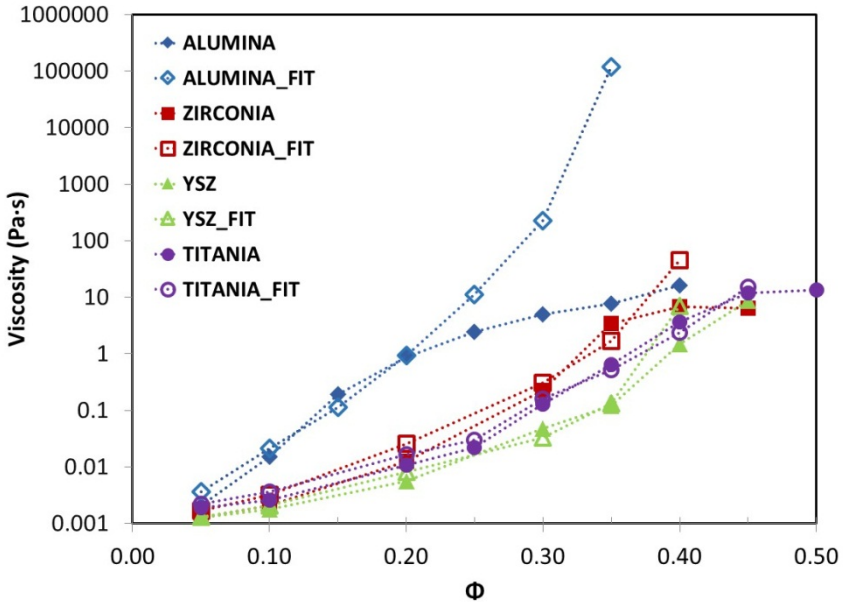

Figure 6: Comparison of experimental data with viscosity predictions by the K-D equation for different oxide systems at a shear rate of 50 s^{-1}.

Intrinsic viscosity is defined as the contribution of particles to the viscosity and is a function of particle size, shape, and flexibility [58]. The intrinsic viscosity of hard spheres was calculated by Einstein as 2.5 [59]. Because there was no size effect included in Einstein's calculations, the effect of particle size was investigated later [58]. Larger particles lead to larger energy dissipation and deviations from the spherical shape lead to higher intrinsic viscosity values because of the increase in particle size caused by free rotation of the particles. Deformable particles, on the other hand, lead to lower intrinsic viscosities.

The TEM micrographs, Figure 1, showed that the YSZ particles were well dispersed individual particles. Zirconia particles, on the other hand, were highly agglomerated resembling fused assemblies. The lowest intrinsic viscosity values were obtained for YSZ systems, which was attributed to the dispersion of the particles. Alumina and titania particles look very similar to each other except from their particle size (Figure1). Lower intrinsic viscosity of titania powders with respect to alumina powders may be attributed to their smaller size (Table 1 and 5).

`

Nanopowders tend to form agglomerates because the smaller separation distances allow for stronger interparticle forces. If the flow units are considered as agglomerates rather than individual particles, an increase in intrinsic viscosity is expected, because of the surface roughness and the higher effective solids content created by the voids between particles [60]. Therefore, in the presence of agglomerates, the intrinsic viscosity becomes not only function of particle properties like size, shape or deformability but also interparticle forces, thus chemistry of particles, solids content and flow conditions [52, 53, 61-63].

At low shear rates, where the interparticle forces are more effective, large agglomerates form resulting in high intrinsic viscosities. With the higher shear rate, agglomerates becomes denser and with lower fractal values, therefore, the values of intrinsic viscosity lower [64, 65]. Table 4 shows the expected decrease in intrinsic viscosities with shear rate for all four oxide systems. The differences between the intrinsic viscosities at lower and higher shear rates indicate the effectiveness of interparticle interactions on viscosity.

At higher shear rates, the effect of interparticle interactions was expected to decrease. Theoretically, shear thinning behavior terminates with the plateau region at very high shear rates. However, as seen in Figure 2, the viscosities did not reach the plateau at a shear rate of 500 s^{-1}, which indicated that the interparticle interactions were still effective. Conversely, at low solids contents, shear thickening was observed in this region as predicted by Jamali *et al*. [44]. Since K-D equation is originated for hard sphere systems, relatively better fitting parameters, R^2, obtained at the shear rate of 50 s^{-1} supports the claim of the minimized effect of interparticle interactions and controllable effect of hydrodynamic interactions at this shear rate.

Estimates using the K-D equation resulted in higher intrinsic viscosity values than estimates using the modified equation. The main differences between the two models were the packing of

`

agglomerates and the deformability of the particles caused by the bound water layer. In the presence of a bound water layer, a denser packing of particles with lower fractal values was expected, especially at high shear rates. Because the packing fraction of the agglomerates is inversely proportional to the intrinsic viscosities, lower predictions of intrinsic viscosities were meaningful when modified K-D was employed.

When the relative intrinsic viscosities of powders were compared, modified relation lead to higher intrinsic viscosity values than zirconia while the K-D relation results in vice versa. The Hamaker constants of titania and zirconia particles are 5.35×10^{-20} J and 8.0×10^{-20} J, respectively [34]. Zeta potential values at the suspensions pH are 45 mV and 30 mV for titania and zirconia powders, respectively. Lower Hamaker constants and higher zeta potential values of titania system indicate the more effective repulsive forces than zirconia systems. Repulsive forces lead to loose packing of agglomerates, thus higher intrinsic viscosities [52, 53, 65]. However, according to K-D equation, zirconia powder has higher intrinsic values than titania powders as opposed to the expectations from relatively better dispersed systems. When the effect of bound water layer was excluded as in modified K-D relation, higher intrinsic viscosities were obtained for titania powders as expected.

In the K-D relation, the estimated intrinsic viscosities $[\eta]$ are directly related to the viscosity of the suspensions. In other words, as Φ_{max} is assumed constant at each specific shear rate, $[\eta]$ is the only adjustable variable in the K-D expression and mirror the suspension viscosity implying that all the variables are imbedded in the intrinsic viscosity term, $[\eta]$. Therefore, elucidating the viscosity mechanism is difficult. With modified Krieger Dougherty equation, the effect of bound water layer on the suspension viscosity was elaborated.

`

Conclusion

The viscosities of different oxide nanopowder suspensions were studied. All suspensions exhibited shear thinning behavior at relatively high solids content because of the small separation distances and enhanced interparticle interactions. With increase in shear rate, hydrodynamic interactions dominate the interparticle interactions. At low solids content, shear thickening behavior was observed at higher shear rates because of the hydrocluster formation.

It was shown that the bound water is not unique to alumina nanopowder suspension, but common for other oxide systems also. Bound water fractions were estimated by deconvolution of LT-DSC plots. Bound water fractions increased with solids content. The melting temperature of bound water and ts magnitude were dependent on the type of oxide. A relationship between the bound water content and ΔpH of the suspensions was distinguished. pH differences was associated with the available charged species and precipitated hydroxides. For the higher ΔpH of suspensions, the lower bound water melting temperatures were observed. Hydrolysis of oxide powders might be responsible for the existence of the bound water layer resulting in increased effective volume fractions and higher viscosities of nanopowder suspensions.

Estimated bound water fractions were introduced to the effective solids content and the maximum achievable volume fraction terms in the K-D equation. Intrinsic viscosities were predicted using the modified Krieger-Dougherty equation as 11.6, 6.6, 5.1 and 3.1 at the shear rate of 50 s^{-1} for alumina, titania, zirconia and YSZ, respectively. The lowest intrinsic value of YSZ was attributed to the better dispersion of particles. The intrinsic viscosity of powders was decreased with increasing shear rate. Introduction of the bound water layer to intrinsic viscosity yield more reasonable intrinsic viscosity values. Since it excludes the effect of bound water layer

`

on intrinsic viscosity, modified equation leads to better understanding of the viscosity mechanism.

Acknowledgement

This research was supported by the National Science Foundation under grant number CBET – 0931038. The authors would like to thank Charles Glatz and Brent H. Shanks for making a Zetasizer and BET surface area unit available for this study. We also would like to thank Tugce Karakulak and Lin Zhou for taking TEM images of nanopowders.

References

[1] Çınar S, Akinc M. Ascorbic Acid as a Dispersant for Concentrated Alumina Nanopowder Suspensions. J Eur Ceram Soc 2013 (accepted)

[2] Çinar S, van Steenhuyse L, Akinc M. Elucidation of Viscosity Reduction Mechanism of Nano Alumina Suspensions with Fructose Addition by DSC. J Am Ceram Soc 2013; 96: 1077-84.

[3] Çınar S, Akinc M. Electrostatic Stabilization of Alumina Nanopowder Suspensions. Sci Adv Mat 2013 (accepted)

[4] Witharana S, Hodges C, Xu D, Lai X, Ding Y. Aggregation and settling in aqueous polydisperse alumina nanoparticle suspensions. J. Nanopart. Res. 2012; 14: 1-11.

[5] Yar Y, Acar FY, Yurtsever E, Akinc M. Reduction of Viscosity of Alumina Nanopowder Aqueous Suspensions by the Addition of Polyalcohols and Saccharides. J Am Ceram Soc 2010; 93: 2630-6.

[6] Wu L, Huang Y, Liu L, Meng L. Interaction and stabilization of DMF-based alumina suspensions with citric acid. Powder Technology 2010; 203: 477-81.

[7] Singh P, Anoop K, Patel H, Sundararajan T, Pradeep T, Das S. Anomalous Size Dependent Rheological Behavior of Alumina Based Nanofluids. Int J Micro-Nano Scale 2010; 1: 179-88.

[8] Azar M, Palmero P, Lombardi M, Garnier V, Montanaro L, Fantozzi G, et al. Effect of initial particle packing on the sintering of nanostructured transition alumina. J Eur Ceram Soc 2008; 28: 1121-8.

`

[9] Studart AR, Amstad E, Gauckler LJ. Colloidal Stabilization of Nanoparticles in Concentrated Suspensions. Langmuir 2006; 23: 1081-90.

[10] Liu JC, Jean JH, Li CC. Dispersion of Nano-Sized γ-Alumina Powder in Non-Polar Solvents. Journal of the American Ceramic Society 2006; 89: 882-7.

[11] Li C, Akinc M, Wiench J, Pruski M, Schilling CH. Relationship Between Water Mobility and Viscosity of Nanometric Alumina Suspensions. J Am Ceram Soc 2005; 88: 2762-8.

[12] Li C, Akinc M. Role of Bound Water on the Viscosity of Nanometric Alumina Suspensions. J Am Ceram Soc 2005; 88: 1448-54.

[13] Bowen P, Carry C, Luxembourg D, Hofmann H. Colloidal processing and sintering of nanosized transition aluminas. Powder Technol 2005; 157: 100-7.

[14] Danelska A, Ulkowska U, Socha RP, Szafran M. Surface properties of nanozirconia and their effect on its rheological behaviour and sinterability. J Eur Ceram Soc 2013; 33: 1875-83.

[15] Khan AU, Haq AU, Mahmood N, Ali Z. Rheological studies of aqueous stabilised nano-zirconia particle suspensions. Materials Research 2012; 15: 21-6.

[16] Horri BA, Ranganathan P, Selomulya C, Wang H. A new empirical viscosity model for ceramic suspensions. Chem Eng Sci 2011; 66: 2798-806.

[17] Wang X, Guo L. Effect of sucrose on rheological properties of aqueous zirconia suspensions with polyacrylate. Powder Technology 2008; 186: 107-12.

[18] Renger C, Kuschel P, Kristoffersson A, Clauss B, Oppermann W, Sigmund W. Rheology studies on highly filled nano-zirconia suspensions. Journal of the European Ceramic Society 2007; 27: 2361-7.

[19] Chera L, Palcevskis E, Berzins M, Lipe A, Jansone I. Dispersion of nanosized ceramic powders in aqueous suspensions. JPCS 2007; 93: 012010.

[20] Bowen P, Carry C. From powders to sintered pieces: forming, transformations and sintering of nanostructured ceramic oxides. Powder Technology 2002; 128: 248-55.

[21] Johnson SB, Franks GV, Scales PJ, Boger DV, Healy TW. Surface chemistry–rheology relationships in concentrated mineral suspensions. Int J Miner Process 2000; 58: 267-304.

[22] Duran C, Jia Y, Hotta Y, Sato K, Watari K. Colloidal processing, surface characterization, and sintering of nano ZrO2 powders. Journal of Materials Research 2005; 20: 1348-55.

[23] Xie Z, Ma J, Xu Q, Huang Y, Cheng Y-B. Effects of dispersants and soluble counter-ions on aqueous dispersibility of nano-sized zirconia powder. Ceramics International 2004; 30: 219-24.

`

[24] Zhang J, Ye F, Sun J, Jiang D, Iwasa M. Aqueous processing of fine ZrO2 particles. Colloids and Surfaces A: Physicochemical and Engineering Aspects 2005; 254: 199-205.

[25] Cannon AS, Warner JC. Structure−Activity Relationship of Organic Acids in Titanium Dioxide Nanoparticle Dispersions. Chemistry of Materials 2004; 16: 5138-40.

[26] Faure B, Sæderup Lindeløv J, Wahlberg M, Adkins N, Jackson P, Bergström L. Spray drying of TiO2 nanoparticles into redispersible granules. Powder Technology 2010; 203: 384-8.

[27] Naina HK, Gupta R, Setia H, Wanchoo RK. Viscosity and Specific Volume of TiO_2/Water Nanofluid. Journal of Nanofluids 2012; 1: 161-5.

[28] Ghadimi A, Saidur R, Metselaar HSC. A review of nanofluid stability properties and characterization in stationary conditions. Int J Heat Mass Transfer 2011; 54: 4051-68.

[29] Mahbubul IM, Saidur R, Amalina MA. Latest developments on the viscosity of nanofluids. Int J Heat Mass Transfer 2012; 55: 874-85.

[30] Rao Y. Nanofluids: Stability, phase diagram, rheology and applications. Particuology 2010; 8: 549-55.

[31] Wang X-Q, Mujumdar AS. A review on nanofluids - part I: theoretical and numerical investigations. Braz J Chem Eng 2008; 25: 613-30.

[32] Yu W, Xie H. A review on nanofluids: preparation, stability mechanisms, and applications. J.Nano Mat. 2012; 2012: 1-17.

[33] Lewis JA. Colloidal processing of ceramics. J Am Ceram Soc 2000; 83: 2341-59.

[34] Sigmund WM, Bell NS, Bergström L. Novel Powder-Processing Methods for Advanced Ceramics. J Am Ceram Soc 2000; 83: 1557-74.

[35] Vickers D, Archer LA, Floyd-Smith T. Synthesis and characterization of cubic cobalt oxide nanocomposite fluids. Colloids Surf, A 2009; 348: 39-44.

[36] Zhou Z, Scales PJ, Boger DV. Chemical and physical control of the rheology of concentrated metal oxide suspensions. Chem. Eng. Sci. 2001; 56: 2901-20.

[37] Khanafer K, Vafai K. A critical synthesis of thermophysical characteristics of nanofluids. International Journal of Heat and Mass Transfer 2011; 54: 4410-28.

[38] Petosa AR, Jaisi DP, Quevedo IR, Elimelech M, Tufenkji N. Aggregation and Deposition of Engineered Nanomaterials in Aquatic Environments: Role of Physicochemical Interactions. Environmental Science & Technology 2010; 44: 6532-49.

`

[39] Wang T, Ni M, Luo Z, Shou C, Cen K. Viscosity and aggregation structure of nanocolloidal dispersions. Chin. Sci. Bull. 2012; 57: 3644-51.

[40] Wang T, Wang X, Luo Z, Ni M, Cen K. Mechanisms of Viscosity Increase for Nanocolloidal Dispersions. J Nanosci Nanotechno 2011; 11: 3141-50.

[41] Krieger IM. Rheology Principles, Measurements, and Applications. J Colloid Interface Sci 1996; 178: 382.

[42] Barnes HA. A handbook of elementary rheology. University of Wales, Institute of Non-Newtonian Fluid Mechanics; 2000.

[43] Genovese DB. Shear rheology of hard-sphere, dispersed, and aggregated suspensions, and filler-matrix composites. Adv Colloid Interface Sci 2012; 171–172: 1-16.

[44] Jamali S, Yamanoi M, Maia J. Bridging the gap between microstructure and macroscopic behavior of monodisperse and bimodal colloidal suspensions. Soft Matter 2013; 9: 1506-15.

[45] Peschard A, Govin A, Grosseau P, Guilhot B, Guyonnet R. Effect of polysaccharides on the hydration of cement paste at early ages. Cement and Concrete Research 2004; 34: 2153-8.

[46] Smith BJ, Rawal A, Funkhouser GP, Roberts LR, Gupta V, Israelachvili JN, et al. Origins of saccharide-dependent hydration at aluminate, silicate, and aluminosilicate surfaces. Proceedings of the National Academy of Sciences 2011; 108: 8949-54.

[47] Smith BJ, Roberts LR, Funkhouser GP, Gupta V, Chmelka BF. Reactions and Surface Interactions of Saccharides in Cement Slurries. Langmuir 2012; 28: 14202-17.

[48] Baes CF, Mesmer RE. The hydrolysis of cations. Wiley; 1976.

[49] Hiemenz PC, Rajagopalan R. Principles of Colloid and Surface Chemistry, Third Edition, Revised and Expanded. Taylor & Francis; 1997.

[50] Krieger IM, Dougherty TJ. A mechanism for non-Newtonian flow in suspensions of rigid spheres. Trans. Soc. Rheol. 1959; 3: 137-52.

[51] Çınar S, Anderson DD, Akinc M. Combined Effect of Fructose and NaCl on the Viscosity of Alumina Nanopowder Suspensions. (under preparation)

[52] Mondragon R, Enrique Julia J, Barba A, Jarque JC. Determination of the packing fraction of silica nanoparticles from the rheological and viscoelastic measurements of nanofluids. Chem Eng Sci 2012; 80: 119-27.

[53] Rubio-Hernández FJ, Ayúcar-Rubio MF, Velázquez-Navarro JF, Galindo-Rosales FJ. Intrinsic viscosity of SiO2, Al2O3 and TiO2 aqueous suspensions. J Colloid Interface Sci 2006; 298: 967-72.

`

[54] Saiki Y, Prestidge CA, Horn RG. Effects of droplet deformability on emulsion rheology. Colloids Surf, A 2007; 299: 65-72.

[55] Chen H, Ding Y, He Y, Tan C. Rheological behaviour of ethylene glycol based titania nanofluids. Chem Phys Lett 2007; 444: 333-7.

[56] Liu D-M. Particle packing and rheological property of highly-concentrated ceramic suspensions: φm determination and viscosity prediction. J Mater Sci 2000; 35: 5503-7.

[57] Xu X, Rice SA, Dinner AR. Relation between ordering and shear thinning in colloidal suspensions. Proc Natl Acad Sci 2013; 110: 3771-6.

[58] García de la Torre J, Amorós D, Ortega A. Intrinsic viscosity of bead models for macromolecules and nanoparticles. Eur Biophys J 2010; 39: 381-8.

[59] Einstein A. Eine neue Bestimmung der Moleküldimensionen. Annalen der Physik 1906; 324: 289-306.

[60] Starov V, Zhdanov V, Meireles M, Molle C. Viscosity of concentrated suspensions: influence of cluster formation. Adv Colloid Interface Sci 2002; 96: 279-93.

[61] Anoop KB, Kabelac S, Sundararajan T, Das SK. Rheological and flow characteristics of nanofluids: Influence of electroviscous effects and particle agglomeration. J Appl Phys 2009; 106:

[62] Biddle D, Walldal C, Wall S. Characterisation of colloidal silica particles with respect to size and shape by means of viscosity and dynamic light scattering measurements. Colloids Surf, A 1996; 118: 89-95.

[63] Brenner H. Rheology of a dilute suspension of axisymmetric Brownian particles. Int J Multiphase Flow 1974; 1: 195-341.

[64] Quemada D. Rheological modelling of complex fluids. I. The concept of effective volume fraction revisited. Eur Phys J - Appl Phys 1998; 1: 119-27.

[65] Smith TL, Bruce CA. Intrinsic viscosities and other rheological properties of flocculated suspensions of nonmagnetic and magnetic ferric oxides. J Colloid Interface Sci 1979; 72: 13-26.

`

CHAPTER VII. GENERAL CONCLUSIONS

Nanopowder suspensions show unexpectedly high viscosities. This thesis addresses the questions regarding the rheological properties of concentrated aqueous suspensions of oxide nanopowders and aimed to understand and control their rheological behavior.

Previous studies showed that the bound water phenomenon is critical not only to reveal the effect of low molecular saccharides on suspension viscosities, but also for a general understanding of the rheological behavior of nanopowder suspensions. However, neither the viscosity reduction mechanism of the fructose nor the origin of the bound water phenomenon was well-understood. The first study elucidated the viscosity reduction mechanism created by low molecular weight saccharides in alumina nanopowder suspension as well as the effects of particle size and solids content. It was shown that the bound water peak was also observed in sub-micron size particle systems where its effect is negligible. The effect of the bound water layer on the effective volume fraction was discussed and it was determined the unexpectedly high viscosities in nanopowder suspensions could be attributed to the bound water layer. The bound water content is directly related to the powder surface. The possible origin of the bound water was suggested as hydration layer. Fructose molecules modified the bound water layer and increased the available solvent, thus decreasing the effective volume fraction and reducing the viscosity.

A literature review revealed that large surface areas, smaller separation distances, and large EDL thickness are the main characteristics of concentrated, nano-size oxide suspensions, causing their complex rheological behavior. However, it was observed that the bound water layer is distinctly different than the EDL layer. The effect of ionic strength and pH in alumina

`

nanopowder suspensions were studied in detail to better understand the bound water layer and the effect of electrostatic forces in concentrated nanopowder suspensions. The application of the DLVO theory to nanoparticle assemblies predicted that small changes in electrolyte concentration would lead to significant changes in the nanopowder system. The effect became more noticable at high solids contents. Contrary to predictions in the literature, very small indifferent electrolyte additions ($0.020\ M \leq [NaCl] \leq 0.040\ M$) led to a significant reduction in suspension viscosity. Zeta potential measurements and DLVO calculations showed that a shrinkage of the double layer and an increase in zeta potential of the powders resulted in lower viscosities. When potential determining ions, HCl and NaOH, were introduced to the system, stable suspensions could be obtained only within a limited pH range ($4 \leq pH \leq 7$). At pH values higher than IEP ($pH \geq 9.5$), the concentrated suspensions could not be stabilized by addition of NaOH, as previously reported in the literature. The low electrostatic repulsion and increased bound layer thickness were identified as the reasons for this behavior. The bound water fraction decreased with the addition of H^+. Therefore, potential determining ions not only adjusted the electrostatic interaction as well known, but also influenced the effective solid volume fraction of the suspensions.

In order to optimize the viscosity reduction, two independent mechanisms – modification of the effective volume fraction achieved by addition of fructose and compressing the electrical double layer by addition of NaCl – were combined. The lowest viscosities were obtained when fructose and NaCl are added simultaneously. LT-DSC and *in situ* ATR-FTIR studies indicated that the two mechanisms operate independently. With the help of the Krieger-Dougherty equation, the individual and combined effects of fructose and NaCl on intrinsic viscosities were estimated. It was determined that the changes in interparticle interactions and bound water

`

content contributed to the intrinsic viscosity. The influence of fructose and NaCl addition on the green body microstructure was illustrated by a limited number of slip cast samples. While slip cast samples without additives were fragile with almost micron size pores, the addition of fructose diminished the pore size and improved the structural integrity of the casts. The combination of fructose and NaCl resulted in stronger samples exhibiting only mesopores.

Although previous studies demonstrated that other mono- and di-saccharides also effective in reducing the viscosity, these studies were all limited to saccharides. In order to demonstrate saccharides are not unique in reducing the viscosity, the use of ascorbic acid for the stabilization of alumina nanopowder suspensions was studied and reported Chapter V. Ascorbic acid was selected as a good candidate to optimize the viscosity of nanopowder suspensions because of the chemical similarity between ascorbic acid and fructose molecules (multiple hydroxyl groups, small molecule) and its acidic nature. With the addition of small amounts of ascorbic acid (1 wt% of dry powder), the viscosity of the suspensions decreased dramatically and Newtonian flow was obtained for moderately concentrated suspensions ($\Phi < 0.30$). With the optimum ascorbic acid concentration, the maximum solids content (where $\eta \leq 1$ Pa·s at a shear rate of 100 s^{-1}) could be increased to about 0.35, which is the highest value reported in the literature for readily available processing additives. In addition, the viscosity reduction mechanism was identified as the adsorption of ascorbic acid molecules on the alumina surface. To the best of our knowledge, this study was the first in open literature to use ascorbic acid to stabilize oxide suspensions.

Lastly, the findings for alumina nanopowder suspensions were extrapolated to other oxide nanopowder systems, such as zirconia, yttria stabilized zirconia, and titania suspensions. These systems were compared in terms of their rheological behavior, bound water content as a function

`

of solids content. Strong shear thinning behavior at higher solids contents and shear thickening behavior at high shear rates of low solids content suspensions were observed in all oxide systems. It was shown that the presence of a bound water event is not unique to alumina nanopowder suspensions, but universal for other aqueous oxide nanopowder systems. An interesting correlation was observed between the ΔpH (pH_{IEP} - pH_{susp}) values of the suspensions and the bound water content. We concluded that the bound water events may be considered as related to hydrolysis of the oxide powders. The application of the Krieger-Dougherty equation showed that the viscosity of the suspensions was not only a function of solids content, DLVO interactions, and geometry of the particles, but also a function of their surface chemistry.

`